Scuola Internazionale Superiore di Studi Avanzati – S.I.S.S.A

International School for Advanced Studies – I.S.A.S

Neurobiology Sector

Trieste, Italy

A structural and functional insight into TMEM16B, a calcium-activated chloride channel.

Thesis submitted for the degree of "*Doctor Philosophiae*"

SUPERVISOR

Prof. Anna Menini

CANDIDATE

Ozhathil Lijo Cherian

CO-SUPERVISOR

Dr. Anna Boccaccio

Declaration

This thesis is the result of four years of work under the supervision of Prof. Anna Menini and co-supervisor Dr. Anna Boccaccio at Neurobiology sector of the International School for Advanced Studies, Trieste from November 2010 till October 2014.

The experiments carried out during this thesis are included in the following three manuscripts either accepted or submitted to peer reviewed journals.

- Valentina Cenedese, Giulia Betto, Fulvio Celsi, *O.Lijo Cherian*, Simone Pifferi, and Anna Menini

The voltage dependence of the TMEM16B/anoctamin2 calcium-activated chloride channel is modified by mutations in the first putative intracellular loop

Journal of General Physiology, March 2012, 139(4), 285-294.

I performed some patch-clamp experiments, data analysis and proof reading of the manuscript.

- Giulia Betto*, *O. Lijo Cherian**, Simone Pifferi*, Valentina Cenedese, Anna Boccaccio, and Anna Menini

Interaction between permeation and gating in the TMEM16B/anoctamin2 calcium-activated chloride channel

Journal of General Physiology, May 2014, 143(6), 703-718.

** Equal contribution*

I was involved in designing and performing some patch-clamp experiments, data analysis and proof reading of the manuscript.

- *O. Lijo Cherian*, Anna Menini, and Anna Boccaccio

Multiple effects of anthracene-9-carboxylic acid on the TMEM16B/anoctamin2 calcium-activated chloride channel

Submitted-2014.

I performed all patch-clamp experiments, and participated to the design of experiments, data analysis, and writing of the manuscript.

Summary

TMEM16B, also known as anoctamin 2 has been recently identified as a calcium-activated chloride channel. It is expressed at the synaptic terminals of photoreceptors, in hippocampal cells, in the cilia of olfactory sensory neurons and in the microvilli of vomeronasal sensory neurons. TMEM16B, as its most known cousin TMEM16A, is activated both by calcium and voltage. When this thesis was started there was no available data correlating the gating function and protein structure in TMEM16B.

In our first manuscript, we show a coupling between calcium and voltage in TMEM16B activation. Primary sequence analysis did not show any canonical calcium binding sites nor S4-like dedicated voltage sensors. However, the first intracellular loop contains several negatively charged amino acids. We performed site directed mutagenesis at $_{367}$E, and $_{386}$EEEEE$_{390}$ in the first intracellular loop and investigated their role in calcium or voltage dependence of TMEM16B. Either neutralizing or deleting these acidic residues strongly shifted the conductance-voltage relation towards more positive voltages without a significant effect on the apparent calcium sensitivity. Our findings indicate involvement of glutamic acids from the first intracellular loop in voltage dependent activation of TMEM16B, and provides an initial structure-function study for this channel.

In our second manuscript, we focused on understanding the effect of permeant anions on TMEM16B activation. Our results show TMEM16B is poorly selective among anions and has a permeability sequence of $SCN^- > I^- > NO_3^- > Br^- > Cl^- > F^-$ > gluconate. The channel kinetics also shows dependence on the permeant anion, with more permeable anions, such as SCN^-, causing a much slower activation and deactivation kinetics than Cl^-. Moreover, SCN^- facilitated the channel activation by

lowering the half-maximal concentration of calcium required for opening the channel and shifting the conductance-voltage relation towards less positive voltages. From this work we report the existence of a crosstalk between calcium, voltage and permeant anion in TMEM16B activation.

Furthermore, we looked for a compound that could modulate the function of TMEM16B. We found that anthracene-9-carboyxlic acid, one of the traditional calcium-activated chloride channel blockers is very interesting since it had multiple effects on TMEM16B. In our third manuscript we report the block by A9C as voltage and concentration dependent, with maximal inhibition at positive voltages. Surprisingly, A9C also potentiated the current at intermediate concentrations and negative voltages. However, anthracene-9-methanol (A9M), a non-charged analog of A9C, completely abolished the voltage dependent inhibition and the potentiation effect seen with A9C. Both A9C and A9M had much slower current kinetics. This indicates the requirement of negative charge of A9C for its voltage dependent block of outward currents and potentiation of inward currents.

In summary, the studies included in this thesis reveal a complex coupling between calcium, voltage, and permeant anion in TMEM16B activation. The identification of a compound have contrasting effects on the channel activation, provides a new tool for future structure-function studies on this channel.

Contents

1. Introduction

1.1 Anion channels

Anion channels are integral membrane proteins that allow the passive diffusion of negatively charged ions along their electrochemical gradient. Since chloride ions are the most abundant permeant physiological anions these channels mostly mediate chloride current and are often called chloride channels. Unlike most cation channels which often show high selectivity for a specific ion, chloride channels are less selective and allow passage of other anions including halides such as I^-, Br^-, NO_3^-, the pseudohalide SCN^-, and also HCO_3^-.

Chloride channels have important roles in regulating electrical excitability, cell volume regulation, transepithelial salt transport, smooth muscle contraction and pH regulation. Mammalian chloride channels can be broadly categorized into five classes based on their regulation as follows (Verkman and Galietta, 2009; Table-1 in Ferrera et al., 2011b): Cystic fibrosis transmembrane conductance regulator (CFTR); voltage-gated or swelling activated chloride channel (CLC); ligand-gated chloride channel (GABA(γ-amiobutyric acid) and glycine-activated); volume-regulated chloride channel (VRAC); and calcium-activated chloride channel (CaCC). Physiological relevance of these chloride channels were appreciated from studies on various inherited diseases and knock-out mouse models (for detailed review Jentsch et al., 2002; Planells-Cases and Jentsch, 2009; Verkman and Galietta, 2009; Duran et al., 2010).

1.2 Calcium activated chloride channels (CaCCs)

CaCCs are activated by an increase in cytosolic calcium. CaCCs were first observed in *Xenopus* oocytes in early 1980`s, where an increase in cytosolic calcium upon egg's fertilization results in rapid chloride efflux through CaCCs, which depolarizes the membrane and prevents polyspermy (Miledi, 1982). Later the discovery of CaCCs in rod inner segments from salamander retina indicated a possible role in sensory processing (Bader et al., 1982). CaCCs were subsequently observed in several other cell types like neurons, various epithelial cells, olfactory and photo-receptors, muscle cells in cardiac, smooth and skeletal tissue. In line with their widespread expression, CaCCs show physiological relevance in epithelial secretion, membrane excitability in cardiac muscle and neurons, olfactory transduction, regulation of vascular tone, modulation of photoreceptors and several other processes (for detail review Hartzell et al., 2005; Eggermont, 2004; Duran and Hartzell, 2011; Ferrera et al., 2011b; Huang et al., 2012a; Kunzelmann et al., 2012).

1.2.1 Biophysical properties of CaCCs

CaCCs show significant variations among different cell types. At the same time share some common biophysical properties: (Huang et al., 2012a)

- They are activated by an increase in cytosolic calcium with half maximal concentration for activation in the submicromolar range, although the exact value varies among cell types.
- At low cytosolic calcium the I-V relation is outward rectifying, while at higher cytosolic calcium it becomes linear.
- The channel allows permeation of larger anions and displays a selectivity sequence of $NO_3^- > I^- > Br^- > Cl^- > F^-$.
- They are inhibited by some of the traditional chloride channel blockers such as DIDS, NPPB, tamoxifen, NFA and A9C (Table 1. in Frings et al., 2000)

Figure 1.1 illustrates the native CaCCs recorded from *Xenopus* oocytes and mammalian cells.

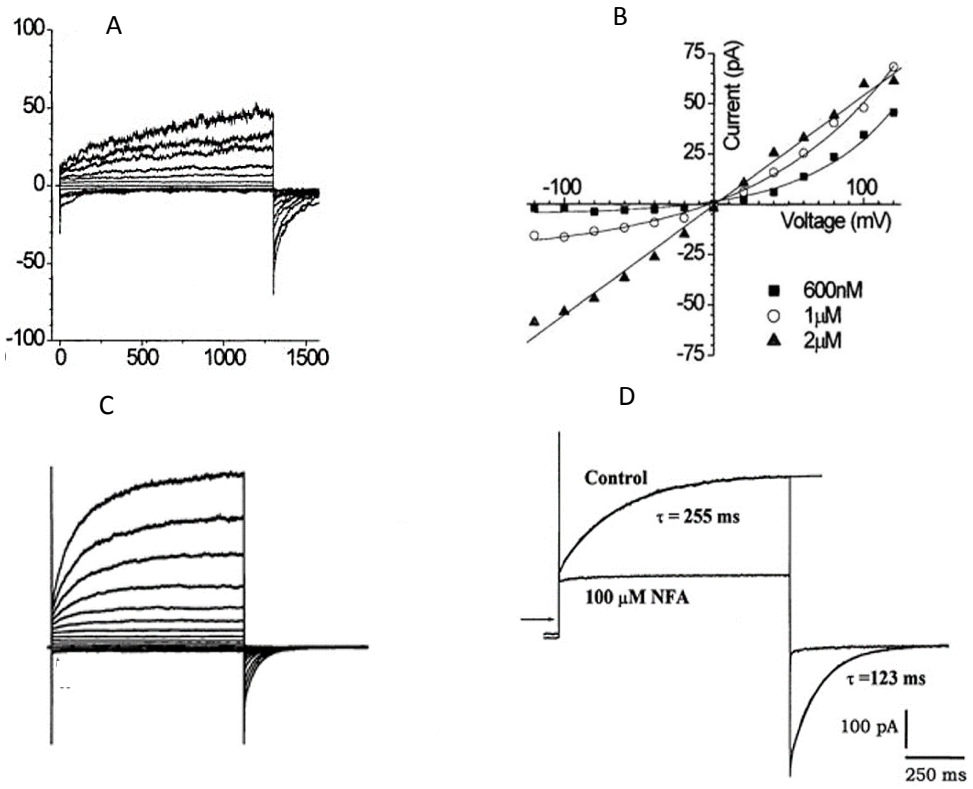

Figure 1.1. **Examples of native CaCCs recorded in *Xenopus* oocytes and mammalian cells.** (*A*) Calcium-activated chloride current in excised patch from *Xenopus* oocytes exposed to 600 nM free calcium on the cytosolic face. The patch was clamped from a holding potential of 0 mV to potentials between 120 and -120 mV for 1.3 s, followed by a 0.3 s pulse step to -100 mV. (*B*) Steady state I-V relations at different cytosolic calcium for the cell shown in *A*. (*Kuruma and Hartzell, 2000*). (*C*) Calcium-activated chloride current evoked in pulmonary artery myocytes in whole cell with 500 nM free cytosolic calcium from a holding potential of -50 mV to potentials between -90 to +130 mV for 1.5 s. and followed by a 1 s step to -80 mV (*D*) Representative current trace recorded from a pulmonary artery myocytes in the absence (Control) or in the presence of 100 μM NFA. At holding potential of -50 mV, a voltage step to +70 mV followed by a step to -80 mV was used. The time dependent activation and deactivation of the current at +70 and -80 mV respectively, were well fitted by a single exponential (continuous line) with respective time constants of 255 and 123 ms *(Greenwood et al., 2001*).

1.2.2 Molecular identity of CaCCs

Despite the wide expression of CaCCs in different tissues and extensive biophysical and physiological studies, the search for a molecular counterpart of CaCCs was challenging for the following reasons (Nilius and Droogmans, 2003; Hartzell et al., 2005):

- The absence of a selective blocker made it difficult to isolate the current electrophysiologically (De La Fuente et al., 2008);
- Heterologous expression of CaCCs in several cell types resulted in up-regulation of endogenous channels producing a false positive result (Hartzell et al., 2009);
- The most common expression system used for ion channel studies, *Xenopus* oocytes, proved unsuitable due to high endogenous expression of CaCCs (Miledi, 1982; Barish, 1983);

Nevertheless, efforts to identify the channel went on with the proposal of several candidates such as CLCA (Cunningham et al., 1995), CLC-3 (Huang et al., 2001), bestrophin (Qu et al., 2003b) and Tweety (Suzuki and Mizuno, 2004). However, researchers failed to clone some of these candidates from tissues expressing endogenous CaCCs (Papassotiriou et al., 2001; Hartzell et al., 2009). Additionally, heterologous expression studies showed that some biophysical properties of these candidates, such as the calcium sensitivity and unitary conductance strongly differ from native CaCCs (Eggermont, 2004; Hartzell et al., 2005). Functional diversity also existed, indeed CLC-3 has been shown to be an electrogenic H^+/Cl^- antiporter (Matsuda et al., 2010) and CLCA to modulate the activity of chloride channels rather than forming the ion channel themselves (Loewen and Forsyth, 2005). Bestrophin was considered to be a promising candidate. However, there were some doubts raised about its calcium sensitivity and lack of voltage and time dependence with hBest-1 and mBest2 (Tsunenari et al., 2003; Qu et al., 2003b; Tsunenari et al., 2006; Hartzell et al., 2008). Indeed the endogenous CaCCs in olfactory sensory neurons and submandibular salivary glands remained unaffected even after knockout of Best2

(Pifferi et al., 2009b; Romanenko et al., 2010). In summary, all the proposed candidates failed to qualify as CaCCs.

1.3 TMEM16/anoctamin titled as CaCCs

Later in 2008, the molecular identity of CaCCs finally came to light when three different research groups independently proposed TMEM16A as CaCCs (Yang et al., 2008; Caputo et al., 2008; Schroeder et al., 2008).

Yang et al., (2008) performed bioinformatic screening for novel proteins with more than two transmembrane domains and pinned TMEM16A. Heterologous expression of TMEM16A, resulted in the appearance of calcium-activated chloride current sensitive to traditional chloride channel blockers. Caputo et al., (2008) followed functional genomic approach for identifying TMEM16A. Previously in 2002, they reported that CaCCs are up-regulated in interleukin-4-treated human bronchial epithelial cells, later in 2008 through global gene expression analysis it was found to be TMEM16A. Schroeder et al., (2008) realized that a different amphibian, the Axolotl salamander is physiologically polyspermic and their oocytes are devoid of CaCCs activity. This made the traditional expression cloning approach for CaCCs possible using Axolotl oocytes, with cDNA extracted from *Xenopus* oocytes. The fact that three different research teams arrived at the same conclusion following different approaches strengthened the proposal of TMEM16A as CaCCs in different cell types.

1.3.1 TMEM16/anoctamin family

The TMEM16 (also called anoctamin) family comprises ten members. They have alphabetical nomenclature from A to K excluding I for TMEM16, whereas they are numbered from 1-10 when named anoctamin (abbreviated as ANO). Hydropathy analysis of TMEM16 predicted eight transmembrane domains with cytoplasmic N and C terminus and a reentrant loop between the 5^{th} and 6^{th} transmembrane domain. The predicted transmembrane topology was later confirmed on TMEM16G with

epitope and N-glycosylation site accessibility approach (Das et al., 2008). However, recently the proposed topology was challenged and remodeled based on epitope and site accessibility approach on TMEM16A (Yu et al., 2012) (Figure 1.3). On the other hand, for the remaining members of TMEM16 family, the topology still remains unclear. Phylogenetic analysis of different TMEM16 family members explains the relatedness among them as shown in figure 1.2. TMEM16A and TMEM16B with 62% amino acid similarity is grouped under the same subfamily whereas TMEM16C/D/J and TMEM16E/F form two separate subgroups followed by TMEM16G/H/K which is the most distant paralogs of TMEM16A (Milenkovic et al., 2010; Flores et al., 2009). Previous studies done on TMEM16A and TMEM16B established that they are CaCCs (Yang et al., 2008; Caputo et al., 2008; Schroeder et al., 2008; Stephan et al., 2009; Pifferi et al., 2009a) whereas the ion channel function and the anion selectivity of the remaining members of the TMEM16 family is still under debate (for example TMEM16F reviewed by Kunzelmann et al., 2014).

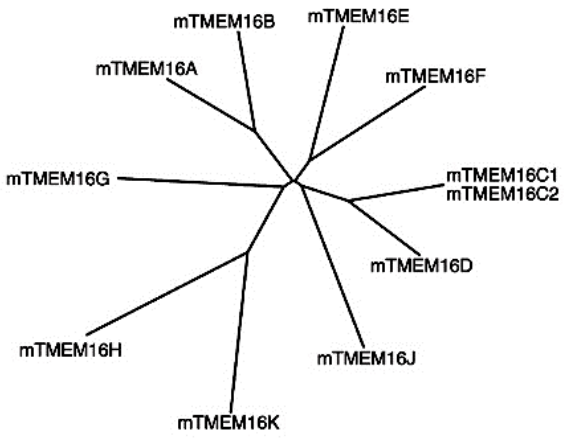

Figure 1.2. **Phylogenetic tree of the mouse TMEM16 family members** (Flores et al., 2009)

1.3.2 Oligomeric structure

Recent studies have indicated TMEM16A probably exist as a homodimer (Sheridan et al., 2011; Fallah et al., 2011). The expression of TMEM16A with two

different fluorescent proteins, mCherry and eGFP demonstrated a significant level of fluorescence resonance energy transfer (FRET), explaining a close physical interaction between them (Sheridan et al., 2011). Biochemical assay with blue native polyacrylamide gel electrophoresis (BN-PAGE) indicated the presence of high-molecular weight complexes of TMEM16A protein, consistent with homodimer formation (Fallah et al., 2011). The property of homodimer formation was also observed for two more members, TMEM16B and TMEM16F (Tien et al., 2013). Additionally, the authors also found the existence of heteromers when TMEM16A and TMEM16B were co-expressed in a heterologous expression system (Tien et al., 2013). However, to date there is no data showing the actual existence of such hybrid channels in native cells.

1.3.3. TMEM16 isoforms

Another reason for the functional differences observed in TMEM16 family may come from alternative splicing of mRNA. At least TMEM16A, TMEM16B and TMEM16F have been reported to exist in different isoforms generated through alternative splicing (Caputo et al., 2008; Ferrera et al., 2009; Stephan et al., 2009; O'Driscoll et al., 2011; Segawa et al., 2011; Ponissery Saidu et al., 2013). TMEM16A can be translated into at least four isoforms depending on either inclusion or exclusion of alternative exons 6b (segment *b*), 13 (segment *c*), 15 (segment *d*) or use of an alternative promoter for the initial 117 amino acids (segment *a*) (segments are marked in figure 1.3). A minimal isoform lacking any of these segment named as TMEM16A(*0*) is also a functional channel with different voltage dependence. It is expressed only in testis and very weakly in kidney (Ferrera et al., 2011a; Sondo et al., 2014). Each segment has its own functional relevance, such as inclusion of segment *b* reduces the sensitivity for cytoplasmic calcium (Ferrera et al., 2009; Galietta, 2009; Ferrera et al., 2011a), whereas deletion of segment *c* can reduce the activation of the channel at positive membrane potentials (Ferrera et al., 2009) along with altered calcium sensitivity (Xiao et al., 2011). TMEM16B isoforms exist with either inclusion or exclusion of exon 14 which resembles segment *c* of TMEM16A. The

presence of exon 14 (ERSQ), found in retina and pineal gland, prevents inactivation at high calcium concentrations differently from the isoform found in olfactory sensory neurons where exon 14 is absent (Ponissery Saidu et al., 2013). Other TMEM16B isoforms include the splicing of exon 4, a 33 amino acid segment coupled with either a longer or shorter NH_2 terminus expressed depending on different start sites (Ponissery Saidu et al., 2013). TMEM16F also have an isoform with inclusion of the first 21 amino acids at NH_2 terminus that increase the calcium dependent scramblase activity of the channel (Segawa et al., 2011). These findings suggest that alternative splicing is a mechanism to regulate the channel properties and basis for generation of CaCCs in different cell types with different voltage and calcium sensitivity.

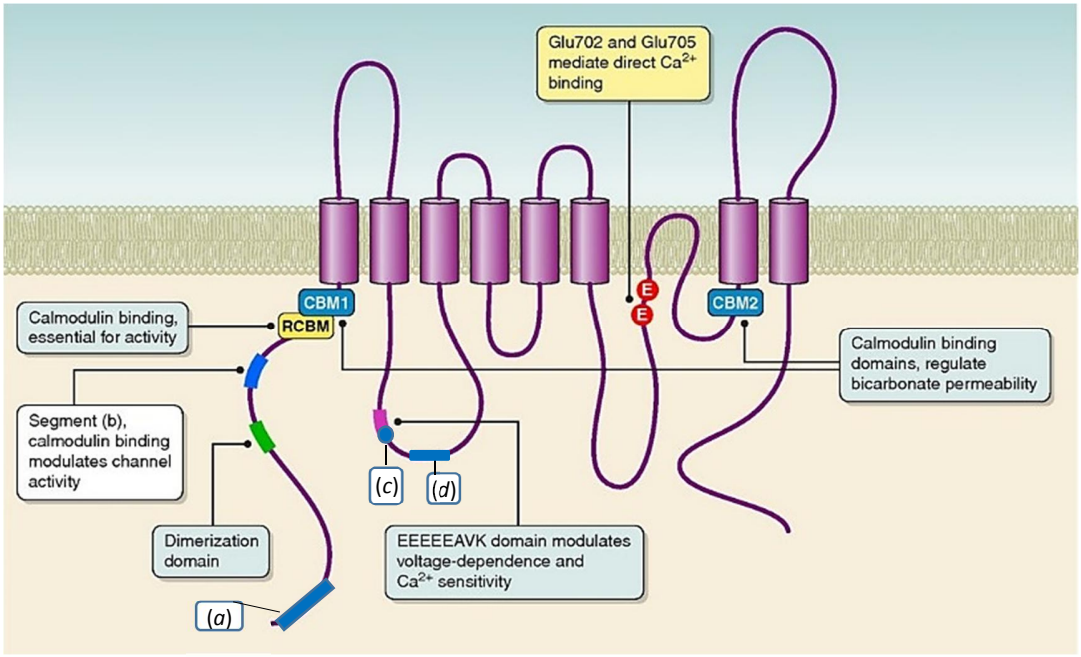

Figure 1.3. **A proposed topology and functional domains of TMEM16A.** A possible topology of TMEM16A slightly modified from Pedemonte and Galietta, (2014) with the sites involved in the regulation of ion channel function. Alternative segments are marked as (*a,b,c,d*). Segment (*b*) is also identified as a calmodulin binding site. Other calmodulin binding sites include RCBM, CBM1 and CBM2. The region EEEEEAVK in the first intracellular loop overlap segment (*c*) which is EAVK. A direct calcium interacting site Glu702 and Glu705 is marked in red (E).

1.3.4 Gating mechanism in TMEM16A and TMEM16B

1.3.4.1 Activation by calcium and voltage

CaCCs are highly sensitive to changes in cytosolic calcium, activating at submicromolar concentrations. This activation is also influenced by the membrane potential. Indeed, the membrane potential can alter the apparent calcium sensitivity of the channel (Arreola et al., 1996; Nilius et al., 1997; Kuruma and Hartzell, 2000; Hartzell et al., 2005). Such a complex interplay between calcium and voltage was also observed for TMEM16A and TMEM16B (Yang et al., 2008; Ferrera et al., 2009; Stephan et al., 2009; Pifferi et al., 2009a; Xiao et al., 2011). The half effective concentration of TMEM16A increased from 0.4 - 0.6 µM at +100 mV to 5.9 - 8.4 µM at -100 mV (Xiao et al., 2011). TMEM16B was comparatively less sensitive to calcium with a half effective concentration in range of 2 µM to 3.5 µM at +50 mV (Pifferi et al., 2009a; Stephan et al., 2009). This difference in calcium sensitivity among TMEM16A and TMEM16B was also reflected on their activation and deactivation kinetics which was at least ten fold faster in TMEM16B (Yang et al., 2008; Caputo et al., 2008; Pifferi et al., 2009a; Stephan et al., 2009). The molecular mechanism behind such a coupling of calcium and voltage in activation of TMEM16A and TMEM16B are still unknown.

1.3.4.2 Direct or indirect activation by calcium

Primary protein sequence analysis of TMEM16A or TMEM16B did not show the presence of a high affinity calcium binding site like EF hands or C2 domain. However, a cluster of highly conserved negatively charged residues (EEEE**E**) is present in the first intracellular loop (Figure 1.3). This negatively charged cluster may resemble the calcium binding pocket as reported for the 'Ca^{2+} bowl' in calcium-activated potassium channel (Bao et al., 2004). Interestingly, the fifth glutamic acid of this cluster is actually a part of segment *c* (exon 13) which codes for four amino acids **E**AVK in TMEM16A. Deletion of segment *c* decreased the apparent calcium sensitivity fifty fold and also shifted the voltage dependence to much positive value

in TMEM16A (Ferrera et al., 2009; Xiao et al., 2011; Xiao and Cui, 2014). The deletion of EEEE abolished the intrinsic voltage dependence with very little effect on apparent calcium sensitivity of the channel (Xiao et al., 2011; Xiao and Cui, 2014). Additionally, Xiao and Cui (2014) recently identified a few more charged residues D452, E464, E470, and E475 in the first intracellular loop having a role in calcium dependent gating of TMEM16A (Xiao and Cui, 2014). Interestingly, neither of these mutants abolished the calcium-dependent gating completely, indicating involvement of more sites for calcium binding or existence of an indirect activation by calcium.

In another study, Yu et al., (2012) identified two acidic residues E702 and E705 in an intracellular loop between 6th and 7th transmembrane of TMEM16A (*ac*) to be important for direct calcium binding (Figure 1.3). Mutation to these residues shifts the calcium sensitivity of the channel from micromolar to millimolar range, further experiments with cysteine-modifying reagents also confirmed their role as direct calcium binding site (Yu et al., 2012).

Earlier this year, Tien et al (2014) confirmed the involvement of E698 and E701 in TMEM16A(*a*) (same as E702 and E705 from the previous study on TMEM16A(*ac*) by Yu et al., 2012) as a calcium binding site. Three additional acidic residues E650 , E730, and D734 were also identified with a possible role in calcium binding (Tien et al., 2014). The authors used an extensive screening by charge neutralization, charge reversal, charge conserving mutagenesis and use of different divalent cations to indicate the direct involvement of E698, E701, E730 and D734 in calcium binding (Tien et al., 2014). The authors remodeled the previous two topologies (Yang et al., 2008; Yu et al., 2012) proposed for TMEM16A with the inclusion of four acidic residues involved in direct calcium binding as shown in figure 1.4.

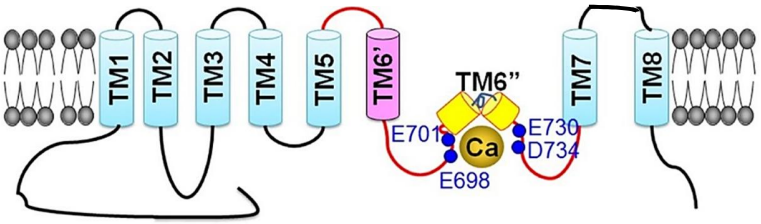

Figure 1.4. **Schematic representation of calcium binding.** Schematic representation for possible calcium binding sites in TMEM16A based on experimental data from Yu et al., (2012) and Tien et al., (2014)

Indirect interactions of intracellular calcium with auxiliary proteins for activation of TMEM16A were also hypothesized. Calmodulin has being postulated as a major factor for indirect activation in native CaCCs (Kaneko et al., 2006). Several calmodulin binding sites including segment *b*, CBM1, CBM2 and RCBM are identified through bioinformatics analysis and also experimentally confirmed to be involved in indirect activation of TMEM16A (Tian et al., 2011; Jung et al., 2013; Vocke et al., 2013) (Figure 1.3). However, these observations were strongly contradicted when purified TMEM16A was activated directly by calcium in proteoliposomes (Terashima et al., 2013). Other studies using mutations in the predicted calmodulin binding domains or use of calcium insensitive calmodulin mutants did not find any alteration in the calcium dependent activation of TMEM16A further confirming the dispensable role of calmodulin in channel activation (Yu et al., 2014; Tien et al., 2014).

In summary, how the channel gating is regulated by calcium and voltage is still an open question. Most of our knowledge about the channel activation comes from the biophysical studies done on TMEM16A, and partially from TMEM16B, while the rest of the family members have not been completely characterized yet and they might not work at all as ion channels.

1.3.4.3 Anion selectivity

It has been observed that native CaCCs, as well as TMEM16A and TMEM16B expressed in heterologous system favor the passage of larger anions such as SCN^-, NO_3^-, I^-, Br^- besides Cl^- (Yang et al., 2008; Schroeder et al., 2008; Pifferi et al., 2009a; Stephan et al., 2009; Sagheddu et al., 2010; Adomaviciene et al., 2013). The permeability ratio among different anions varied for different cell types. However, it followed a permeability sequence inversely proportional to anion's dehydration energy (Wright and Diamond, 1977; Zhang and Cremer, 2006). More permeant anions such as SCN^- strongly affect the channel kinetics with a slow time constant for deactivation and favoring a channel open state by increasing the mean open time (Evans and Marty, 1986; Greenwood and Large, 1999; Perez-Cornejo et al., 2004). Moreover, the effect of a permeant anion on channel activation is far more complex, with the apparent calcium affinity and voltage dependence of the channel found to be dependent on the permeant anion in endogenous CaCCs as well as in TMEM16A (Evans and Marty, 1986; Qu and Hartzell, 2000; Perez-Cornejo et al., 2004; Xiao et al., 2011).

1.4 Pharmacology of CaCCs

The "pharmacology" of a protein comprises the description of its interactions with small organic or inorganic molecules, whose binding can alter protein function. Such a selective and potent molecule is always a valuable research tool to study ion channel function and their tissue distribution. Much of our early knowledge of the functional architecture of ion channels came from pharmacological experiments (Hille, 2001). Unfortunately, pharmacological studies on CaCCs remain limited due to lack of specific potent agents, and knowledge about a structurally defined pore region. Thus, the possibility to develop specific and high affinity inhibitors is potentially very useful to elucidate the physiological function of CaCCs in different tissue types.

1.4.1 Traditional blockers

In early times, endogenous CaCCs in different tissues were inhibited with compounds such as niflumic acid (NFA) (Hogg et al., 1994b; Greenwood and Large, 1995), 4,4'-diisothiocyanato-stilbene-2,2'-disulfonic acid (DIDS) (Hogg et al., 1994a), and anthracene-9-carboxylic acid (A9C) (Hogg et al., 1994a) (Figure 1.5). However, the effect of most of these traditional blockers is nonspecific and target chloride channels in general, and they are less efficacious with potency in the micromolar to millimolar range.

NFA is considered to be the most potent among available traditional blockers tried and tested on CaCCs. However, the action of NFA is quite complex and varies according to cell type. In pulmonary artery myocytes 100 μM of extracellular NFA has multiple effects: at positive membrane voltages it inhibit the outward current, while at negative membrane potentials it increases the inward current and lastly on washing out extracellular NFA, it increases both the inward and outward current (Piper et al., 2002; Ledoux et al., 2005). In contrast, NFA inhibits endogenous CaCCs in *Xenopus* oocytes from both the sides of the membrane with less voltage dependence but, without any increase in inward current (White and Aylwin, 1990; Qu and Hartzell, 2001).

NFA has also been reported to block TMEM16A and TMEM16B expressed in heterologous system (Yang et al., 2008; Caputo et al., 2008; Schroeder et al., 2008; Pifferi et al., 2009a; Sagheddu et al., 2010; Romanenko et al., 2010; Kunzelmann et al., 2012). As shown in figure 1.6 A, extracellular 30 μM NFA reduced the amplitude of outward TMEM16A current along with a slow deactivation of tail current. Although NFA reduced TMEM16A current at all the voltages, its inhibition was slightly voltage dependent at positive voltages. Moreover, likewise in pulmonary smooth muscle cells, at lower concentrations (< 30 μM) NFA potentiated the inward current of TMEM16A in heterologous expression systems (Bradley et al., 2014; Liu et al., 2014).

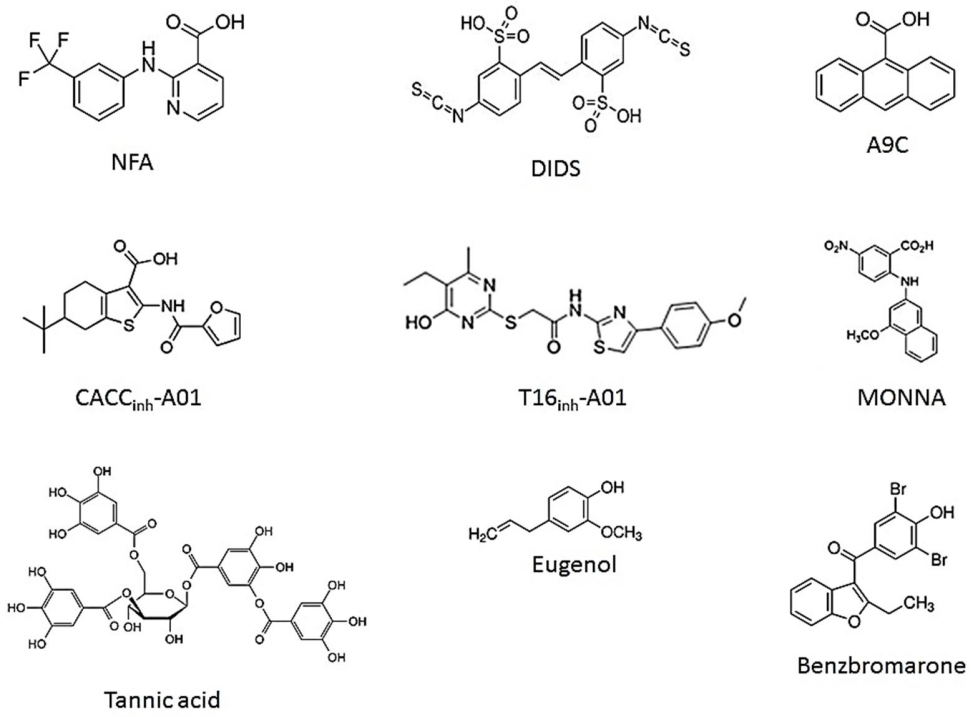

Figure 1.5. **Pharmacological modulators of CaCCs.** Structure of traditional CaCCs blockers (NFA, DIDS, and A9C) and of new TMEM16A inhibitors (CACC$_{inh}$-A01, T16$_{inh}$-A01, MONNA, Benzbromarone, Tannic acid, and Eugenol).

The property of voltage dependent interaction of NFA with CaCCs was also extended to other structurally dissimilar compound like A9C. A9C is an aromatic carboxylate, used in study of several chloride channels. It is less efficient compared to NFA but has much steeper voltage dependence as reported for endogenous CaCCs (Hogg et al., 1993, 1994a; Akbarali and Giles, 1993; Cotton et al., 1997; Wayman et al., 1997; Toland et al., 2000; Qu et al., 2003a; Qu and Hartzell, 2001) and heterologously expressed TMEM16A. (Figure 1.6 B) (Bradley et al., 2014). Like NFA, A9C also has complex mode of action. Piper and Greenwood (2003), carefully studied the effect of A9C on endogenous CaCCs from pulmonary artery smooth muscle cells. Application of extracellular A9C strongly inhibited the outward current in a concentration and voltage dependent manner. Whereas, the inward current at negative potential increased 3.7 times with A9C compared to control (Piper and Greenwood, 2003). The

authors further confirmed by changing external anions that the observed increase in inward current was in fact chloride dependent and not due to background channel activation (Piper and Greenwood, 2003).

The effect of A9C on TMEM16A current in heterologous expression system was studied only recently, and had similar concentration and voltage dependent inhibition of outward current as shown in figure 1.6 B (Bradley et al., 2014). Furthermore, A9C potentiated the inward tail current as for endogenous CaCCs. It also made the deactivation kinetics of the channel much slower compared to control (Bradley et al., 2014). Although a nonspecific blocker, having a strong voltage dependent interaction and multiple effect on channel activation makes A9C an interesting compound for future structure-function studies of TMEM16 family members.

1.4.2 Specific blockers

$CACC_{inh}$-A01:

The absence of a potent and selective blocker has limited the studies of CaCCs. De La Fuente et al., (2008) screened 50,000 small molecules using high throughput screening methods in search for a candidate with inhibitory action against endogenous CaCCs in epithelial cell line HT-29. The authors screened out two classes of drugs (Class A and Class B) based on their potency, water solubility, chemical stability and CaCCs targeting (De La Fuente et al., 2008). Among these, a compound labelled $CACC_{inh}$-A01 (Figure 1.5) was further used because of its potency and specificity towards endogenous CaCCs in several cell types (Bevers and Williamson, 2010; Ousingsawat et al., 2011) and TMEM16A in heterologous expression system (Bradley et al., 2014; Liu et al., 2014). It inhibited 90% of the current across the voltage range and enhanced the rate of tail current deactivation with much faster kinetics compared to control as shown in figure 1.6 C (Bradley et al., 2014).

$T16A_{inh}$-A01:

After identification of TMEM16A as a CaCCs, high throughput screening of ~110,000 small molecules library revealed four novel chemical classes of TMEM16A blockers that fully inhibited TMEM16A chloride current with an IC_{50} < 10 µM and without interfering with calcium dependent activation of the channel. Further structure-activity analysis screened $T16A_{inh}$-A01 (Figure 1.5) to be the most potent with an IC_{50} of ~1 µM (Namkung et al., 2011). $T16A_{inh}$-A01 inhibited more than 60% TMEM16A current and increased the rate of channel closure as shown in figure 1.6 D (Bradley et al., 2014). $T16A_{inh}$-A01 show specificity towards CaCCs as it failed to have inhibitory action on CFTR but it still remains to be confirmed for other chloride channels (Namkung et al., 2011). Recently, Davis et al., (2013) used $T16A_{inh}$-A01 to confirm that TMEM16A constitutes a major component of endogenous CaCCs in isolated vascular smooth muscle cells. Moreover, the authors found $T16A_{inh}$-A01 to be a potent vasorelaxant for the smooth muscle cells in comparison to the traditional chloride channel blocker, NFA (Davis et al., 2013).

Several reports have shown that TMEM16A is overexpressed in many tumor types including esophageal cancer (Huang et al., 2002), gastrointestinal stromal tumors (West et al., 2004) and head and neck squamous cell carcinoma (SCCHN) (Akervall et al., 1995). Duvvuri et al (2012) reported that TMEM16A expression directly impacts cellular proliferation in SCCHN by activating RAS-REF-MEK-ERK1/2 pathway. Here the authors found that application of T16Ainh-A01 inhibited tumor cell proliferation *in vitro*. In a similar study, T16Ainh-A01 inhibited the cell proliferation in interstitial cells of Cajal (ICC) by acting on TMEM16A and blocked the tumor formation (Mazzone et al., 2012). These studies present TMEM16A as an interesting pharmacological target for control of tumor proliferation, however its ubiquitous expression and involvement in different physiological processes might cause side-effects.

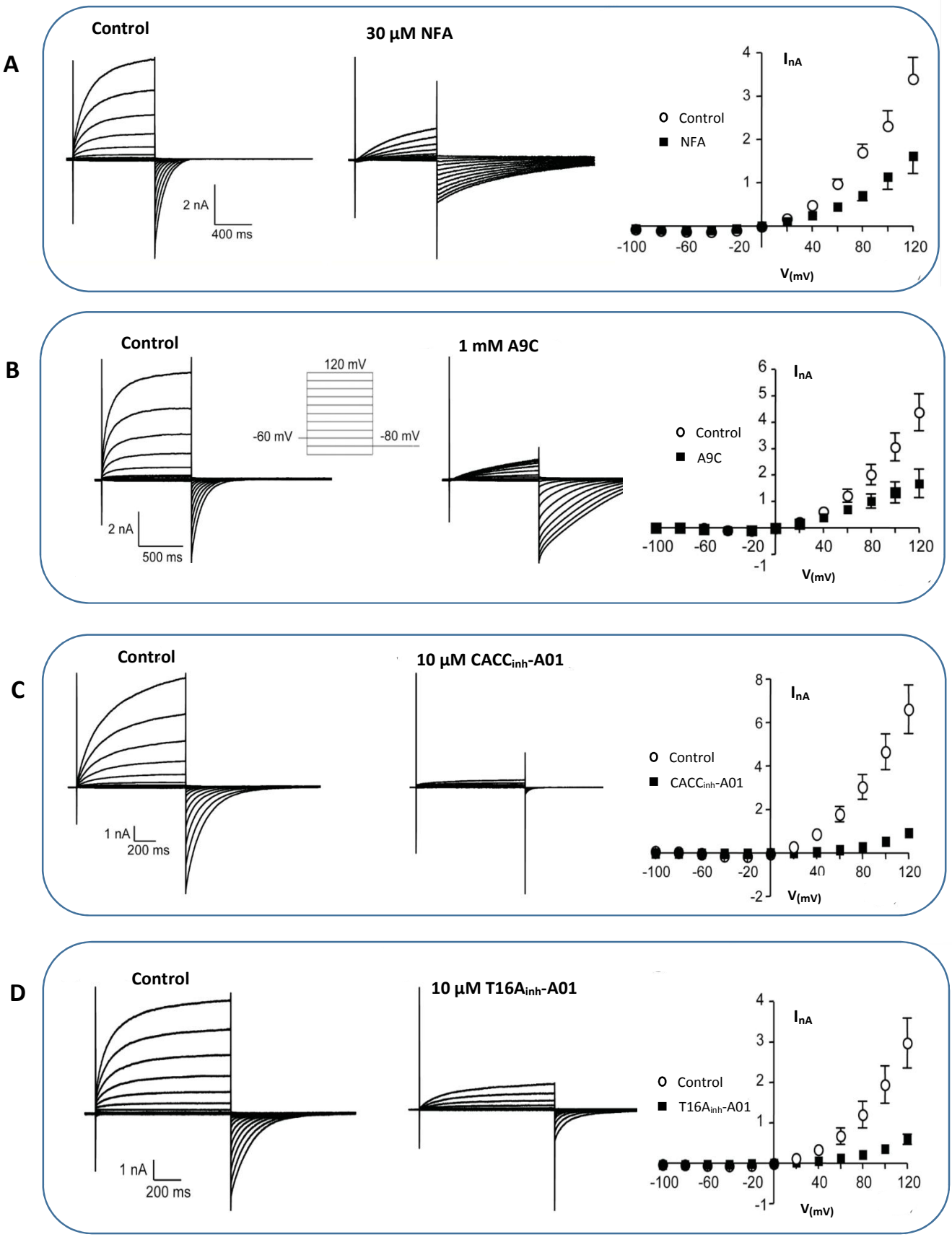
A
Control
30 µM NFA
2 nA
400 ms
I_nA
Control
NFA
V(mV)
B
Control
120 mV
-60 mV
-80 mV
1 mM A9C
2 nA
500 ms
I_nA
Control
A9C
V(mV)
C
Control
10 µM CACC_inh-A01
1 nA
200 ms
I_nA
Control
CACC_inh-A01
V(mV)
D
Control
10 µM T16A_inh-A01
1 nA
200 ms
I_nA
Control
T16A_inh-A01
V(mV)

Figure 1.6. **Effect of chloride channel blockers on TMEM16A current.** Whole cell current recorded from HEK293 cells transfected with hTMEM16A (*ac*) in the presence of 171 nM intracellular calcium. Panel represent current in control, in presence of extracellular blocker and steady state I-V relation from respective control and blocker. *A*) 30 µM NFA, *B*) 1 mM A9C, *C*) 10 µM $CACC_{inh}$-A01, *D*) 10 µM $T16A_{inh}$-A01. (Bradley et al., 2014).

Other:

In another study, small scale screening for TMEM16A blocker identified compounds such as benzbromarone, dichlorophen, and hexachlorophene. These compounds in future could be potential candidates for the treatment of asthma, as they inhibited the airway smooth muscle contraction and mucin release from goblet cells (Huang et al., 2012b). A search for compounds with inhibitory properties is not just limited to available chemical libraries, instead chemical modification of different anthranilic acid derivatives identified N-((4-methoxy)-2-naphthyl)-5-nitroanthranilic acid (MONNA) (Figure 1.5). This compound was most potent among the reported with an IC_{50} of 0.08 µM for xTMEM16A. MONNA appeared selective and did not block CFTR, CLC or bestrophin (Oh et al., 2013). Very recently, compounds with inhibitory action from natural sources were also studied. Compounds such as tannic acid and its derivatives, and eugenol (Figure 1.5) from sources such as green tea, red wine and medicinal herbal preparations were found to have inhibitory effect against TMEM16A (Namkung et al., 2010; Yao et al., 2012). A large panel of blockers for TMEM16A is now available. In contrast, the pharmacology of remaining TMEM16 members is still unknown.

2. Project Aim

Several reports from different laboratories helped to increase our understanding about TMEM16A as a CaCC and its biophysical properties. In comparison only few countable reports exist for the close cousin TMEM16B. In this thesis we conducted a first structure-function analysis of TMEM16B expressed in heterologous system.

Here we addressed the following questions:

- What is the role of some conserved glutamic acid residues in the first intracellular loop in channel activation?
- How extracellular and intracellular anions affect the gating?
- What is the effect of the traditional chloride channel blocker A9C and its non-charged analogue A9M on channel activation?

3. Materials and methods

3.1 Cell culture and transfection

HEK293T cells (American Type Culture Collection, USA) were cultured in DMEM (Gibco, Italy) with 10% fetal bovine serum (Sigma, Italy), 100 UI/ml penicillin and 100 µg/ml streptomycin (Sigma, Italy) at 37 ^{o}C in humidified atmosphere of 5% CO_2, and passaged every second day.

Full-length mouse TMEM16B cDNA in pCMV-Sport6 mammalian expression plasmid was obtained from RZPD (clone identification, IRAVp968H1167D; NCBI Protein database accession no. NP_705817.1). Mutations were made using a PCR-based site directed mutagenesis kit (Gene tailor mutagenesis kit, Invitrogen, OR, USA) and confirmed by DNA sequence.

HEK293T cells were transfected with 2 µg TMEM16B cDNA using transfection reagent FUGENE 6 (Roche diagnostic, USA). For positive identification of transfected cells they were also co-transfected with 0.2 µg enhanced green fluorescent protein, eGFP (Takara Bio Inc, USA). After 24 h of transfection the cells were trypsinised and plated at a lower density to 35-mm Nunc petri dishes (Thermo Scientific, USA) and later used for patch clamp experiments between 48-72 h from transfection.

3.2 Electrophysiological recording

HEK293T cells were visualized under an Olympus IX70 inverted microscope (Olympus, Japan) placed on anti-vibration table (TMC, USA) and shielded from external noise with a homemade Faraday cage. All the instruments kept inside the

Faraday cage was connected to a single ground to avoid current loops. TMEM16B and its mutants currents were recorded in whole-cell or inside-out configuration using a Axopatch 1-D amplifier controlled by Clampex 9.2 via Digidata 1322A (Axon Instruments, USA). The data was acquired at rate of 10 kHz and the signals were low-pass filtered at 5 kHz. Patch electrodes were made of borosilicate glass (WPI, USA) and pulled with a PP-830 micropipette puller (Narishige, Japan). Pulled patch electrodes had resistance of 5-7 MΩ for whole cell and 2-5 MΩ for inside-out configuration when filled with internal solution. The patch electrode was mounted on electrode holder with Ag/AgCl electrode, connected to CV-4 headstage (Axon Instrument, USA). The movement of this headstage is controlled either by MM3 mechanical micromanipulator (Narishige, Japan) for coarse adjustment or through MWO-3 three dimensional oil hydraulic micromanipulator (Narishige, Japan) for fine movement. The bath was grounded with a 1 mM KCl agar bridge connected with Ag/AgCl reference electrode. All the experiments were conducted at room temperature.

The tip of patch electrode is pressed against the cell membrane and suction is applied to form a high resistance gigaseal (>1 GΩ). After gigaseal formation, the membrane patch under the electrode tip is excised by pulling the patch electrode away from the cell to achieve inside-out configuration and to expose the cytoplasmic face of the patch to different bath solutions. Alternatively for whole-cell configuration, after gigaseal formation slow and constant suction is applied to rupture the membrane patch enclosed within the tip of patch electrode. The intracellular solution filled in patch pipette is dialyzed into the cell and currents from ion channels expressed on the plasma membrane of the cell can be measured. The recording chamber was continuously perfused with gravity fed Ringer solution, while an aspiration tube connected to a suction pump placed on the opposite side provided a controlled level of solution in the recording chamber.

3.3 Perfusion setup

Rapid exchange of solutions in close vicinity to patched cells either in whole-cell or excised patch configuration was achieved using a multibarrel glass tube each with an internal diameter of 0.9 mm. The movement of these pipes was motorized by perfusion fast-step SF-77B (Warner Instrument Corp. USA) with user defined voltage commands relayed through Digidata 1332A (Axon instruments, USA). Exchange of solutions was efficiently achieved within less than 20ms for inside-out experiment and approx. 30ms for whole-cell experiments. The perfusion system was entirely gravity fed from the solutions stored in 50 ml syringe connected with polyethylene tubes of 1.14 mm internal diameter to the multibarrel opening. The flow of solution was controlled by solenoid valves operated manually. A schematic representation of the perfusion setup is shown in figure 3.1.

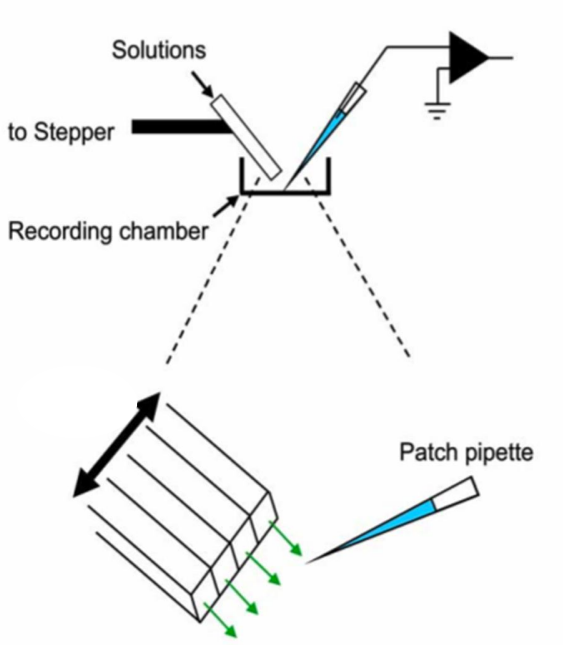

Figure 3.1 Perfusion system used for patch clamp recording. Four parallel streams of solutions emerging from glass pipes, were delivered in front of the patch pipette. Through motorized movement of pipes, it was possible to change rapidly the solutions bathing the cells (or the excised patch) attached to the patch pipette. (Scheme from Dr. Simone Pifferi)

3.4 Solutions

Solutions with different ionic composition were used for experiments, the composition was tailored as per the experimental design and is being clearly reported in respective manuscripts in the result section. The standard extracellular mammalian Ringer contained (mM) 140 NaCl, 5 KCl, 2 $CaCl_2$, 1 $MgCl_2$, 10 glucose and 10 HEPES to buffer pH which was adjusted to 7.2 with NaOH or HCl as appropriate.

Intracellular solutions with different concentrations of free calcium were calculated with program WINMAX C (C. Patton, Stanford university, Palo Alto, CA USA) (Patton et al., 2004). The composition for different intracellular solutions is as reported in the table 3.1. pH was adjusted to 7.2 using CsOH and HCl. Osmolarity for all the solutions were balanced in range of 280-300 mosm with glucose.

Free Ca^{2+} ***(µM)***	**CsCl** ***(mM)***	**$CaCl_2$** ***(mM)***	**HEDTA** ***(mM)***	**HEPES** ***(mM)***
0	140	--	10	10
0.5	140	1.242	10	10
1.5	140	3.209	10	10
3.8	140	5.866	10	10
13	140	8.263	10	10
100	140	9.980	10	10

Table 3.1 Composition of intracellular solution with variable calcium concentrations.

Stock solutions of blockers were prepared in either DMSO for A9C or in chloroform for A9M. Final concentrations were achieved by diluting these stocks in standard mammalian Ringer solution. These compounds had very low solubility so they were sonicated at 37 ^{o}C until a clear solution was obtained. Preparation and application of these blockers were done with minimal light exposure.

3.5 Data analysis

The electrophysiology data saved in *.abf* format in Clampex 9.2 (Axon Instruments, USA) were further analyzed using IGOR Pro software (Wavemetrics, Lake Oswego, OR, USA). IGOR procedures used for analysis were written by Dr. Simone Pifferi. All the figures presented in the three manuscripts in the Results section has been prepared using IGOR. Data are presented as mean ± SEM, with n indicating the number of cells. Statistical significance was determined using paired t-tests or ANOVA as appropriate. When a statistically significant difference was determined with ANOVA, a post hoc Tukey test was done to evaluate which data groups showed significant differences. P values < 0.05 were considered significant.

4. Results

4.1 The voltage dependence of the TMEM16B/anoctamin2 calcium-activated chloride channel is modified by mutations in the first putative intracellular loop.

Published March 12, 2012

The voltage dependence of the TMEM16B/anoctamin2 calcium-activated chloride channel is modified by mutations in the first putative intracellular loop

Valentina Cenedese, Giulia Betto, Fulvio Celsi, O. Lijo Cherian, Simone Pifferi, and Anna Menini

Neurobiology Sector, International School for Advanced Studies, and Italian Institute of Technology, SISSA Unit, 34136 Trieste, Italy

Ca^{2+}-activated Cl^- channels (CaCCs) are involved in several physiological processes. Recently, TMEM16A/anoctamin1 and TMEM16B/anoctamin2 have been shown to function as CaCCs, but very little information is available on the structure–function relations of these channels. TMEM16B is expressed in the cilia of olfactory sensory neurons, in microvilli of vomeronasal sensory neurons, and in the synaptic terminals of retinal photoreceptors. Here, we have performed the first site-directed mutagenesis study on TMEM16B to understand the molecular mechanisms of voltage and Ca^{2+} dependence. We have mutated amino acids in the first putative intracellular loop and measured the properties of the wild-type and mutant TMEM16B channels expressed in HEK 293T cells using the whole cell voltage-clamp technique in the presence of various intracellular Ca^{2+} concentrations. We mutated E367 into glutamine or deleted the five consecutive glutamates $_{386}$EEEEE$_{390}$ and $_{399}$EYE$_{401}$. The EYE deletion did not significantly modify the apparent Ca^{2+} dependence nor the voltage dependence of channel activation. E367Q and deletion of the five glutamates did not greatly affect the apparent Ca^{2+} affinity but modified the voltage dependence, shifting the conductance–voltage relations toward more positive voltages. These findings indicate that glutamates E367 and $_{386}$EEEEE$_{390}$ in the first intracellular putative loop play an important role in the voltage dependence of TMEM16B, thus providing an initial structure–function study for this channel.

INTRODUCTION

Ca^{2+}-activated Cl^- channels (CaCCs) are expressed in many cell types, where they play various physiological roles. For example, CaCCs are involved in fast block of polyspermy in *Xenopus laevis* oocytes, in the regulation of smooth muscle contraction, in fluid secretion from exocrine glands, in the control of excitability in cardiac myocytes, as well as in olfactory, taste, and phototransduction (Frings et al., 2000; Hartzell et al., 2005; Leblanc et al., 2005; Petersen, 2005; Wray et al., 2005; Bers, 2008; Kleene, 2008; Lalonde et al., 2008; Petersen and Tepikin, 2008; Duran et al., 2010; Kunzelmann et al., 2011a).

Despite the fact that CaCCs are broadly present in several tissues, their molecular identity had remained elusive until 2008, when three independent studies reported that the expression of TMEM16A/anoctamin1 was associated with CaCCs (Caputo et al., 2008; Schroeder et al., 2008; Yang et al., 2008). The TMEM16 family comprises 10 members, and another member of the family, TMEM16B/anoctamin2, has also been shown to function as a CaCC when heterologously expressed in axolotl oocytes (Schroeder et al., 2008) or in HEK 293T cells (Pifferi et al., 2009; Stephan et al., 2009; Stöhr et al., 2009; Rasche et al., 2010; Sagheddu et al., 2010).

The study of knockout mice for TMEM16A (Rock and Harfe, 2008) and for TMEM16B (Billig et al., 2011) further confirmed that CaCC activity was reduced or abolished in several cells (Flores et al., 2009; Galietta, 2009; Hartzell et al., 2009; Kunzelmann et al., 2011b, 2012; Huang et al., 2012; Pifferi et al., 2012; Sanders et al., 2012; Scudieri et al., 2012).

Hydropathy analysis indicates that TMEM16 proteins have eight putative transmembrane domains with both N- and C-terminal domains located at the intracellular side of the membrane, and the predicted topology has been experimentally confirmed for TMEM16G/anoctamin7 (Das et al., 2008). At present, TMEM16A and TMEM16B have been shown to function as CaCCs, whereas it is unclear whether the other members of the family are CaCCs (Duran and Hartzell, 2011; Huang et al., 2012; Scudieri et al., 2012). Furthermore, splice variants have been identified both for TMEM16A (Caputo et al., 2008; Ferrera et al., 2009, 2011) and for TMEM16B

Correspondence to Anna Menini: menini@sissa.it

S. Pifferi's present address is Max Delbrück Center for Molecular Medicine, 13125 Berlin, Germany.

Abbreviations used in this paper: CaCC, Ca^{2+}-activated Cl^- channel; WT, wild type.

The Rockefeller University Press $30.00
J. Gen. Physiol. Vol. 139 No. 4 285–294
www.jgp.org/cgi/doi/10.1085/jgp.201110764

Published March 12, 2012

(Stephan et al., 2009). However, although the functional properties of different isoforms have been extensively investigated for TMEM16A, only preliminary data have been presented for TMEM16B (Saidu, S.P., A.B. Stephan, S.M. Caraballo, H. Zhao, and J. Reisert. 2010. Association for Chemoreception Sciences Meeting. Abstr. P68).

At present, very little is known about the structure–function relations for these channels. The analysis of the sequence of TMEM16A and TMEM16B did not reveal any canonical voltage-sensing or Ca^{2+}-binding domains (Yang et al., 2008), but a comparison among the biophysical properties of the TMEM16A splice variants pointed to the functional relevance of the first putative intracellular loop (Caputo et al., 2008; Ferrera et al., 2009, 2011). Moreover, a recent study performed site-directed mutagenesis experiments on TMEM16A modifying some amino acids in the first putative intracellular loop and found that deletion of EAVK affected both the Ca^{2+} and voltage dependence of TMEM16A (Xiao et al., 2011).

Here, we aimed to perform a first site-directed mutagenesis investigation of TMEM16B to contribute to the understanding of the molecular mechanisms underlying the channel voltage and Ca^{2+} dependence. We identified some acidic amino acids in the first intracellular loop of TMEM16B ($_{367}$E, $_{386}$EEEEE$_{390}$, $_{399}$EYE$_{401}$), which are conserved in TMEM16A, where some of them have been studied (Xiao et al., 2011). We mutated or deleted the indicated glutamates and made a comparison between the electrophysiological properties measured in the whole cell configuration of the wild-type (WT) TMEM16B and its mutants. We have found that $_{367}$E and $_{386}$EEEEE$_{390}$ contribute to the voltage-dependent regulation of the TMEM16B channel.

MATERIALS AND METHODS

Site-directed mutagenesis of TMEM16B and heterologous expression

Full-length mouse TMEM16B cDNA in pCMV-Sport6 mammalian expression plasmid was obtained from RZPD (clone identification, IRAVp968H1167D; NCBI Protein database accession no. NP_705817.1). Mutations were made using a PCR-based site-directed mutagenesis kit (Gene Tailor; Invitrogen) and confirmed by DNA sequencing. HEK 293T cells (American Type Culture Collection) were transfected with 2 µg TMEM16B by using transfection reagent (FuGENE 6; Roche). Cells were co-transfected with 0.2 µg enhanced green fluorescent protein (eGFP; Takara Bio Inc.) for fluorescent identification of transfected cells. After 24 h, transfected cells were replated at a lower density and used for patch-clamp experiments between 48 and 72 h from transfection.

Electrophysiological recordings and ionic solutions

Current recordings from HEK 293T cells expressing TMEM16B or its mutants were performed in the whole cell voltage-clamp configuration, as described previously (Pifferi et al., 2006, 2009). Patch pipettes were made of borosilicate glass (World Precision Instruments, Inc.) and pulled with a PP-830 puller (Narishige). Patch pipettes filled with the intracellular solution had a resistance of ~3–5 MΩ when immersed in the bath solution. Currents were recorded with an Axopatch 1D or Axopatch 200B amplifier controlled by Clampex 9 or 10 via a Digidata 1332A or 1440 (Molecular Devices). Data were low-pass filtered at 5 kHz and sampled at 10 kHz. Experiments were performed at room temperature (20–25°C). As reported previously (Pifferi et al., 2006), control experiments in nontransfected and only eGFP-transfected cells did not show any significant Ca^{2+}-activated current.

The standard extracellular solution contained (in mM): 140 NaCl, 5 KCl, 2 $CaCl_2$, 1 $MgCl_2$, 10 glucose, and 10 HEPES, adjusted to pH 7.4 with NaOH. The intracellular solution filling the patch pipette contained (in mM): 140 CsCl, 10 HEPES, and 10 HEDTA, adjusted to pH 7.2 with CsOH, and no added Ca^{2+} for the nominally 0 Ca^{2+} solution, or various added Ca^{2+} concentrations, as calculated with the program WinMAXC (Patton et al., 2004), to obtain free Ca^{2+} in the range between 0.5 and 100 µM. The free Ca^{2+} concentrations were experimentally determined by Fura-4F (Invitrogen) measurements by using a luminescence spectrophotometer (LS-50B; PerkinElmer), as described previously (Pifferi et al., 2006). The total Cl^- concentration was 158 mM in the extracellular solution, whereas in the pipette solution it ranged from 140 mM in 0 Ca^{2+} to 160 mM in 100 µM Ca^{2+}, with a calculated

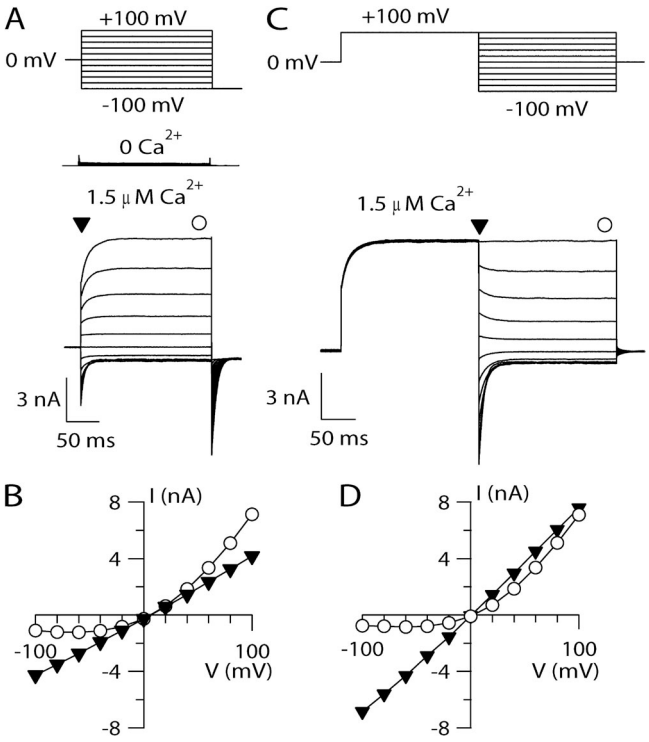

Figure 1. I-V relations of TMEM16B. (A) Representative whole cell voltage-clamp recordings obtained with an intracellular solution containing nominally 0 Ca^{2+} or 1.5 µM Ca^{2+}, as indicated. Voltage steps of 200-ms duration were given from a holding voltage of 0 mV to voltages between −100 and +100 mV in 20-mV steps, followed by a step to −100 mV, as indicated in the top part of the panel. (B) Steady-state I-V relation measured at the end of the voltage steps (circles) or instantaneous I-V measured at the beginning of each voltage step (inverted triangles) from the cell shown in B. (C) Representative recordings at 1.5 µM Ca^{2+} obtained with a voltage protocol consisting of a prepulse to +100 mV from a holding voltage of 0 mV, followed by voltage steps between −100 and +100 mV in 20-mV steps, as shown in the top part of the panel. (D) I-V relations measured from tail currents (inverted triangles) or at the steady state (circles).

Published March 12, 2012

equilibrium potential for Cl^- of −1.5 and +1.9 mV, respectively. All chemicals, unless otherwise stated, were purchased from Sigma-Aldrich.

In most experiments, we applied voltage steps of 200-ms duration from a holding potential of 0 mV ranging from −100 to +100 mV (or from −200 to +200 mV), followed by a step to −100 mV. A single-exponential function was fitted to tail currents to extrapolate the current value at the beginning of the step to −100 mV. In another set of experiments, channels were activated by a 200-ms pulse to +100 mV, and then rapidly closed by the application of hyperpolarizing steps. Single-exponential functions were fitted to tail currents at each voltage step.

Membrane capacitance and series resistance were compensated with the amplifier during the experiments. Membrane current density was calculated by dividing the current by the cell capacitance. The conductance, *G*, was calculated as $G = I/(V - V_{rev})$, where *I* is the tail current, V is the membrane voltage, and V_{rev} is the current reversal potential. Because in our experimental conditions the calculated equilibrium potential for Cl^- ranged between −1.5 and +1.9 mV and the measured V_{rev} was close to 0 mV, V_{rev} was set to 0 mV in all calculations.

Data analysis

Data are presented as mean ± SEM, with *n* indicating the number of cells. Statistical significance was determined using paired or unpaired *t* tests or ANOVA, as appropriate. When a statistically significant difference was determined with ANOVA, a post-hoc Tukey test was done to evaluate which data groups showed significant differences. P-values of <0.05 were considered significant. Data analysis and figures were made with Igor Pro software (WaveMetrics).

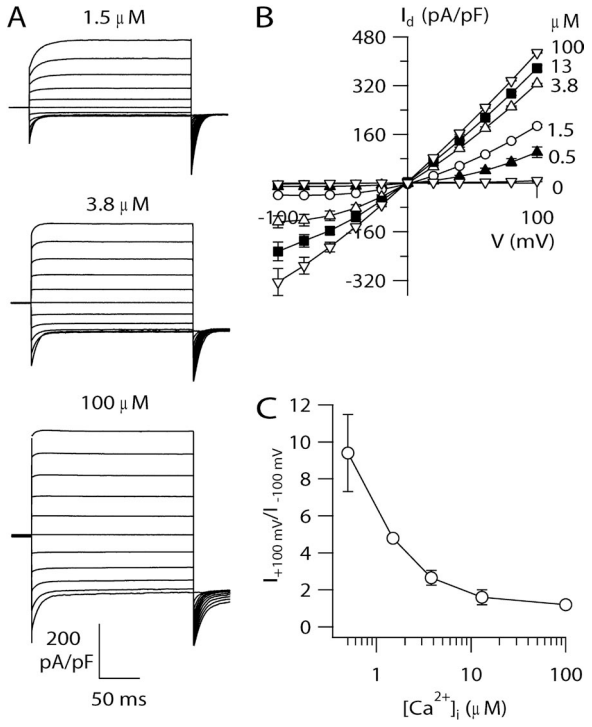

Figure 2. Ca^{2+}-dependent rectification of TMEM16B. (A) Whole cell currents activated by the indicated $[Ca^{2+}]_i$. Voltage protocol as in Fig. 1 A. (B) Average steady-state I-V relations from several cells (n = 3–6). (C) Average ratios between steady-state currents measured at +100 and −100 mV at various $[Ca^{2+}]_i$ (n = 3–6).

RESULTS

TMEM16B activation by Ca^{2+} and voltage

To study the activation of TMEM16B by $[Ca^{2+}]_i$ and voltage, we performed whole cell voltage-clamp recordings on HEK 293T cells transiently transfected with TMEM16B using intracellular solutions containing different free $[Ca^{2+}]_i$. Fig. 1 A shows that voltage steps between −100 and +100 mV from a holding voltage of 0 mV elicited very small currents with a nominally 0-Ca^{2+} pipette solution (8 ± 3 pA/pF at +100 mV; n = 8), whereas it induced large outward currents in the presence of 1.5 µM Ca^{2+}.

In the presence of Ca^{2+}, depolarizing voltage steps elicited an instantaneous outward current, indicating that channels were open at the holding potential of 0 mV, followed by a time-dependent outward relaxation (see also Fig. 5). Hyperpolarizing voltage steps induced instantaneous inward currents followed by a relaxation toward less negative values, in agreement with previous results (Pifferi et al., 2009; Stöhr et al., 2009; Rasche et al., 2010). The I-V relation measured at the steady state showed a pronounced outward rectification, whereas the instantaneous I-V curve measured at the beginning of each step was linear (Fig. 1 B). A similar result was obtained by activating TMEM16B with a different voltage protocol: channels were first activated by a 200-ms prepulse to +100 mV, and then tail currents were induced by voltage steps between −100 and +100 mV in 20-mV steps (Fig. 1 C). The I-V relation obtained by plotting the tail currents measured at the beginning of each step versus the step voltage was linear, whereas the steady-state I-V curve showed an outward rectification (Fig. 1 D), as in Fig. 1 B. These results clearly demonstrate that the I-V relation of the open channel is linear, and therefore the outward rectification is a result of a voltage-dependent mechanism that favors channel opening at

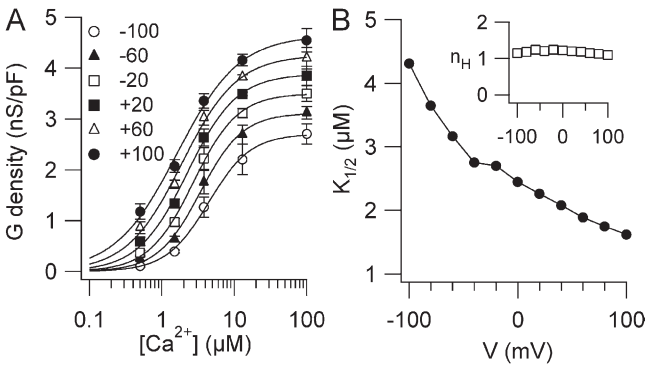

Figure 3. Ca^{2+} sensitivity of TMEM16B. (A) Conductance density calculated from tail currents measured at −100 mV after prepulses between −100 and +100 mV as indicated was plotted versus $[Ca^{2+}]_i$ (n = 3–6). Voltage protocol as in Fig. 1 A. Lines are the fit to the Hill equation (Eq. 1). (B) $K_{1/2}$ and n_H (inset) values plotted versus voltage.

Published March 12, 2012

depolarizing voltages. Thus, TMEM16B is activated by $[Ca^{2+}]_i$ and modulated by voltage at low $[Ca^{2+}]_i$.

To further examine the interplay between $[Ca^{2+}]_i$ and voltage in channel activation, we varied $[Ca^{2+}]_i$ (Fig. 2 A). Steady-state I-V relations measured at low $[Ca^{2+}]_i$ showed an outward rectification that became less pronounced as $[Ca^{2+}]_i$ increased (Fig. 2 B). We calculated a rectification index as the ratio between the steady-state current at +100 and −100 mV at each $[Ca^{2+}]_i$. The rectification index was 4.8 ± 0.2 at 1.5 µM Ca^{2+} and decreased to 1.4 ± 0.2 at 100 µM Ca^{2+}, showing that the I-V relation is Ca^{2+} dependent and becomes more linear as $[Ca^{2+}]_i$ increases (Fig. 2 C).

To analyze the Ca^{2+} dependence of TMEM16B activation at various voltages, we measured the dose–response relations. Tail currents at each $[Ca^{2+}]_i$ were measured at the beginning of the step to −100 mV after prepulses ranging from −100 to +100 mV. Fig. 3 A shows the average conductance densities plotted versus $[Ca^{2+}]_i$ and fit at each voltage by the Hill equation:

$$G = G_{max}\left[Ca^{2+}\right]_i^{nH} / \left(\left[Ca^{2+}\right]_i^{nH} + {K_{1/2}}^{nH}\right), \quad (1)$$

where G is the current density, G_{max} is the maximal current density, $K_{1/2}$ is the half-maximal $[Ca^{2+}]_i$, and n_H is the Hill coefficient.

The Hill coefficient was not voltage dependent with a value of 1.2 at −100 mV and 1.1 at +100 mV. The finding that the Hill coefficient was >1 indicates that the binding of more than one Ca^{2+} ion is necessary to open the channel. $K_{1/2}$ slightly decreased with membrane depolarization from 4.3 µM at −100 mV to 1.6 µM at +100 mV, as illustrated in Fig. 3 B. These data show that the Ca^{2+} sensitivity of TMEM16B is moderately voltage dependent, in agreement with previous results obtained with inside-out patches (Pifferi et al., 2009; Stephan et al., 2009).

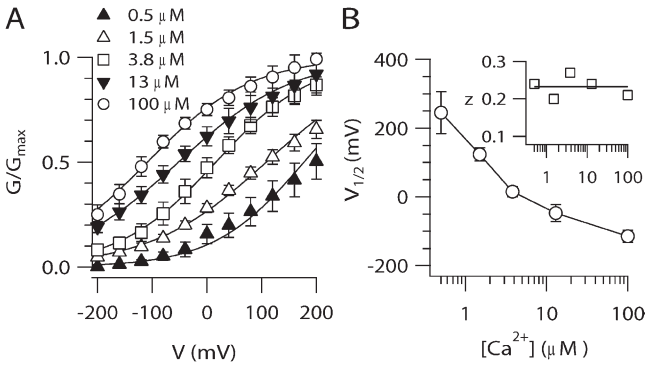

Figure 4. Voltage dependence of TMEM16B. (A) Normalized conductances at the indicated $[Ca^{2+}]_i$ calculated from tail currents at −100 mV after prepulses between −200 and +200 mV were plotted versus the prepulse voltage (n = 4–9). Lines are the fit to the Boltzmann equation (Eq. 2). (B) $V_{1/2}$ and z (inset) values plotted versus $[Ca^{2+}]_i$.

The voltage dependence of steady-state activation (G-V relation) was analyzed by measuring tail currents at the beginning of a step to −100 mV after prepulse voltages between −200 and +200 mV. The range of voltages was extended from the previous voltage protocols to obtain a better estimate of voltage dependence. Fig. 4 A shows the average conductance activated at a given $[Ca^{2+}]_i$ plotted versus membrane voltage and fit by the Boltzmann equation:

$$G / G_{max} = 1 / \left\{1 + \exp\left[z\left(V_{1/2} - V\right)F / RT\right]\right\}, \quad (2)$$

where G/G_{max} is the normalized conductance, z is the equivalent gating charge associated with voltage-dependent channel opening, V is the membrane potential, $V_{1/2}$ is the membrane potential producing half-maximal activation, F is the Faraday constant, R is the gas constant, and T is the absolute temperature.

The maximal conductance density G_{max} was determined by a global fit of G-V relations, and G at each $[Ca^{2+}]_i$ was then normalized to the same G_{max}. Because at the smaller $[Ca^{2+}]_i$ the prediction of G_{max} from the fit could be affected by a large error, we also estimated G_{max} at each $[Ca^{2+}]_i$. G_{max} at 0.5 µM Ca^{2+} was 4.1 ± 0.4 nS/pF, not significantly different from the value of 4.7 ± 0.4 nS/pF at 100 µM Ca^{2+}, indicating that the estimate of G_{max} was little affected by $[Ca^{2+}]_i$. Fig. 4 A shows that increasing

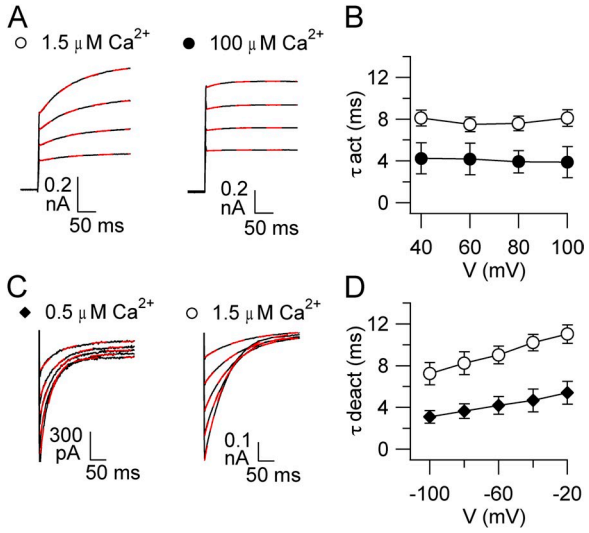

Figure 5. Activation and deactivation kinetics of TMEM16B. (A) Representative recordings at the indicated $[Ca^{2+}]_i$. Voltage protocol as in Fig. 1 A, with voltage steps from a holding voltage of 0 between +40 to +100 mV in 20-mV steps. Red dashed lines are the fit to a single-exponential function. (B) Average activation time constants (τ_{act}) plotted versus voltage (n = 6–8). (C) Representative recordings at the indicated $[Ca^{2+}]_i$. Voltage protocol as in Fig. 1 C, with a prepulse to +100 mV and tail currents induced by voltage steps between −100 and +100 mV in 20-mV steps. Only tail currents are illustrated. Red dashed lines are the fit to a single-exponential function. (D) Average deactivation time constants (τ_{deact}) plotted versus voltage (n = 4–9).

Published March 12, 2012

$[Ca^{2+}]_i$ produced a leftward shift in the G-V relation: $V_{1/2}$ was 124 ± 20 mV at 1.5 µM Ca^{2+} and became −115 ± 18 mV at 100 µM Ca^{2+}, whereas the equivalent gating charge was not largely modified (z = 0.23–0.30). Thus, $V_{1/2}$ decreased as $[Ca^{2+}]_i$ increased, indicating that more channels can be activated by depolarization in the presence of a high $[Ca^{2+}]_i$ (Fig. 4 B). At a given $[Ca^{2+}]_i$, the conductance increased with depolarization, showing that the conductance depends both on $[Ca^{2+}]_i$ and voltage.

Activation and deactivation kinetics are regulated by $[Ca^{2+}]_i$ and voltage

To characterize activation and deactivation kinetics, we analyzed the time-dependent components in response to voltage steps in the presence of a given $[Ca^{2+}]_i$. As shown in Figs. 2 A and 5 A, current activation in response to depolarizing voltage steps had two components: an instantaneous time-independent current, related to the fraction of channels open at the holding voltage of 0 mV, followed by an outward time-dependent relaxation, a

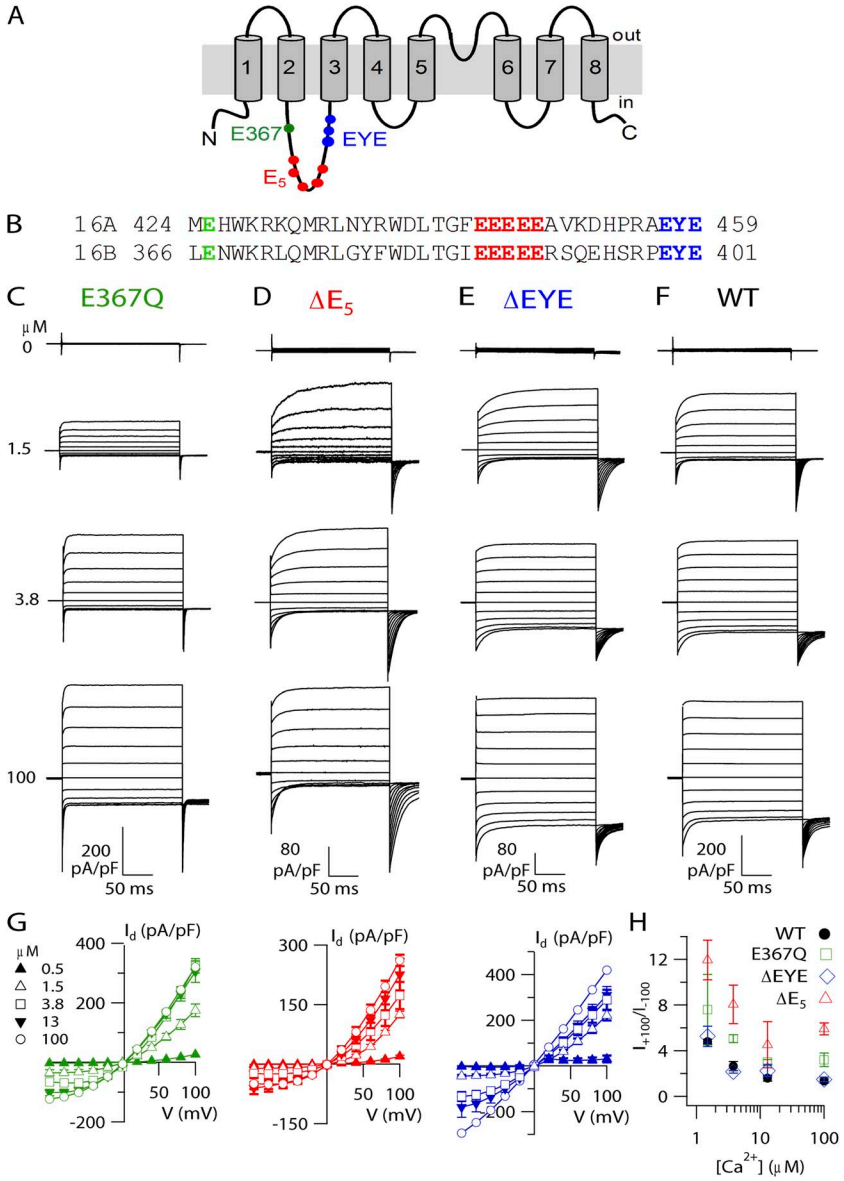

Figure 6. TMEM16B mutations. (A) Predicted topology of TMEM16A and TMEM16B from hydropathy analysis. (B) Alignment between mouse TMEM16A (*a,c*; available from GenBank/EMBL/DDBJ under accession no. NM_178642.4) and the retinal isoform of TMEM16B used in this study (NP_705817.1), with the mutations or deletions highlighted in color. (C–F) Representative recordings at the indicated $[Ca^{2+}]_i$ for E367Q (C), ΔE_5 (D), ΔEYE (E) mutants, and WT (F). Traces for WT are the same as in Fig. 2 A. Voltage protocol as in Fig. 1 A. (G) I-V steady-state relations (n = 3–8). (H) Average ratios between currents measured at +100 and −100 mV plotted versus $[Ca^{2+}]_i$ for each mutant (n = 3–8).

Published March 12, 2012

result of the increase in the fraction of channels opened by depolarization. The time-independent component became larger as voltage or $[Ca^{2+}]_i$ increased.

To examine the activation kinetics, we analyzed the time-dependent component of the current elicited by depolarizing voltage steps. Fig. 5 A shows that most of the time course of time-dependent relaxations was well fit by a single-exponential function. The time constant of current activation, τ_{act}, in the presence of 1.5 µM Ca^{2+} was 8.1 ± 0.8 ms at +100 mV and did not vary as a function of voltage at a given $[Ca^{2+}]_i$ (Fig. 5 B). At +100 mV, τ_{act} at 100 µM Ca^{2+} was 3.9 ± 1.4 ms, significantly smaller than the value of 8.1 ± 0.8 ms at 1.5 µM Ca^{2+}, showing that an increase in $[Ca^{2+}]_i$ accelerated activation.

The time constant of current deactivation (τ_{deact}) was calculated by fitting with a single-exponential function the tail currents obtained after a prepulse at +100 mV by voltage steps ranging between −100 and −20 mV (Fig. 5 C). In the presence of 0.5 µM Ca^{2+}, τ_{deact} was 3.0 ± 0.2 ms at −100 mV and 5.4 ± 0.5 ms at −20 mV, showing that less negative voltages slowed deactivation (Fig. 5 D). At −100 mV, τ_{deact} at 1.5 µM Ca^{2+} was 7.2 ± 0.8 ms, significantly different from the value of 3.0 ± 0.2 ms at 0.5 µM Ca^{2+}, showing that an increase in $[Ca^{2+}]_i$ slowed deactivation.

In summary, the activation kinetics are voltage independent and become faster by increasing $[Ca^{2+}]_i$, whereas the deactivation kinetics are prolonged by depolarization and by increasing $[Ca^{2+}]_i$.

Functional characterization of mutations in the first putative intracellular loop

To investigate the molecular mechanisms responsible for channel activation by Ca^{2+} and by voltage, we performed a site-directed mutagenesis study. Hydropathy analysis indicates that each member of the TMEM16 family has eight transmembrane domains (Fig. 6 A). Analysis of the sequence of TMEM16B does not reveal the presence of any typical voltage sensor or Ca^{2+}-binding domain. However, some acidic amino acids are located in the first putative intracellular loop between transmembrane segment 2 and 3, and we hypothesized that some of them may be involved in Ca^{2+} and/or voltage activation of TMEM16B. As illustrated in Fig. 6 B, we mutated glutamate at position 367 into glutamine (E367Q), deleted the five consecutive glutamate residues $_{386}$EEEEE$_{390}$ (ΔE_5), or deleted $_{399}$EYE$_{401}$ (ΔEYE), and measured their biophysical properties.

Fig. 6 (C–F) illustrates recordings from each mutant channel in the presence of various $[Ca^{2+}]_i$. Similar to WT

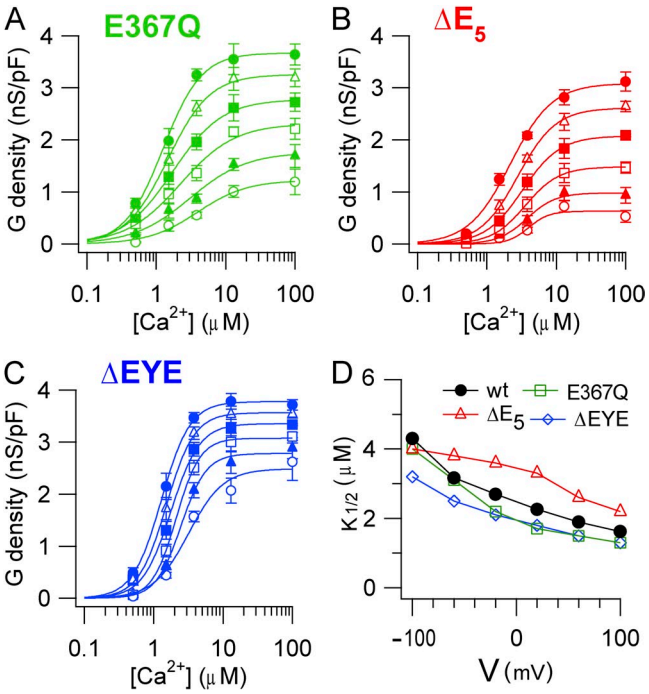

Figure 7. Ca^{2+} sensitivity of TMEM16B mutants. Conductance density calculated from tail currents measured at −100 mV after prepulses between −100 and +100 mV as indicated was plotted versus $[Ca^{2+}]_i$ for E367Q (A; n = 3–6), ΔE_5 (B; n = 3–5), and ΔEYE (C; n = 3–8) mutants. Lines are the fit to the Hill equation (Eq. 1). (D) $K_{1/2}$ values plotted versus voltage for each mutant.

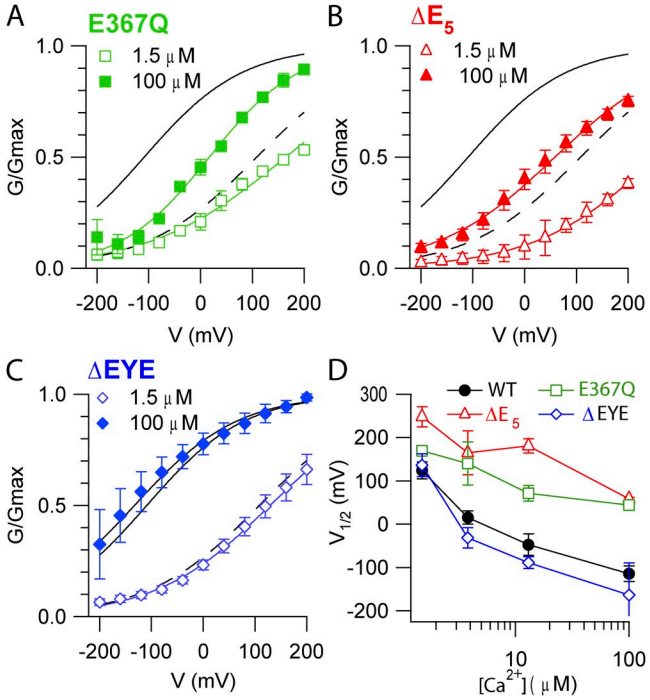

Figure 8. Voltage dependence of TMEM16B mutants. Normalized conductances at the indicated $[Ca^{2+}]_i$ calculated from tail currents at −100 mV after prepulses between −200 and +200 mV were plotted versus the prepulse voltage. Black lines are the fit to the Boltzmann equation (Eq. 2) for WT from Fig. 4 at 100 µM Ca^{2+} (solid line) or at 1.5 µM Ca^{2+} (dashed line). Colored lines are the fits to the Boltzmann equation for E367Q (A; n = 3–4), ΔE_5 (B; n = 3–5), and ΔEYE (C; n = 3–6) mutants. (D) Average $V_{1/2}$ values plotted versus $[Ca^{2+}]_i$.

Published March 12, 2012

(Fig. 2 A), the steady-state I-V relation for each mutant was Ca^{2+} dependent, showing an outward rectification at low $[Ca^{2+}]_i$ that became less pronounced as $[Ca^{2+}]_i$ increased (Fig. 6 G). However, although the overall Ca^{2+} dependence was similar, the rectification index, measured from the ratio between steady-state currents at +100 and −100 mV, was significantly higher at every $[Ca^{2+}]_i$ in E367Q and ΔE_5 mutants than in WT, whereas it remained similar in ΔEYE mutant channel (Fig. 6 H).

The dose–response relations for each mutant channel, evaluated from tail currents as described previously for the WT channel (Fig. 3), were fit by the Hill equation (Fig. 7, A–C). Fig. 7 D shows that $K_{1/2}$ at +100 mV (−100 mV) was 1.6 µM (4.3 µM) in WT, 1.3 µM (4.0 µM) in E367Q, 2.2 µM (4.0 µM) in ΔE_5, and 1.3 µM (3.2 µM) in ΔEYE. The Hill coefficient n_H at +100 mV (−100 mV) was 1.1 (1.2) in WT, 1.6 (1.2) in E367Q, 1.4 (2.9) in ΔE_5, and 2.0 (1.7) in ΔEYE. Thus, the mutations produced only some very small changes in $K_{1/2}$ or n_H, but overall no strong modifications in Ca^{2+} sensitivity were observed.

The G-V relations in mutant channels were measured at each $[Ca^{2+}]_i$ and compared with the corresponding relations in WT channels. Fig. 8 A shows that the E367Q mutation produced a rightward shift of the G-V relation at a given $[Ca^{2+}]_i$ with respect to WT; indeed, $V_{1/2}$ changed from 124 ± 20 mV in WT to 169 ± 6 mV in E367Q at 1.5 µM Ca^{2+}, and from −115 ± 18 mV in WT to 44 ± 8 mV in E367Q at 100 µM Ca^{2+} (Fig. 8 D). The deletion ΔE_5 also shifted the G-V relations to the right (Fig. 8, B and D): $V_{1/2}$ changed from 124 ± 20 mV in WT to 248 ± 39 mV in ΔE_5 at 1.5 µM Ca^{2+}, and from −115 ± 18 mV in WT to 58 ± 15 mV in ΔE_5 at 100 µM Ca^{2+}. Differently from the previous mutants, the ΔEYE deletion did not produce any significant change in the G-V relations (Fig. 8, C and D). The equivalent gating charge for each mutant varied between 0.15 and 0.32, values similar to those of the WT channel (z = 0.23–0.30). Thus, E367Q and the ΔE_5 deletion modified the voltage sensitivity: at a given $[Ca^{2+}]_i$, fewer channels can be open by depolarization compared with WT.

The kinetic properties of activation and deactivation of mutant channels also showed some interesting changes compared with WT channels. Upon depolarizing voltage steps, the activation of mutant channels was still characterized by two components: an instantaneous time-independent current, followed by an outward time-dependent relaxation (Fig. 6), which was well fit by a single-exponential function as in WT channels. In the presence of 1.5 µM Ca^{2+}, τ_{act} at +100 mV was 2.8 ± 0.3 ms in E367Q, faster than 7.5 ± 0.7 ms in the WT channel, whereas it became slower than WT in ΔE_5 (17.7 ± 3.0 ms) and in ΔEYE (25.5 ± 2.3 ms). These results indicate that each mutation altered the time course of activation. Indeed, the time necessary to respond to a depolarization decreased in E367Q, whereas it was progressively prolonged in ΔE_5 and in ΔEYE compared with WT. As in the WT channel, τ_{act} in each mutant was not significantly modified by voltage (Fig. 9 A).

Deactivation kinetics was also well fit by a single-exponential function and, similarly to WT, τ_{deact} showed an increase at less negative voltages for each mutant channel (Fig. 9 B). In the presence of 1.5 µM Ca^{2+}, τ_{deact} at −100 mV was 1.6 ± 0.3 ms in E367Q, smaller than 7.2 ± 0.8 ms in the WT channel, whereas it was not significantly different from WT in ΔE_5 (6.8 ± 0.3 ms) and became larger than WT in ΔEYE (12.3 ± 1.5 ms). The time necessary for channels to close upon repolarization decreased in E367Q but remained similar in ΔE_5, and it was prolonged in ΔEYE compared with WT. Thus, E367Q and ΔEYE mutants also showed a modified time course of deactivation.

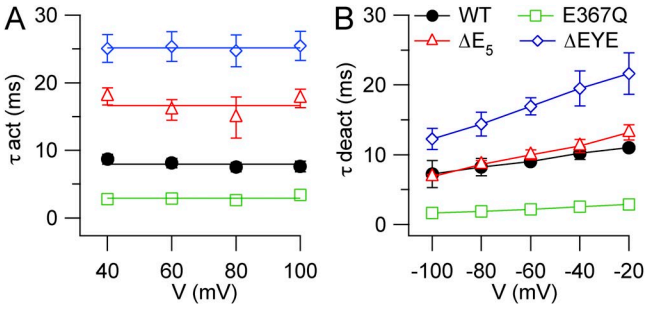

Figure 9. Activation and deactivation kinetics of TMEM16B mutants. Kinetics were measured as explained in Fig. 5. (A) Average activation time constants (τ_{act}) plotted versus voltage for E367Q (n = 5), ΔE_5 (n = 3), and ΔEYE (n = 6) mutants. (B) Average deactivation time constants (τ_{deact}) plotted versus voltage for E367Q (n = 4), ΔE_5 (n = 4), and ΔEYE (n = 5) mutants.

DISCUSSION

Here, we have provided the first site-directed mutagenesis study to investigate structure–function relations of the TMEM16B channel. Because previous studies have shown that TMEM16B in excised inside-out patches has a significant rundown (Pifferi et al., 2009, Fig. 5; Stephan et al., 2009, Fig. 3 A), whereas whole cell recordings are rather stable (Pifferi et al., 2009, Fig. 1 h), we decided to use the whole cell configuration.

We first characterized the WT TMEM16B channel and established one important difference between TMEM16A and TMEM16B activation properties in the absence of $[Ca^{2+}]_i$. Indeed, we found that TMEM16B cannot be activated by voltages up to +200 mV in the absence of Ca^{2+} (32 ± 10 pA/pF; n = 6; not depicted), whereas recent data from Hartzell's laboratory showed that TMEM16A was activated by strong depolarization in the absence of Ca^{2+} (∼140 pA/pF at +200 mV; Fig. 5 A in Xiao et al., 2011). Thus, our data show that TMEM16B needs Ca^{2+} to be activated differently from TMEM16A, which can be activated by voltage also in the absence of Ca^{2+} (Xiao et al., 2011).

Published March 12, 2012

In the presence of Ca^{2+}, dose–response relations for TMEM16A and TMEM16B obtained by different laboratories reported variable values for $K_{1/2}$. For TMEM16A, from inside-out recordings, $K_{1/2}$ at +60 mV (−60 mV) was 0.3 µM (2.6 µM) (Yang et al., 2008), and at +100 mV (−100 mV) it was 0.4 µM (5.9 µM) (Xiao et al., 2011), whereas from whole cell recordings at +100 mV (−40 mV) it was 332 nM (∼700 nM) (Ferrera et al., 2009). For TMEM16B, from previous work in inside-out patches, $K_{1/2}$ at +50 mV (−50 mV) was 3.3 µM (4.9 µM) (Pifferi et al., 2009), and at +40 mV (−40 mV) it was 1.2 µM (1.8 µM) (Stephan et al., 2009), whereas from whole cell recordings we found that $K_{1/2}$ at +40 mV (−40 mV) was 2.0 µM (2.7 µM), and at +100 mV (−100 mV) it was 1.6 µM (4.3 µM) (Fig. 3). Although there are some differences among studies reported from different laboratories, every report showed that the apparent affinity for Ca^{2+} is slightly voltage dependent, with higher apparent Ca^{2+} affinity at positive voltages, and the Hill coefficients are consistently higher than one, indicating that more than a Ca^{2+} ion is necessary to activate the channels. A comparison between TMEM16A and TMEM16B shows a fourfold difference between $K_{1/2}$ values at +100 mV: 0.4 µM (Xiao et al., 2011) for TMEM16A and 1.6 µM for TMEM16B (Fig. 3), indicating a lower apparent affinity for Ca^{2+} of TMEM16B compared with TMEM16A.

A critical question about the function of TMEM16A and TMEM16B is the following: what are the molecular mechanisms responsible for Ca^{2+} and voltage modulation of channel gating in each channel? Galietta's laboratory (Ferrera et al., 2009) has shown that human TMEM16A has various protein isoforms generated by alternative splicing, and it has labeled the four identified alternative segments as *a*, *b*, *c*, and *d*. A rare minimal version of TMEM16A lacking all alternative segments, TMEM16A (0), still shows CaCC properties, although the voltage dependence is reduced, (Caputo et al., 2008; Ferrera et al., 2009, 2011). Ferrera et al. (2009) showed that segment *b* modified the Ca^{2+} sensitivity by nearly fourfold, decreasing the apparent half-effective concentration at +80 mV from 350 to 90 nM, whereas segment *c* affected the voltage dependence but not the Ca^{2+} sensitivity of human TMEM16A (*abc*). Segment *c* is composed of the four amino acids EAVK, which have also been recently deleted from mouse TMEM16A (*ac*) in a study from Hartzell's laboratory (Xiao et al., 2011). Differently from Ferrera et al. (2009), Xiao et al. (2011) found that deletion of EAVK modified both Ca^{2+} and voltage dependence of TMEM16A. The discrepancy between the results can be a result of differences between human TMEM16A (*ab*) and mouse TMEM16A (*a*), and/or to the different techniques, whole cell versus inside-out recordings, used for the experiments in the different laboratories. Although the two studies reached some different conclusions, they both pointed to the relevance of the segment *c* in the regulation of the TMEM16A functional activity.

TMEM16B is expressed in the retina, at the synaptic terminal of photoreceptors (Stöhr et al., 2009; Billig et al., 2011), in the cilia of olfactory sensory neurons, and in the microvilli of vomeronasal sensory neurons (Stephan et al., 2009; Rasche et al., 2010; Sagheddu et al., 2010; Billig et al., 2011; Pifferi et al., 2012). Zhao's laboratory showed that the major TMEM16B olfactory isoform differs from the retinal isoform in the absence of the exon encoding the four amino acids ERSQ in the first putative intracellular loop (Stephan et al., 2009). It is worth pointing out here that segment *c* (EAVK) in TMEM16A is not present in TMEM16B, but that ERSQ residues are located in the corresponding positions in the retinal isoform of TMEM16B (Fig. 6). A comparison between the biophysical properties measured in inside-out patches from the retinal isoform (Pifferi et al., 2009) and from the olfactory isoform (missing ERSQ; Stephan et al., 2009) did not reveal any major difference in the rectification properties and in the dose–response relations between the two isoforms, although we cannot exclude that more detailed biophysical studies may reveal subtle differences. Indeed, the functional properties of additional isoforms for TMEM16B are under investigation (Saidu, S.P., A.B. Stephan, S.M. Caraballo, H. Zhao, and J. Reisert. 2010. Association for Chemoreception Sciences Meeting. Abstr. P68).

Although the amino acidic sequences of both TMEM16A and TMEM16B lack any classical voltage-sensor or Ca^{2+}-binding domain, a series of five consecutive glutamates located in the first putative intracellular loop has been identified as a good candidate to play a role in channel gating. Moreover, we have investigated if other glutamates in the same loop could also be involved in the activation of TMEM16B by Ca^{2+} and voltage. We found that deletion of the five glutamates, ΔE_5, did not greatly affect the apparent affinity for Ca^{2+} (Fig. 7), but it significantly shifted the activation curve to the right. Indeed, $V_{1/2}$ at 1.5 µM Ca^{2+} changed from 124 mV in WT to 248 mV, whereas the equivalent gating charge was not modified. In addition, the time necessary to respond to a depolarization was prolonged in ΔE_5, whereas the deactivation constant was not significantly affected (Fig. 9). Thus, the five consecutive glutamates are involved in the voltage dependence of the TMEM16B channel, whereas they do not seem to play a significant role in the apparent affinity for Ca^{2+}. These results are in agreement with a recent study in TMEM16A, showing that the substitution of the four correspondent glutamates into alanines ($_{444}$EEEE/AAAA$_{447}$) did not greatly affect the apparent affinity for Ca^{2+} but modified the voltage dependence, producing a shift of the activation curve to the right (Xiao et al., 2011).

In the TMEM16B mutant E367Q, both activation and deactivation kinetics were shortened; the dose–response relation for Ca^{2+} was not strongly modified, while the activation curve was shifted to the right. Finally, the deletion ΔEYE produced an increase in the time constants

for activation and deactivation, whereas it did not cause any large change in apparent affinity for Ca^{2+} or in voltage sensitivity.

Collectively, our results indicate that glutamates E367 and $_{386}$EEEEE$_{390}$ in the first putative intracellular loop play a relevant role in the modulation of the voltage dependence of TMEM16B.

Conclusions

In conclusion, we have found evidence that the five consecutive glutamates in the first putative intracellular loop are not involved in Ca^{2+} sensitivity in TMEM16B but have an important role in voltage dependence. Another glutamate in position 367 plays a similar role, further indicating that the first intracellular loop is involved in voltage-dependent activation of TMEM16B.

At present, the location of the Ca^{2+}-binding site in TMEM16A and TMEM16B remains unknown. It is possible that several residues in different regions contribute to bind Ca^{2+} ions, but it cannot be excluded that the Ca^{2+}-binding site is located in an accessory subunit expressed both in HEK 293T cells and in axolotl oocytes. Future work will have to shed light on the intricate mechanisms that couple Ca^{2+} gating and voltage dependence, including intriguing interactions between gating and permeation.

We thank Anna Boccaccio, Arin Marchesi, and Riccardo Scala for discussions; Federica Ferrero for help with cell cultures; and all members of the laboratory for discussions.

This study was supported by grants from the Italian Ministry of Education, University and Research, and from the Italian Institute of Technology.

Christopher Miller served as editor.

Submitted: 27 December 2011
Accepted: 17 February 2012

REFERENCES

Bers, D.M. 2008. Calcium cycling and signaling in cardiac myocytes. *Annu. Rev. Physiol.* 70:23–49. http://dx.doi.org/10.1146/annurev.physiol.70.113006.100455

Billig, G.M., B. Pál, P. Fidzinski, and T.J. Jentsch. 2011. Ca2+-activated Cl− currents are dispensable for olfaction. *Nat. Neurosci.* 14:763–769. http://dx.doi.org/10.1038/nn.2821

Caputo, A., E. Caci, L. Ferrera, N. Pedemonte, C. Barsanti, E. Sondo, U. Pfeffer, R. Ravazzolo, O. Zegarra-Moran, and L.J.V. Galietta. 2008. TMEM16A, a membrane protein associated with calcium-dependent chloride channel activity. *Science.* 322:590–594. http://dx.doi.org/10.1126/science.1163518

Das, S., Y. Hahn, D.A. Walker, S. Nagata, M.C. Willingham, D.M. Peehl, T.K. Bera, B. Lee, and I. Pastan. 2008. Topology of NGEP, a prostate-specific cell:cell junction protein widely expressed in many cancers of different grade level. *Cancer Res.* 68:6306–6312. http://dx.doi.org/10.1158/0008-5472.CAN-08-0870

Duran, C., and H.C. Hartzell. 2011. Physiological roles and diseases of tmem16/anoctamin proteins: are they all chloride channels? *Acta Pharmacol. Sin.* 32:685–692. http://dx.doi.org/10.1038/aps.2011.48

Duran, C., C.H. Thompson, Q. Xiao, and H.C. Hartzell. 2010. Chloride channels: often enigmatic, rarely predictable. *Annu. Rev. Physiol.* 72:95–121. http://dx.doi.org/10.1146/annurev-physiol-021909-135811

Ferrera, L., A. Caputo, I. Ubby, E. Bussani, O. Zegarra-Moran, R. Ravazzolo, F. Pagani, and L.J.V. Galietta. 2009. Regulation of TMEM16A chloride channel properties by alternative splicing. *J. Biol. Chem.* 284:33360–33368. http://dx.doi.org/10.1074/jbc.M109.046607

Ferrera, L., P. Scudieri, E. Sondo, A. Caputo, E. Caci, O. Zegarra-Moran, R. Ravazzolo, and L.J.V. Galietta. 2011. A minimal isoform of the TMEM16A protein associated with chloride channel activity. *Biochim. Biophys. Acta.* 1808:2214–2223. http://dx.doi.org/10.1016/j.bbamem.2011.05.017

Flores, C.A., L.P. Cid, F.V. Sepúlveda, and M.I. Niemeyer. 2009. TMEM16 proteins: the long awaited calcium-activated chloride channels? *Braz. J. Med. Biol. Res.* 42:993–1001. http://dx.doi.org/10.1590/S0100-879X2009005000028

Frings, S., D. Reuter, and S.J. Kleene. 2000. Neuronal Ca2+-activated Cl− channels—homing in on an elusive channel species. *Prog. Neurobiol.* 60:247–289. http://dx.doi.org/10.1016/S0301-0082(99)00027-1

Galietta, L.J.V. 2009. The TMEM16 protein family: a new class of chloride channels? *Biophys. J.* 97:3047–3053. http://dx.doi.org/10.1016/j.bpj.2009.09.024

Hartzell, C., I. Putzier, and J. Arreola. 2005. Calcium-activated chloride channels. *Annu. Rev. Physiol.* 67:719–758. http://dx.doi.org/10.1146/annurev.physiol.67.032003.154341

Hartzell, H.C., K. Yu, Q. Xiao, L.-T. Chien, and Z. Qu. 2009. Anoctamin/TMEM16 family members are Ca2+-activated Cl− channels. *J. Physiol.* 587:2127–2139. http://dx.doi.org/10.1113/jphysiol.2008.163709

Huang, F., X. Wong, and L.Y. Jan. 2012. International Union of Basic and Clinical Pharmacology. LXXXV: calcium-activated chloride channels. *Pharmacol. Rev.* 64:1–15. http://dx.doi.org/10.1124/pr.111.005009

Kleene, S.J. 2008. The electrochemical basis of odor transduction in vertebrate olfactory cilia. *Chem. Senses.* 33:839–859. http://dx.doi.org/10.1093/chemse/bjn048

Kunzelmann, K., P. Kongsuphol, K. Chootip, C. Toledo, J.R. Martins, J. Almaca, Y. Tian, R. Witzgall, J. Ousingsawat, and R. Schreiber. 2011a. Role of the Ca2+-activated Cl− channels bestrophin and anoctamin in epithelial cells. *Biol. Chem.* 392:125–134. http://dx.doi.org/10.1515/BC.2011.010

Kunzelmann, K., Y. Tian, J.R. Martins, D. Faria, P. Kongsuphol, J. Ousingsawat, F. Thevenod, E. Roussa, J. Rock, and R. Schreiber. 2011b. Anoctamins. *Pflugers Arch.* 462:195–208. http://dx.doi.org/10.1007/s00424-011-0975-9

Kunzelmann, K., R. Schreiber, A. Kmit, W. Jantarajit, J.R. Martins, D. Faria, P. Kongsuphol, J. Ousingsawat, and Y. Tian. 2012. Expression and function of epithelial anoctamins. *Exp. Physiol.* 97:184–192.

Lalonde, M.R., M.E. Kelly, and S. Barnes. 2008. Calcium-activated chloride channels in the retina. *Channels (Austin).* 2:252–260. http://dx.doi.org/10.4161/chan.2.4.6704

Leblanc, N., J. Ledoux, S. Saleh, A. Sanguinetti, J. Angermann, K. O'Driscoll, F. Britton, B.A. Perrino, and I.A. Greenwood. 2005. Regulation of calcium-activated chloride channels in smooth muscle cells: a complex picture is emerging. *Can. J. Physiol. Pharmacol.* 83:541–556. http://dx.doi.org/10.1139/y05-040

Patton, C., S. Thompson, and D. Epel. 2004. Some precautions in using chelators to buffer metals in biological solutions. *Cell Calcium.* 35:427–431. http://dx.doi.org/10.1016/j.ceca.2003.10.006

Petersen, O.H. 2005. Ca2+ signalling and Ca2+-activated ion channels in exocrine acinar cells. *Cell Calcium.* 38:171–200. http://dx.doi.org/10.1016/j.ceca.2005.06.024

Petersen, O.H., and A.V. Tepikin. 2008. Polarized calcium signaling in exocrine gland cells. *Annu. Rev. Physiol.* 70:273–299. http://dx.doi.org/10.1146/annurev.physiol.70.113006.100618

Pifferi, S., G. Pascarella, A. Boccaccio, A. Mazzatenta, S. Gustincich, A. Menini, and S. Zucchelli. 2006. Bestrophin-2 is a candidate calcium-activated chloride channel involved in olfactory transduction. *Proc. Natl. Acad. Sci. USA*. 103:12929–12934. http://dx.doi.org/10.1073/pnas.0604505103

Pifferi, S., M. Dibattista, and A. Menini. 2009. TMEM16B induces chloride currents activated by calcium in mammalian cells. *Pflugers Arch.* 458:1023–1038. http://dx.doi.org/10.1007/s00424-009-0684-9

Pifferi, S., V. Cenedese, and A. Menini. 2012. Anoctamin 2/TMEM16B: a calcium-activated chloride channel in olfactory transduction. *Exp. Physiol.* 97:193–199.

Rasche, S., B. Toetter, J. Adler, A. Tschapek, J.F. Doerner, S. Kurtenbach, H. Hatt, H. Meyer, B. Warscheid, and E.M. Neuhaus. 2010. Tmem16b is specifically expressed in the cilia of olfactory sensory neurons. *Chem. Senses.* 35:239–245. http://dx.doi.org/10.1093/chemse/bjq007

Rock, J.R., and B.D. Harfe. 2008. Expression of TMEM16 paralogs during murine embryogenesis. *Dev. Dyn.* 237:2566–2574. http://dx.doi.org/10.1002/dvdy.21676

Sagheddu, C., A. Boccaccio, M. Dibattista, G. Montani, R. Tirindelli, and A. Menini. 2010. Calcium concentration jumps reveal dynamic ion selectivity of calcium-activated chloride currents in mouse olfactory sensory neurons and TMEM16b-transfected HEK 293T cells. *J. Physiol.* 588:4189–4204. http://dx.doi.org/10.1113/jphysiol.2010.194407

Sanders, K.M., M.H. Zhu, F.C. Britton, S.D. Koh, and S.M. Ward. 2012. Anoctamins and gastrointestinal smooth muscle excitability. *Exp. Physiol.* 97:200–206.

Schroeder, B.C., T. Cheng, Y.N. Jan, and L.Y. Jan. 2008. Expression cloning of TMEM16A as a calcium-activated chloride channel subunit. *Cell.* 134:1019–1029. http://dx.doi.org/10.1016/j.cell.2008.09.003

Scudieri, P., E. Sondo, L. Ferrera, and L.J. Galietta. 2012. The anoctamin family: TMEM16A and TMEM16B as calcium-activated chloride channels. *Exp. Physiol.* 97:177–183. http://dx.doi.org/10.1113/expphysiol.2011.058198

Stephan, A.B., E.Y. Shum, S. Hirsh, K.D. Cygnar, J. Reisert, and H. Zhao. 2009. ANO2 is the cilial calcium-activated chloride channel that may mediate olfactory amplification. *Proc. Natl. Acad. Sci. USA.* 106:11776–11781. http://dx.doi.org/10.1073/pnas.0903304106

Stöhr, H., J.B. Heisig, P.M. Benz, S. Schöberl, V.M. Milenkovic, O. Strauss, W.M. Aartsen, J. Wijnholds, B.H.F. Weber, and H.L. Schulz. 2009. TMEM16B, a novel protein with calcium-dependent chloride channel activity, associates with a presynaptic protein complex in photoreceptor terminals. *J. Neurosci.* 29:6809–6818. http://dx.doi.org/10.1523/JNEUROSCI.5546-08.2009

Wray, S., T. Burdyga, and K. Noble. 2005. Calcium signalling in smooth muscle. *Cell Calcium.* 38:397–407. http://dx.doi.org/10.1016/j.ceca.2005.06.018

Xiao, Q., K. Yu, P. Perez-Cornejo, Y. Cui, J. Arreola, and H.C. Hartzell. 2011. Voltage- and calcium-dependent gating of TMEM16A/Ano1 chloride channels are physically coupled by the first intracellular loop. *Proc. Natl. Acad. Sci. USA.* 108:8891–8896. http://dx.doi.org/10.1073/pnas.1102147108

Yang, Y.D., H. Cho, J.Y. Koo, M.H. Tak, Y. Cho, W.-S. Shim, S.P. Park, J. Lee, B. Lee, B.-M. Kim, et al. 2008. TMEM16A confers receptor-activated calcium-dependent chloride conductance. *Nature.* 455:1210–1215. http://dx.doi.org/10.1038/nature07313

4.2 Interactions between permeation and gating in the TMEM16B/anoctamin2 calcium-activated chloride channel.

Published May 26, 2014

Interactions between permeation and gating in the TMEM16B/anoctamin2 calcium-activated chloride channel

Giulia Betto,[1] O. Lijo Cherian,[1] Simone Pifferi,[1] Valentina Cenedese,[1] Anna Boccaccio,[2] and Anna Menini[1]

[1]Neurobiology Group, International School for Advanced Studies (SISSA), 34136 Trieste, Italy
[2]Istituto di Biofisica, Consiglio Nazionale delle Ricerche, 16149 Genova, Italy

At least two members of the TMEM16/anoctamin family, TMEM16A (also known as anoctamin1) and TMEM16B (also known as anoctamin2), encode Ca^{2+}-activated Cl^- channels (CaCCs), which are found in various cell types and mediate numerous physiological functions. Here, we used whole-cell and excised inside-out patch-clamp to investigate the relationship between anion permeation and gating, two processes typically viewed as independent, in TMEM16B expressed in HEK 293T cells. The permeability ratio sequence determined by substituting Cl^- with other anions (P_X/P_{Cl}) was $SCN^- > I^- > NO_3^- > Br^- > Cl^- > F^-$ > gluconate. When external Cl^- was substituted with other anions, TMEM16B activation and deactivation kinetics at 0.5 µM Ca^{2+} were modified according to the sequence of permeability ratios, with anions more permeant than Cl^- slowing both activation and deactivation and anions less permeant than Cl^- accelerating them. Moreover, replacement of external Cl^- with gluconate, or sucrose, shifted the voltage dependence of steady-state activation (G-V relation) to more positive potentials, whereas substitution of extracellular or intracellular Cl^- with SCN^- shifted G-V to more negative potentials. Dose–response relationships for Ca^{2+} in the presence of different extracellular anions indicated that the apparent affinity for Ca^{2+} at +100 mV increased with increasing permeability ratio. The apparent affinity for Ca^{2+} in the presence of intracellular SCN^- also increased compared with that in Cl^-. Our results provide the first evidence that TMEM16B gating is modulated by permeant anions and provide the basis for future studies aimed at identifying the molecular determinants of TMEM16B ion selectivity and gating.

INTRODUCTION

Permeation and gating properties in most ion channels have been traditionally considered to be independent, with the opening and closing of the ion channel (gating) as a separate process from ion entrance and passage in the channel pore (permeation). However, several studies on many ion channels have described interactions between permeation and gating, suggesting that these two processes are not always independent (Hille, 2001).

Ca^{2+}-activated Cl^- channels (CaCCs) play important physiological functions, including regulation of cell excitability, fluid secretion, and smooth muscle contraction and block of polyspermy in some oocytes (Frings et al., 2000; Hartzell et al., 2005; Leblanc et al., 2005; Petersen, 2005; Wray et al., 2005; Lalonde et al., 2008; Duran et al., 2010; Berg et al., 2012; Huang et al., 2012a). Evidence that anions modify gating of endogenous CaCCs was reported in several cell types. Indeed, partial replacement of Cl^- with other anions caused alterations in CaCC kinetics or conductance in lacrimal gland cells (Evans and Marty, 1986), parotid secretory cells (Ishikawa and Cook, 1993; Perez-Cornejo and Arreola, 2004), portal vein smooth muscle cells (Greenwood and Large, 1999), and *Xenopus laevis* oocytes (Centinaio et al., 1997; Kuruma and Hartzell, 2000; Qu and Hartzell, 2000). Moreover, Qu and Hartzell (2000) showed that the sensitivity for Ca^{2+} of CaCCs in *Xenopus* oocytes depended on the permeant anion, indicating that the permeant anion is able to affect channel gating.

The molecular identity of CaCCs has been controversial for a long time, but there is now a general consensus that at least two members of the TMEM16 (anoctamin) gene family, TMEM16A/anoctamin1 and TMEM16B/anoctamin2, encode for CaCCs (Caputo et al., 2008; Schroeder et al., 2008; Yang et al., 2008; Pifferi et al., 2009; Stephan et al., 2009; Stöhr et al., 2009). TMEM16A is expressed in secretory cells, smooth muscle cells, and several other cell types (Huang et al., 2009, 2012a), including supporting cells in the olfactory and vomeronasal epithelium (Billig et al., 2011; Dauner et al., 2012; Dibattista et al., 2012; Maurya and Menini, 2013) and microvilli of vomeronasal sensory neurons (Dibattista et al., 2012). TMEM16B is expressed at the synaptic terminal of

G. Betto, O.L. Cherian, and S. Pifferi contributed equally to this paper and are listed in alphabetical order.

Correspondence to Anna Boccaccio: boccaccio@ge.ibf.cnr.it

V. Cenedese's present address is Netherlands Institute for Neuroscience (NIN), 1105 BA Amsterdam, Netherlands.

Abbreviation used in this paper: CaCC, Ca^{2+}-activated Cl^- channel.

The Rockefeller University Press $30.00
J. Gen. Physiol. Vol. 143 No. 6 703–718
www.jgp.org/cgi/doi/10.1085/jgp.201411182

Published May 26, 2014

photoreceptors (Stöhr et al., 2009; Billig et al., 2011; Dauner et al., 2013), in hippocampal cells (Huang et al., 2012b), in the cilia of olfactory sensory neurons, and in the microvilli of vomeronasal sensory neurons (Stephan et al., 2009; Hengl et al., 2010; Rasche et al., 2010; Sagheddu et al., 2010; Billig et al., 2011; Dauner et al., 2012; Dibattista et al., 2012; Maurya and Menini, 2013). Studies with knockout mice for TMEM16A or TMEM16B (Rock and Harfe, 2008; Billig et al., 2011) or knockdown of these channels further confirmed a reduction in CaCC activity (Flores et al., 2009; Galietta, 2009; Hartzell et al., 2009; Huang et al., 2012a; Kunzelmann et al., 2012a,b; Pifferi et al., 2012; Sanders et al., 2012; Scudieri et al., 2012).

At present little is known about the structure-function relations for TMEM16A and TMEM16B. Bioinformatic models based on hydropathy analysis indicate that TMEM16 proteins have eight putative transmembrane domains (Caputo et al., 2008; Schroeder et al., 2008; Yang et al., 2008). In TMEM16A, the first putative intracellular loop contains regions that are involved both in the Ca^{2+} and voltage dependence (Caputo et al., 2008; Ferrera et al., 2009, 2011; Xiao et al., 2011). In TMEM16B, some glutamic acids in the first putative intracellular loop contribute to voltage dependence (Cenedese et al., 2012). A recent study identified splice variants for TMEM16B and found that N-terminal sequences affect Ca^{2+} sensitivity (Ponissery Saidu et al., 2013).

A region located between transmembrane domains 5 and 6 was proposed to form a reentrant loop exposed to the extracellular membrane side and to be part of the channel pore. Indeed, mutations of some basic amino acids in this region of TMEM16A, such as R621E, altered ion selectivity (Yang et al., 2008), although another study did not confirm the change in ion selectivity with this mutation (Yu et al., 2012). The same group proposed a different topology in which a reentrant loop is exposed to the intracellular membrane side of the membrane, also forming the third intracellular loop. Indeed, mutagenesis of two amino acids in this region, E702 and E705, largely modified Ca^{2+} sensitivity of TMEM16A (Yu et al., 2012). Experiments with chimeras between TMEM16A and TMEM16B support the finding that the third intracellular loop is important for Ca^{2+} sensitivity (Scudieri et al., 2013). At present, no mutations significantly altering ion selectivity have been found (Yu et al., 2012).

Recent studies reported that anions modify gating of TMEM16A. Ferrera et al. (2011) showed that membrane conductance increased at all voltages when extracellular Cl^- was replaced with I^- or SCN^-. Xiao et al. (2011) found that voltage-dependent gating of TMEM16A was facilitated by anions with high permeability or by an increase in extracellular Cl^-. Here, we investigate how extracellular and intracellular anions affect gating in TMEM16B and show the presence of a strong coupling between permeation and gating.

MATERIALS AND METHODS

Heterologous expression

Full-length mouse TMEM16B cDNA in pCMV-Sport6 mammalian expression plasmid was obtained from RZPD (clone identification: IRAVp968H1167D; NCBI Protein accession no. NP_705817.1). This is the retinal isoform with the same start site of the olfactory isoform used in Stephan et al. (2009) and contained exon 14 (Ponissery Saidu et al., 2013; named exon 13 in Stephan et al. [2009]). 2 µg cDNA was transfected into HEK 293T cells using FuGENE-6 or X-tremeGENE 9 (Roche). Cells were cotransfected with 0.2 µg pEGFP-C1 (Takara Bio Inc.) for fluorescent identification of transfected cells.

Electrophysiology

Electrophysiological recordings were performed in the whole-cell or inside-out patch-clamp configurations between 48 and 72 h from transfection, as previously described (Pifferi et al., 2006, 2009; Cenedese et al., 2012). Patch pipettes, made of borosilicate glass (World Precision Instruments, Inc.) with a PP-830 puller (Narishige), had a resistance of ∼3–5 MΩ or 1–2 MΩ, respectively, for whole-cell or inside-out experiments. Currents were recorded with an Axopatch 1D or Axopatch 200B amplifier controlled by Clampex 9 or 10 via a Digidata 1332A or 1440 (Axon Instruments or Molecular Devices). Data were low-pass filtered at 4 or 5 kHz and sampled at 10 kHz. Experiments were performed at room temperature (20–25°C). The bath was grounded via a 1 or 3 M KCl agar salt bridge connected to an Ag/AgCl reference electrode. A modified rapid solution exchanger (Perfusion Fast-Step SF-77B; Warner Instruments Corp.) was used to expose cells or excised membrane patches to different solutions.

In whole-cell recordings, one stimulation protocol consisted of voltage steps of 200-ms duration from a holding potential of 0 mV ranging from −100 to +100 mV (or from −200 to +200 mV), followed by a step to −100 mV. A single-exponential function was fitted to tail currents to extrapolate the tail current value at the beginning of the step to −100 mV. The conductance, G, was calculated as $G = I_t/(V_t - V_{rev})$, where I_t is the tail current, V_t is the tail voltage, −100 mV, and V_{rev} is the current reversal potential.

To estimate V_{rev}, channels were activated by a 200-ms pulse to +100 mV and then rapidly closed by application of hyperpolarizing steps. Single-exponential functions were fitted to tail currents to extrapolate the tail current value at each voltage step. Tail current values were plotted as a function of voltage, and the V_{rev} was estimated from a linear fit in a ±20-mV interval around V_{rev}.

In inside-out recordings, currents were recorded after the initial rundown, as described in Pifferi et al. (2009). Moreover, to allow the current to partially inactivate, patches were preexposed to the various Ca^{2+} concentrations for 500 ms before applying voltage protocols (Pifferi et al., 2009). Stimulation protocols consisted of a 100-mV voltage step of 200-ms duration from a holding potential of 0 mV, followed by a step to −100 mV or by double voltage ramps from −100 to +100 mV and back to −100 mV at 1-mV/ms rate, and the two I-V relations were averaged. The dose–response curves were obtained by exposing the patches for one second to solutions with increasing free Ca^{2+} concentrations. Leak currents measured in nominally 0 Ca^{2+} solutions were subtracted.

Ionic solutions

The same solutions were used for whole-cell and inside-out recordings, unless otherwise indicated. The standard extracellular solution contained (mM) 140 NaCl, 5 KCl, 2 $CaCl_2$, 1 $MgCl_2$, 10 glucose, and 10 HEPES, pH 7.4. The standard intracellular solution contained (mM) 140 CsCl, 10 HEPES, 10 HEDTA (or 5 EGTA), pH 7.2, and no added Ca^{2+} for the nominally 0 Ca^{2+} solution, or various amounts of $CaCl_2$, as calculated with the program WinMAXC (C. Patton, Stanford University, Stanford, CA), to

Published May 26, 2014

obtain free Ca^{2+} in the range between 0.18 and 100 µM (Patton et al., 2004). The intracellular solution with 1 mM Ca^{2+} contained (mM) 140 NaCl, 10 HEPES, and 1 $CaCl_2$, pH 7.2.

Cl^- in the extracellular solution was substituted with other anions by replacing NaCl on an equimolar basis (unless otherwise indicated) with NaX, where X is the substituted anion. The control extracellular solution (140 mM Cl) used in Fig. 4 contained (mM) 140 NaCl, 2.5 K_2SO_4, 2 $CaSO_4$, 1 $MgSO_4$, and 10 HEPES, pH 7.4. For the 11 mM Cl^- and 1 mM Cl^- solutions, NaCl was replaced on an equimolar basis with Na-gluconate or sucrose. The osmolarity was adjusted with sucrose. In the extracellular solutions containing NaF, divalent cations were omitted. When NaF was tested in the presence of 1 mM Ca^{2+} at the intracellular side of inside-out patches, no current was measured, probably because of the insolubility of CaF_2. When the patch pipette contained SCN^-, I^-, and Br^-, a 1 M KCl agar salt bridge was used to connect the Ag/AgCl wire to the recording solutions. Applied voltages were not corrected for liquid junction potentials. All chemicals were purchased from Sigma-Aldrich, except K_2SO_4 from Carlo Erba and $CaSO_4$ from J.T.Baker.

Data analysis

Data are presented as mean ± SEM, with *n* indicating the number of cells or patches. Statistical significance was determined using paired or unpaired *t* tests or ANOVA, as appropriate. When a statistically significant difference was determined with ANOVA, a post hoc Tukey's test was used to evaluate which data groups showed significant differences. P-values <0.05 were considered significant. Data analysis and figures were made with Igor Pro software (WaveMetrics). For the sake of clarity in the figures, the capacitative transients of some traces were trimmed.

RESULTS

Anion selectivity of TMEM16B

To determine the selectivity of TMEM16B to anions, we measured currents in the presence of various extracellular anions by replacing 140 mM NaCl in the Ringer solution with the Na salt of other anions. Fig. 1 A shows representative whole-cell recordings at 0.5 µM Ca^{2+} in the presence of Cl^-, after replacement of Cl^- with the indicated anions, and in Cl^- after wash out. Steady-state I-V relations are plotted in Fig. 1 B. To obtain a better estimate of V_{rev}, we also measured tail currents (Fig. 1, C and D). When Cl^- was replaced with gluconate, the outward currents decreased and V_{rev} shifted to positive values, revealing a lower permeability of gluconate than Cl^-. On the contrary, in the presence of SCN^-, I^-, NO_3^-, and Br^-, the outward currents were larger than those measured in Cl^- and V_{rev} shifted to negative values, indicating a higher permeability of the substituted anions than Cl^-. Permeability ratios (P_X/P_{Cl}) were SCN^- (3.0) > I^- (2.6) > NO_3^- (2.3) > Br^- (1.7) > Cl^- (1.0) > F^- (0.5) > gluconate (0.2). Fig. 1 (E and F) shows that the selectivity of TMEM16B estimated both from permeability ratios (P_X/P_{Cl}) and from chord conductance ratios (G_X/G_{Cl}) had the same sequence: $SCN^- > I^- > NO_3^- > Br^- > Cl^- > F^-$ > gluconate.

To obtain a direct comparison of selectivity in whole-cell and inside-out configurations, we also performed experiments in inside-out patches with different anions in the pipette solution, at the extracellular side of the membrane patch. Fig. 2 A shows currents activated at 1.5 µM Ca^{2+} using voltage ramps from −100 to +100 mV, in the presence of the indicated extracellular anions. P_X/P_{Cl} ratios were SCN^- (18.2) > I^- (7.1) > NO_3^- (4.1) > Br^- (2.3) > Cl^- (1.0) > F^- (0.3) > gluconate (0.1).

The sequence of P_X/P_{Cl} in inside-out patches was the same as that measured in whole-cell experiments, although the value of P_X/P_{Cl} for some anions was significantly higher when measured in inside-out than in whole-cell recordings (see Discussion). Moreover, we compared selectivity when anions were replaced at the extracellular or intracellular side of inside-out patches and showed that for each internal or external anion P_X/P_{Cl} was not significantly different (Fig. 2 B; data for intracellular I^-, NO_3^-, and Br^- are from Pifferi et al. [2009]).

We plotted P_X/P_{Cl} for extracellular anion substitution versus ionic radius (Fig. 2 C) or free energy of hydration (Fig. 2 D) of the test anion X. These plots show that P_X/P_{Cl} increases with the ionic radius, with the exception of F^- and gluconate. On the other side, P_X/P_{Cl} increases monotonically as the free energy of hydration decreases, indicating that the facility with which the anion enters the channel is related to its free energy of hydration.

Activation and deactivation kinetics

To characterize activation and deactivation kinetics in the presence of various anions, we analyzed the time-dependent components in response to voltage steps in whole-cell recordings at 0.5 µM Ca^{2+}. We measured the activation kinetics of currents in response to a voltage step to +100 mV from 0-mV holding voltage. The current in Cl^- had an instantaneous component, related to the fraction of channels open at 0 mV, followed by a time-dependent component caused by the increase in channel opening at +100 mV. The time-dependent component was fit by a single-exponential function to calculate the time constant of activation, τ_{act}. Fig. 3 A shows superimposed normalized currents from the same cell in Cl^- or with the indicated extracellular anion. No time-dependent component at +100 mV was observed when Cl^- was replaced with gluconate or F^- (not depicted). On average, τ_{act} at +100 mV in the presence of 0.5 µM Ca^{2+} was 7.7 ± 0.4 ms in Cl^-, whereas it became slower with more permeant anions: 28 ± 3 ms in SCN^-, 14.8 ± 1.2 ms in I^-, 12.5 ± 1.0 ms in NO_3^-, and 11.1 ± 1.4 ms in Br^-. The mean τ_{act} is plotted as a function of P_X/P_{Cl} in Fig. 3 C, showing that more permeant anions significantly prolonged the time course of activation, increasing the time necessary to respond to a depolarization compared with Cl^-.

To examine the deactivation kinetics, we calculated the time constant of current deactivation (τ_{deact}) by fitting with a single exponential function the tail currents obtained by a voltage step to −60 mV after a prepulse at

Published May 26, 2014

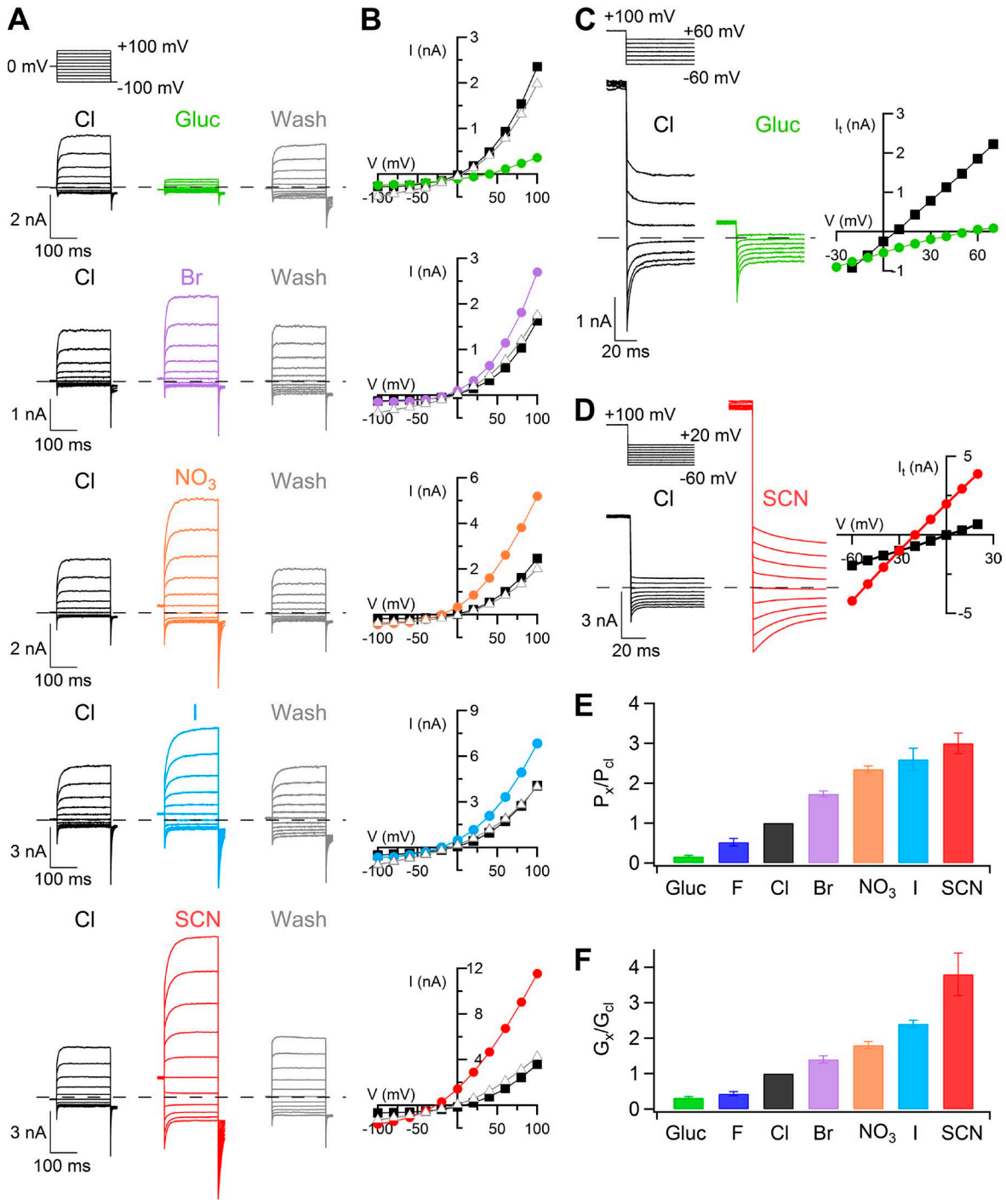

Figure 1. Extracellular anion selectivity in whole-cell recordings. (A) Representative whole-cell voltage-clamp recordings obtained with an intracellular solution containing 0.5 µM Ca^{2+}. Voltage steps of 200-ms duration were given from a holding voltage of 0 mV to voltages between −100 and +100 mV in 20-mV steps followed by a step to −100 mV, as indicated in the top part of the panel. Each cell was exposed to a control solution containing NaCl (black traces) and NaX, where X was the indicated anion, followed by wash out in NaCl (gray traces). (B) Steady-state I-V relations measured at the end of the voltage steps from the cells shown at the left (A) in control (squares), NaX (circles), or after wash out from the NaX solution (triangles). (C and D) Representative recordings from two cells at 0.5 µM Ca^{2+} obtained with a voltage protocol consisting of a prepulse to +100 mV from a holding voltage of 0 mV, followed by voltage steps between −60 and +70 mV (C) or −60 and +20 mV (D) in 10-mV steps. Only current recordings every 20 mV are shown in C. I-V relations measured from tail currents in Cl^- (squares) or in the indicated anion (circles) are shown on the right of each cell. (E) Mean permeability ratios (P_X/P_{Cl}) calculated with the Goldman-Hodgkin-Katz equation (n = 11–14). (F) Mean chord conductance ratios (G_X/G_{Cl}) measured in a 40-mV interval around V_{rev} per each anion (n = 4–14). Error bars indicate SEM.

Published May 26, 2014

+100 mV. Fig. 3 B shows superimposed normalized currents from the same cells of Fig. 3 A. In the presence of 0.5 µM Ca^{2+}, the mean τ_{deact} at −60 mV was 4.6 ± 0.3 ms in Cl^-, whereas it became faster with less permeant anions (2.3 ± 0.5 ms in F^- and 1.9 ± 0.2 ms in gluconate) and slower with more permeant anions (23.3 ± 4.8 ms in SCN^-, 9.3 ± 1.4 ms in I^-, 7.5 ± 0.5 ms in NO_3^-, and 5.8 ± 0.9 ms in Br^-). The mean τ_{deact} is plotted as a function of P_X/P_{Cl} in Fig. 3 C, showing that the deactivation kinetics prolonged as a function of permeability ratios.

Voltage dependence

To investigate the effect of anions on the voltage dependence of channel activation in whole-cell recordings, we extended voltage steps from −200 to +200 mV to obtain a better estimate of voltage dependence (Fig. 4). The voltage dependence of steady-state activation (G-V relation) was analyzed measuring tail currents at the beginning of a step to −100 mV after the prepulse voltage steps. The conductance was plotted versus membrane voltage and fit by the Boltzmann equation:

$$G = G_{max} / \left\{1 + \exp\left[z\left(V_{1/2} - V\right)F/RT\right]\right\}, \quad (1)$$

where G is the conductance, z is the equivalent gating charge associated with voltage-dependent channel opening, V is the membrane potential, $V_{1/2}$ is the membrane potential producing half-maximal activation, F is the Faraday constant, R is the gas constant, and T is the absolute temperature. G_{max} was evaluated for each cell from a global fit of G-V relations in control, after anion substitutions, and after wash out.

In a first set of experiments, we decreased the extracellular Cl^- concentration from 140 to 11 mM or 1 mM by replacing Cl^- with equimolar concentrations of the less permeant anion gluconate, in the presence of 1.5 µM Ca^{2+} (Fig. 4, A and B). Fig. 4 C shows that the decrease of $[Cl^-]_o$ produced a rightward shift of the G-V relation. From a global fit of G-V relations with the same G_{max} and equivalent gating charge (z), $V_{1/2}$ significantly changed from +79 ± 13 mV in 140 mM Cl^- to +187 ± 14 mV in 11 mM $[Cl^-]_o$. When Cl^- was further decreased to 1 mM, $V_{1/2}$ was +205 ± 17 mV, which was not significantly different from the $V_{1/2}$ value in 11 mM.

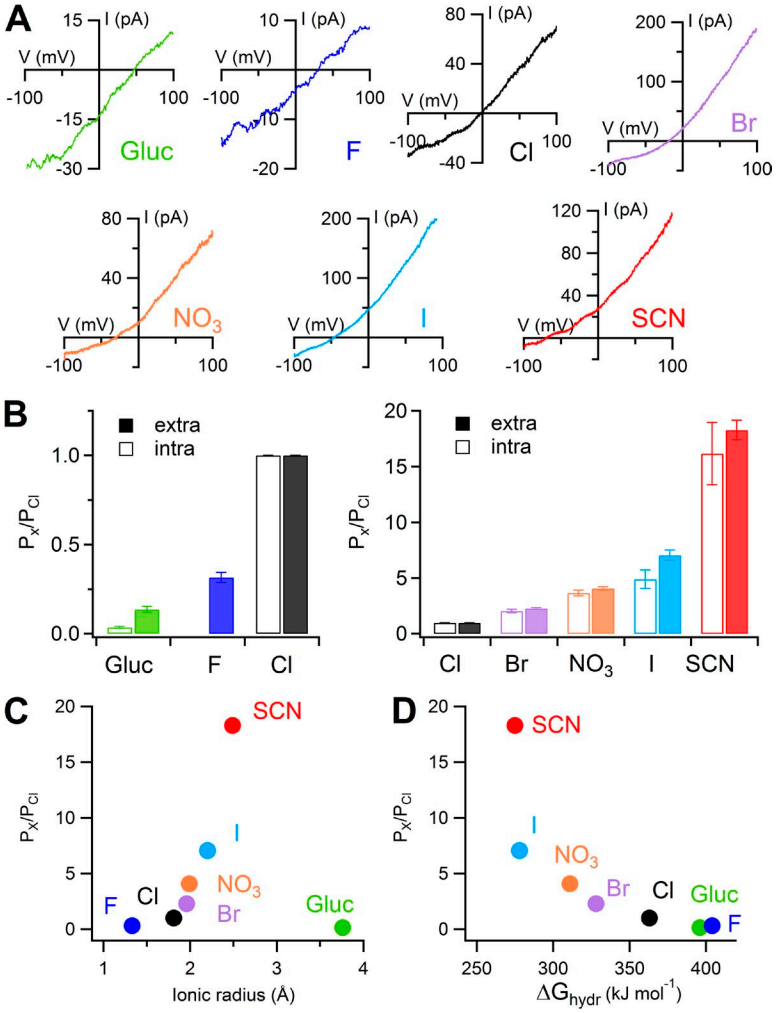

Figure 2. Anion selectivity in inside-out patches. (A) I-V relations in 1.5 µM Ca^{2+} obtained from a ramp protocol in inside-out membrane patches. In each patch, the pipette solution contained 140 mM NaCl or the Na salt of the indicated anion. Leakage currents measured in 0 Ca^{2+} were subtracted. (B) Comparison of mean permeability ratios (P_X/P_{Cl}) calculated with the Goldman-Hodgkin-Katz equation with different anions in the internal (n = 5–6; data for intracellular I^-, NO_3^-, and Br^- are from Pifferi et al. [2009]) or external solution (n = 6–12; as experiments shown in A). Error bars indicate SEM. (C and D) Permeability ratios (P_X/P_{Cl}), obtained from experiments as in A, plotted versus ionic radius (C) or free energy of hydration (D) of the extracellular anion. Ionic radius and free energy of hydration were taken from Table 1 of Smith et al. (1999).

Published May 26, 2014

The mean z value was 0.29 ± 0.02 (n = 10). Similar results were obtained when $[Cl^-]_o$ was reduced by partial substitution with sucrose: $V_{1/2}$ changed from +70 ± 19 mV in 140 mM Cl^- to +209 ± 23 mV in 11 mM Cl^- and +199 ± 23 mV in 1 mM Cl^-, confirming that the shift was caused by $[Cl^-]_o$ reduction rather than the presence of gluconate (Fig. 4 D).

These results show that $V_{1/2}$ increased when extracellular Cl^- was reduced by substitution with gluconate or with sucrose, indicating that fewer channels can be activated by depolarization when the external Cl^- concentration is reduced. The opposite trend, consisting of a leftward shift of the G-V relation at a given $[Ca^{2+}]_i$, was observed when Cl^- was partially replaced by the more permeant anion SCN^- (Fig. 5). Indeed, in the presence of 0.5 µM Ca^{2+} (Fig. 5, A–C) or 1.5 µM Ca^{2+} (Fig. 5, D–F), the substitution of Cl^- with SCN^- produced a leftward shift of the G-V relations. Upon a further increase of Ca^{2+} concentration to 13 µM (Fig. 5, G and H), the substitution of Cl^- with SCN^- caused an almost complete activation of the current at all membrane potentials in all of the experiments, preventing the possibility to numerically estimate $V_{1/2}$, which was shifted to very negative potentials << −200 mV (Fig. 5, G and H).

Data from several cells at 0.5 or 1.5 µM Ca^{2+} are summarized in Fig. 5 I, in which mean $V_{1/2}$ values are shown. At 0.5 µM Ca^{2+}, the mean $V_{1/2}$ significantly changed from +195 ± 19 mV in Cl^- to +11 ± 35 mV in SCN^- (n = 4). At 1.5 µM Ca^{2+}, the mean $V_{1/2}$ significantly changed from +84 ± 20 mV in Cl^- to −189 ± 20 mV in SCN^- (n = 9; in some experiments with SCN^- at 1.5 µM Ca^{2+}, in which the current was fully activated and $V_{1/2}$ could not be evaluated, we considered $V_{1/2}$ = −250 mV). The mean z value was not significantly different: 0.33 ± 0.04 and 0.26 ± 0.01, respectively, in 0.5 and 1.5 µM Ca^{2+}.

To investigate whether the leftward shift of the G-V relation was specific to SCN^- or was present also with other anions more permeant than Cl^-, we performed experiments changing the external anion from Cl^- to NO_3^- in the presence of 1.5 µM Ca^{2+} (representative recordings not depicted). A leftward shift of the G-V relation was observed also with NO_3^-, and the mean $V_{1/2}$ significantly changed from +52 ± 16 mV in Cl^- to −101 ± 18 mV in NO_3^- (n = 6), as shown in the right columns of Fig. 5 I. Thus, $V_{1/2}$ decreased in the presence of SCN^- or NO_3^-, indicating that more channels can be activated by depolarization in the presence of some anions more permeant than Cl^-.

Ca^{2+} dependence

To investigate whether different anions modify the Ca^{2+} dependence of TMEM16B activation, we measured dose–response relations. The best technique to measure the Ca^{2+} dependence of TMEM16B is to use excised inside-out patches because channels can be activated by several $[Ca^{2+}]_i$ in the same patch and the leakage current in the absence of Ca^{2+} can be subtracted from each measurement. However, as we have previously shown, the current induced by TMEM16B presents a rundown in activity in inside-out patches (Pifferi et al., 2009), limiting the number of recordings that can be compared on the same patch. For this reason, we measured currents activated by various $[Ca^{2+}]_i$ at only two voltage steps of +100 or −100 mV, as shown in Fig. 6 A. Currents in the presence of each extracellular anion were measured at the end of each voltage step by

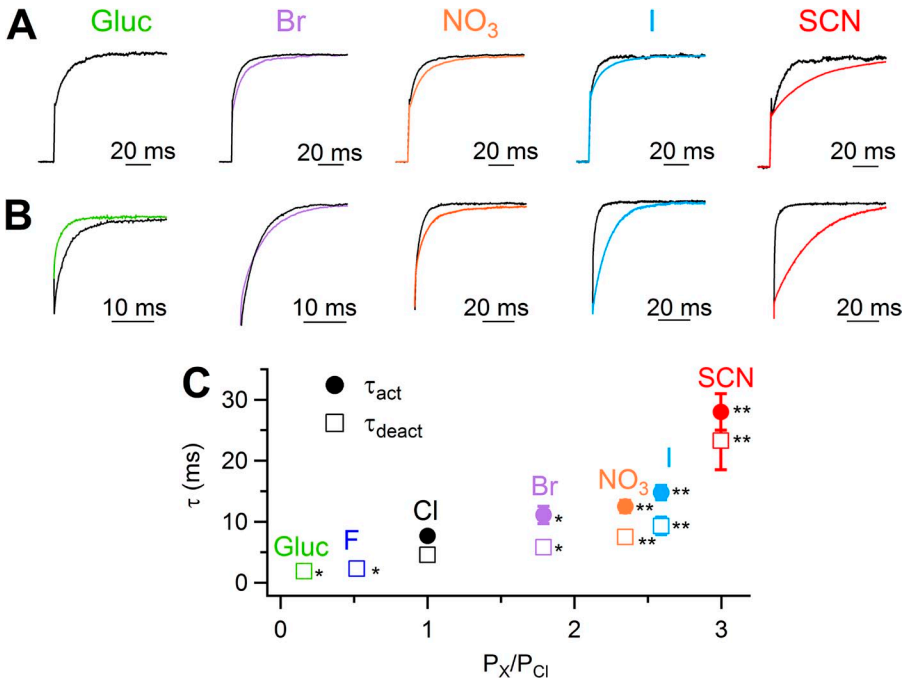

Figure 3. Activation and deactivation kinetics in whole cell with various extracellular anions. (A and B) Normalized single traces from whole-cell currents in the presence of extracellular NaCl or the Na salt of the indicated anion in 0.5 µM Ca^{2+}. Voltage protocol similar to Fig. 1 (C and D), with a voltage step to +100 mV (A) from a holding voltage of 0 mV and followed by a step to −60 mV (B). Trace in gluconate in A is not shown because at the test potential there is a negligible time-dependent component. (C) Current activation and deactivation were fitted with a single exponential (fit not depicted for clarity). Mean activation time constants (τ_{act}) at +100 mV and deactivation time constants (τ_{deact}) at −60 mV were plotted versus permeability ratios (n = 8–14; *, P < 0.05; **, P < 0.01, paired t test with Cl^-). Error bars indicate SEM.

Published May 26, 2014

taking the mean current between 150 and 190 ms, normalized to the maximal current at the same voltage and plotted versus $[Ca^{2+}]_i$ (Fig. 6 B). Data were fitted by the Hill equation:

$$I / I_{max} = \left[Ca^{2+}\right]_i^{n_H} / \left(\left[Ca^{2+}\right]_i^{n_H} + K_{1/2}{}^{n_H}\right), \quad (2)$$

where I is the current, I_{max} is the maximal current, $K_{1/2}$ is the half-maximal $[Ca^{2+}]_i$, and n_H is the Hill coefficient.

Mean $K_{1/2}$ values at +100 mV were lower for anions more permeant than Cl^- but increased for less permeant anions (Fig. 6, B, C, and E). At −100 mV, the mean $K_{1/2}$ value for SCN^- was smaller than the value in Cl^-, whereas there was no significant difference for values between the other anions and Cl^- (Fig. 6 C). Moreover, we observed a significant increase for Hill coefficient values (n_H) both at −100 and +100 mV for NO_3^-, I^-, and SCN^- compared with Cl^- (Fig. 6 D). These results indicate that, at +100 mV, a lower $[Ca^{2+}]_i$ is sufficient to activate 50% of the maximal current in the presence of external anions more permeant than Cl^-, whereas a higher $[Ca^{2+}]_i$ is required for less permeant anions.

To further investigate how external SCN^- modifies the Ca^{2+} dependence of TMEM16B compared with Cl^-, we measured dose–response relations in whole-cell recordings at different voltages and compared the results with values measured with voltage ramps in inside-out patches (Fig. 7). The whole-cell configuration has the advantage of allowing the comparison of recordings with different extracellular anions in the same cell but has the disadvantage that different $[Ca^{2+}]_i$ values have to be tested on different cells. To compare currents from different cells, current densities were calculated by dividing current amplitudes by the cell capacitance. Fig. 7 A shows whole-cell currents at various $[Ca^{2+}]_i$ in external Cl^- or SCN^-. In each cell, at a given $[Ca^{2+}]_i$, both inward and outward currents in SCN^- significantly increased with respect to those in Cl^-. Dose–response relations in whole-cell were analyzed by measuring tail currents at the beginning of the step to −100 mV after prepulses ranging from −100 to +100 mV in steps of 20 mV. Mean conductance densities in the presence of external Cl^- or SCN^- were calculated, plotted versus $[Ca^{2+}]_i$, and fit at each voltage by the Hill equation:

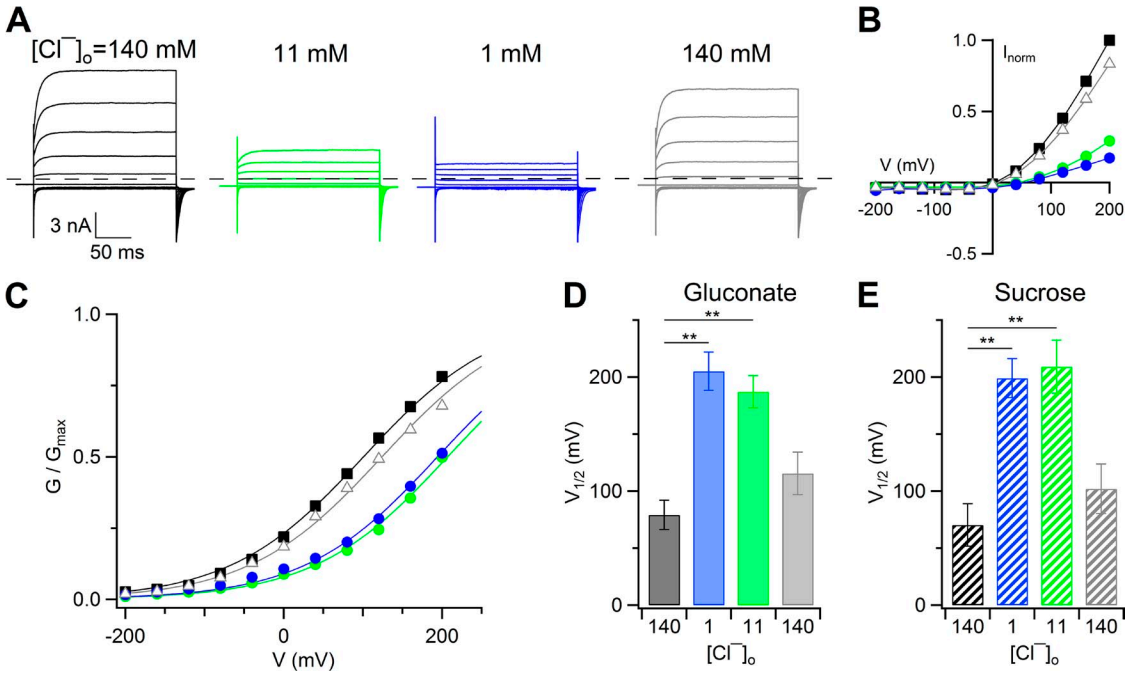

Figure 4. Changes of voltage dependence in whole cell when extracellular Cl^- was substituted with less permeant gluconate or sucrose. (A) Representative whole-cell voltage-clamp recordings at 1.5 µM Ca^{2+}. The same cell was exposed to a solution containing NaCl (black traces), Na-gluconate (green and blue traces), and back to NaCl (gray traces). Voltage steps of 200-ms duration were given from a holding voltage of 0 mV to voltages between −200 and +200 mV in 40-mV steps, followed by a step to −100 mV. (B) Steady-state I-V relations measured at the end of the voltage steps from the cell shown at the left (A) normalized to the control value at +200 mV. Control values are represented by black squares, wash out by gray triangles, and 11 mM and 1 mM Cl^-, respectively, by the green and blue circles. (C) Normalized conductances calculated from tail currents at −100 mV after prepulses between −200 and +200 mV plotted versus the prepulse voltage for the experiment shown in A. Symbols as in B. Lines are the fit to the Boltzmann equation (Eq. 1). (D and E) Mean $V_{1/2}$ values in the presence of gluconate (D; $n = 10$) or sucrose (E; $n = 3$) at the indicated $[Cl^-]_o$ (**, $P < 0.01$, Tukey's test after ANOVA for repeated measurements). Error bars indicate SEM.

Published May 26, 2014

$$G = G_{max}\left[Ca^{2+}\right]_i^{n_H} / \left(\left[Ca^{2+}\right]_i^{n_H} + K_{1/2}{}^{n_H}\right), \quad (3)$$

where G is the conductance density, G_{max} is the maximal conductance density, $K_{1/2}$ is the half-maximal $[Ca^{2+}]_i$, and n_H is the Hill coefficient.

The comparison between dose–response relations at +100 and −100 mV in external Cl^- and SCN^- is illustrated in Fig. 7 B. At +100 mV, $K_{1/2}$ was 1.2 µM in Cl^- and decreased to 0.4 µM in SCN^-. Fig. 7 C shows that $K_{1/2}$ slightly decreased as a function of voltage from 7.6 µM at −100 mV to 1.2 µM at +100 mV in Cl^- and from 1.1 µM at −100 mV to 0.4 µM at +100 mV in SCN^-. The Hill coefficient in Cl^- was not voltage dependent, with a value of 1.1 at both −100 and +100 mV, whereas in SCN^- n_H was 2.2 at −100 mV and 3.5 at +100 mV (Fig. 7 D). Similar results were obtained from experiments in the inside-out configuration. Currents at various $[Ca^{2+}]_i$ were activated with voltage ramps with Cl^- (Fig. 7 E) or SCN^- (Fig. 7 F) in the patch pipette.

Normalized dose–response relations were fit with the Hill equation (Eq. 2 and Fig. 7 G). Fig. 7 (H and I) shows that $K_{1/2}$ and n_H values at different voltages were similar in inside-out and in whole-cell configurations, further confirming that external SCN^- increased the apparent Ca^{2+} affinity at all voltages compared with Cl^- and increased n_H at some positive voltages.

To determine whether SCN^- modifies channel gating also from the intracellular side, we measured the voltage dependence of activation in whole-cell recordings in the presence of SCN^- instead of Cl^- at 0.5 µM Ca^{2+} (Fig. 8 A). G-V relations showed that $V_{1/2}$ was −0.4 ± 11 mV in intracellular SCN^- (n = 11; z = 0.33 ± 0.01), whereas it was +195 ± 19 mV in intracellular Cl^- (Fig. 8, B and C; for Cl^- data from Fig. 5 I).

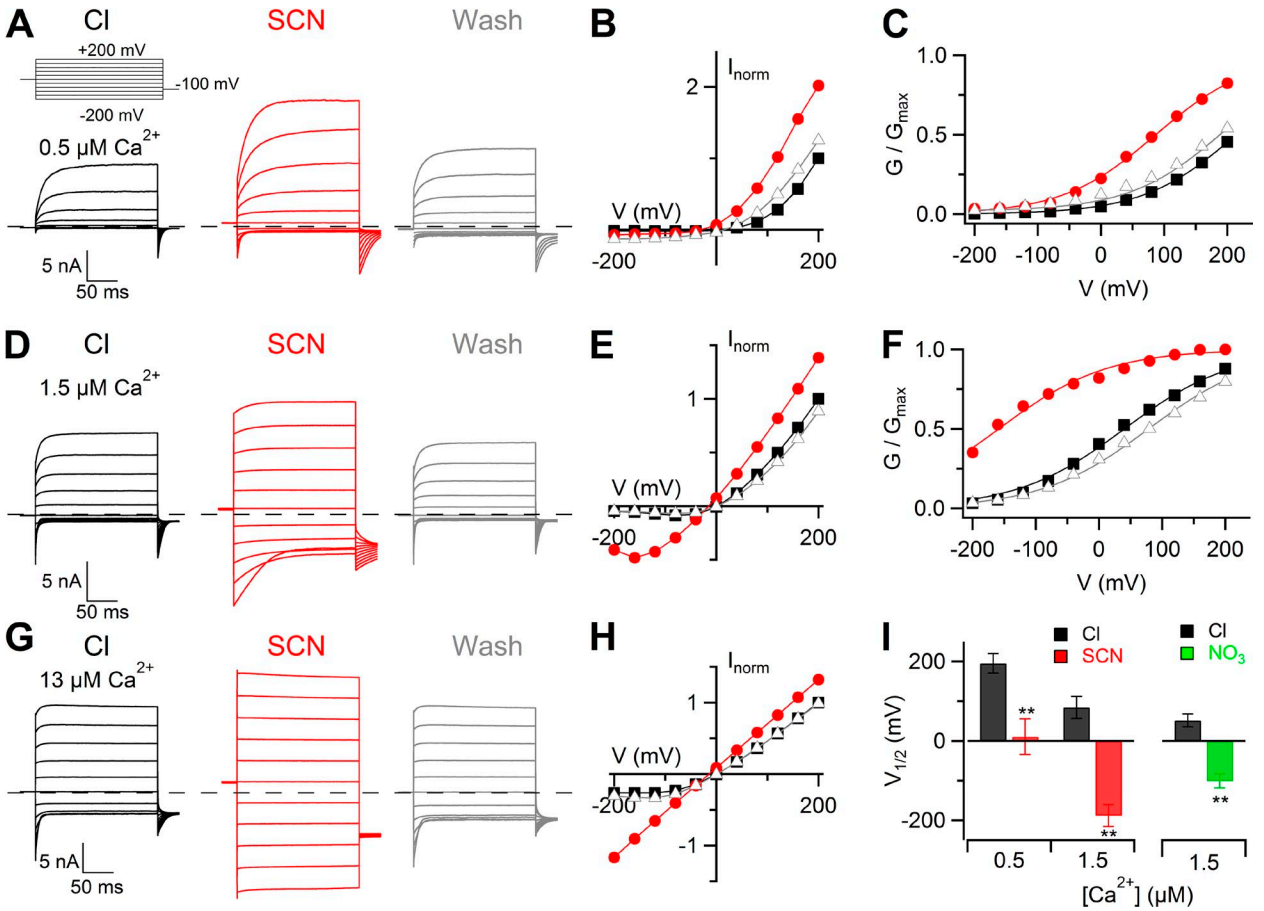

Figure 5. Changes of voltage dependence in whole cell when extracellular Cl^- was substituted with more permeant anions. (A, D, and G) Representative whole-cell voltage-clamp recordings at the indicated $[Ca^{2+}]_i$. The same cell was exposed to a solution containing NaCl (black traces), NaSCN (red traces), and back to NaCl (gray traces). Voltage steps of 200-ms duration were given from a holding voltage of 0 mV to voltages between −200 and +200 mV in 40-mV steps, followed by a step to −100 mV, as indicated in the top part of A. (B, E, and H) Steady-state I-V relations measured at the end of the voltage steps from the cell shown at the left (A, D, and G, respectively) in control (squares), NaSCN (circles), and after wash out (triangles). (C and F) Normalized conductances calculated from tail currents at −100 mV after prepulses between −200 and +200 mV plotted versus the prepulse voltage. Symbols as in B and E. Lines are the fit to the Boltzmann equation (Eq. 1). (I) Mean $V_{1/2}$ values at 0.5 µM Ca^{2+} (n = 4) or 1.5 µM Ca^{2+} (n = 9 in Cl^-, 6 in NO_3^-) for Cl^-, SCN^-, or NO_3^- (**, P < 0.01 paired t test). Error bars indicate SEM.

Published May 26, 2014

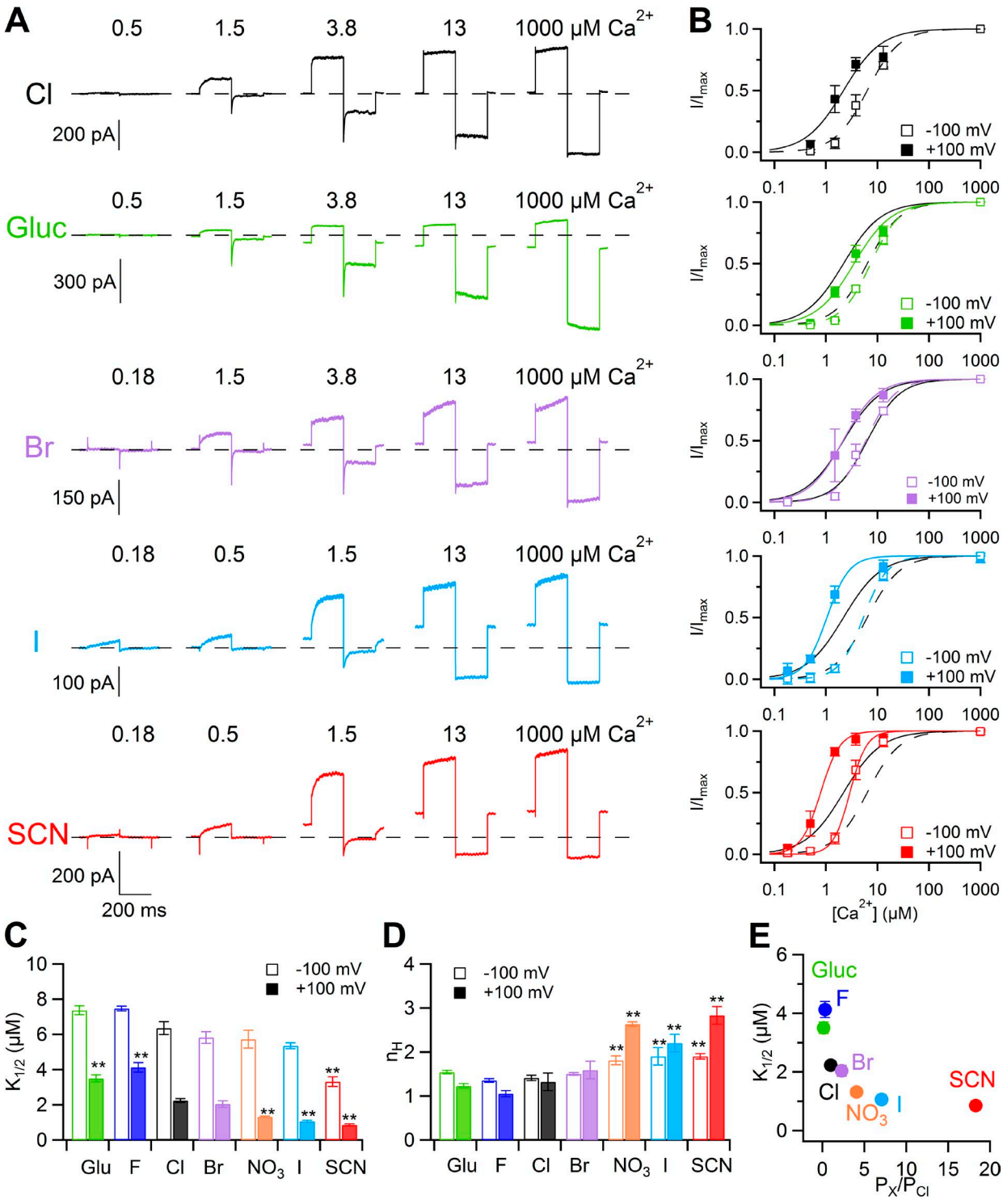

Figure 6. Ca^{2+} sensitivity in inside-out patches with various extracellular anions. (A) Each row shows current traces from the same inside-out patch with the indicated anion in the pipette. The cytoplasmic side was exposed to $[Ca^{2+}]_i$ ranging from 0.18 to 1 mM. Voltage steps of 200-ms duration were given from a holding voltage of 0 mV to +100 mV, followed by a 200-ms step to −100 mV. Leakage currents measured in 0 Ca^{2+} were subtracted. (B) Dose–response relations of activation by Ca^{2+} obtained by normalized currents at −100 or +100 mV, fitted to the Hill equation (Eq. 2). Black lines are the fit to the Hill equation in external Cl^-. (C) Comparison of the mean $K_{1/2}$ values at −100 or +100 mV in the presence of various anions (n = 5–13; **, P < 0.01 comparison with Cl^- by Tukey's test after ANOVA). (D) Comparison of the mean n_H values at −100 or +100 mV in the presence of various anions (n = 5–13; **, P < 0.01 comparison with Cl^- by Tukey's test after ANOVA). (E) Mean $K_{1/2}$ values at +100 mV plotted versus permeability ratios. Error bars indicate SEM.

Published May 26, 2014

Moreover, we measured dose–response relations for Ca^{2+} in inside-out patches in the presence of SCN^- in the bathing solution (Fig. 8 D). The comparison between dose–response relations at +100 and −100 mV in intracellular Cl^- and SCN^- is illustrated in Fig. 8 E. At +100 mV, $K_{1/2}$ was 2.2 ± 0.1 µM in Cl^- and decreased to 0.85 ± 0.06 µM in SCN^-; at −100 mV, $K_{1/2}$ was 6.4 ± 0.4 µM in Cl^- and 3.3 ± 0.3 µM in SCN^-. The Hill coefficient in Cl^- was not voltage dependent, with a value of 1.41 ± 0.06 at −100 mV and 1.4 ± 0.3 at +100 mV, whereas in SCN^- n_H was 1.90 ± 0.06 at −100 mV and 2.2 ± 0.2 at +100 mV. These results show that not only extracellular, but also intracellular SCN^- affects gating of TMEM16B by producing a leftward shift of the voltage dependence and an increase of the apparent affinity for Ca^{2+}.

DISCUSSION

In this study, we have provided evidence that, in the TMEM16B channel, permeant anions modulate the kinetics of current activation and deactivation, as well as the voltage and apparent Ca^{2+} sensitivity. Indeed, extracellular anions more permeant than Cl^- prolonged both τ_{act} and τ_{deact} at low Ca^{2+}, shifted $V_{1/2}$ toward more negative values, and decreased $K_{1/2}$, favoring the channel's opening. In contrast, extracellular anions less permeant than Cl^- shortened τ_{deact}, shifted $V_{1/2}$ toward more positive values, and increased $K_{1/2}$, contributing to channel closure. Moreover, a decrease of extracellular Cl^- by replacement with sucrose also shortened τ_{deact} (not depicted) and shifted $V_{1/2}$ toward more positive values, favoring the closed state of the channel. Overall, these results indicate that the most permeant anions

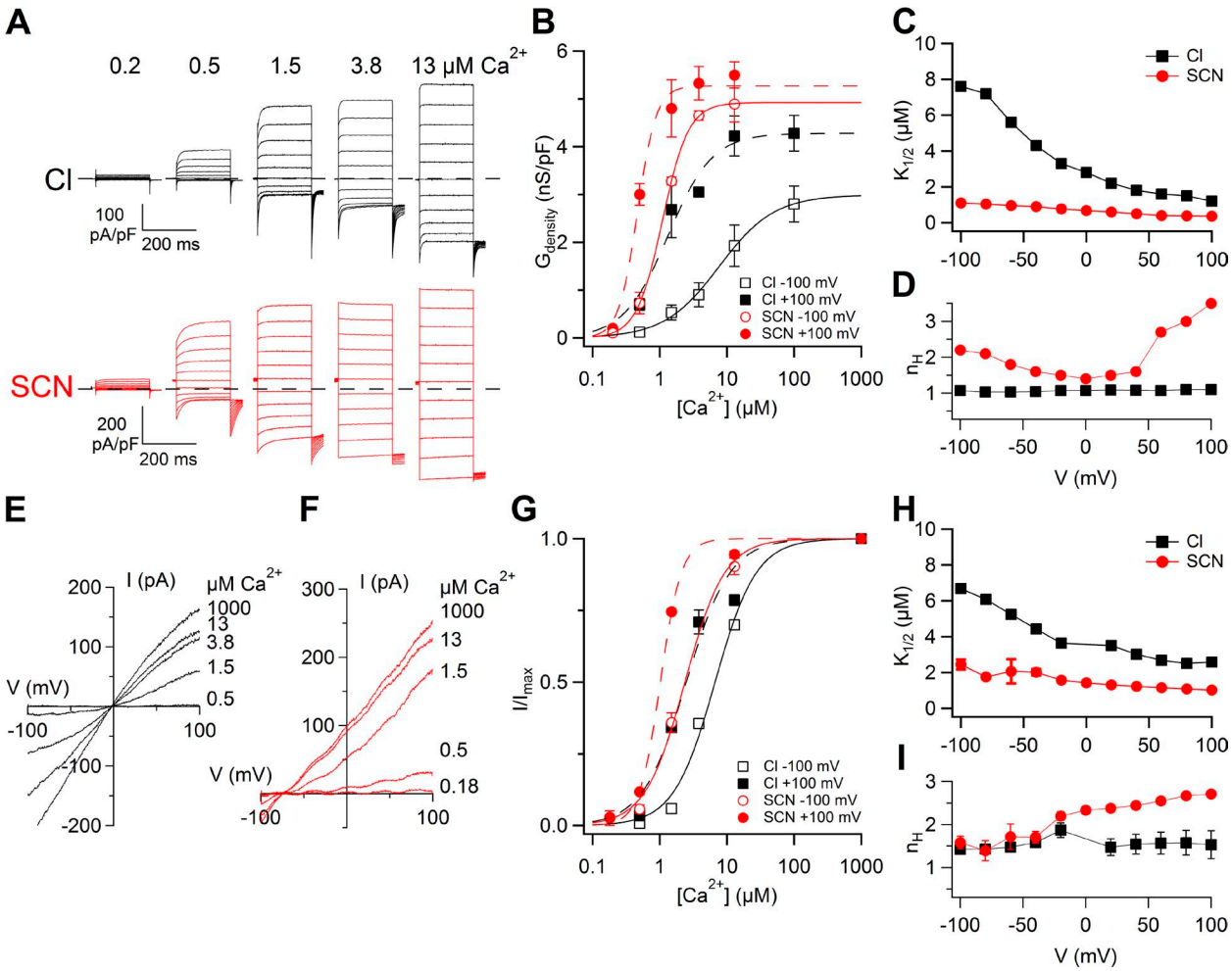

Figure 7. Comparison of Ca^{2+} sensitivity in whole-cell and inside-out patches. (A) Whole-cell recordings obtained with various $[Ca^{2+}]_i$ in extracellular Cl^- or SCN^-. The same cells were recorded in Cl^- or SCN^- for each $[Ca^{2+}]_i$. Voltage protocol as in Fig. 1 A. (B) Comparison of dose–responses in Cl^- or SCN^- at −100 and +100 mV in whole cell obtained from conductance density calculated from tail currents plotted versus $[Ca^{2+}]_i$ (n = 3–5). Lines are the fit to the Hill equation (Eq. 3). (C and D) Mean $K_{1/2}$ and n_H values from whole-cell recordings plotted versus voltage. (E and F) Currents in an inside-out patch activated by voltage ramps at the indicated $[Ca^{2+}]_i$ in symmetrical Cl^- (E) or in extracellular SCN^- (F). Leakage currents measured in 0 Ca^{2+} were subtracted. (G) Comparison of dose–responses in Cl^- or SCN^- obtained by normalized currents at −100 or +100 mV, fitted to the Hill equation (Eq. 2). (H and I) Mean $K_{1/2}$ and n_H values from inside-out patch recordings plotted versus voltage (n = 6–7). Error bars indicate SEM.

Published May 26, 2014

and Cl^- itself favor the open state of TMEM16B. Furthermore, we investigated the effect of replacing Cl^- with SCN^- at the intracellular side of the channel and found similar gating modifications as from the extracellular side.

Anion selectivity

The sequence of permeability ratios measured in whole-cell recordings when extracellular Cl^- was replaced with other anions was SCN^- (3.0) > I^- (2.6) > $NO3^-$ (2.3) > Br^- (1.7) > Cl^- (1.0) > F^- (0.5) > gluconate (0.2). Moreover, the sequence of relative chord conductance followed the same order. Both sequences are in agreement, for the corresponding anions, with measurements obtained by Adomaviciene et al. (2013; see their Fig. 4) on TMEM16B and TMEM16A.

The order of anions in the sequence was the same when measurements were obtained both from whole-cell and inside-out patches. However, permeability ratios in inside-out patches were SCN^- (18.2) > I^- (7.1) > NO_3^- (4.1) > Br^- (2.3) > Cl^- (1.0) > F^- (0.3) > gluconate (0.1), showing larger differences among anions than in whole-cell recordings. Indeed, we measured a difference in V_{rev} when anions were exchanged in the whole-cell or inside-out configurations. For example, when external Cl^- was replaced with SCN^-, the mean V_{rev} in whole cell was -27 ± 2 mV, whereas in the same ionic conditions with SCN^- in the pipette, V_{rev} in inside out was -70 ± 1 mV. We measured a less negative V_{rev} in whole-cell than in inside-out recordings also with the other anions more permeant than Cl^-. This difference may be the result of several reasons, including the loss of some intracellular factor after patch excision, such as calmodulin, and/or ion accumulation effects caused by restricted ion diffusion altering the ion concentration gradient. If SCN^- or other anions entering the cell accumulated at the intracellular side of the membrane, the concentration gradient between the intracellular and extracellular side would decrease, producing a less negative V_{rev} value. The differences we observed are consistent with anion accumulation at the intracellular surface membrane in whole cell, whereas the continuous flow of solutions containing Cl^- in inside-out membrane patches is likely to prevent or reduce the possibility of anion accumulation at the intracellular side of the membrane. In addition, we cannot exclude a difference induced by effects after patch excision. Jung et al. (2013) reported that the anion selectivity of TMEM16A is dynamically regulated by the Ca^{2+}–calmodulin complex, whereas the effect of Ca^{2+}–calmodulin on selectivity of TMEM16B has not been investigated yet. In any case, despite the difference in some values of permeability ratios, we obtained the same sequence for anion permeability ratios measured with different patch-clamp configurations, confirming that the permeability ratio sequence for TMEM16B follows the Hofmeister sequence or lyotropic sequence, in which anions with lower dehydration energy (lyotropos) have higher permeability compared with anions with higher dehydration energy (Wright and Diamond, 1977; Zhang and Cremer, 2006). As previously pointed out, "the relationship between anion permeability and anion energy of hydration supports the notion that anion dehydration

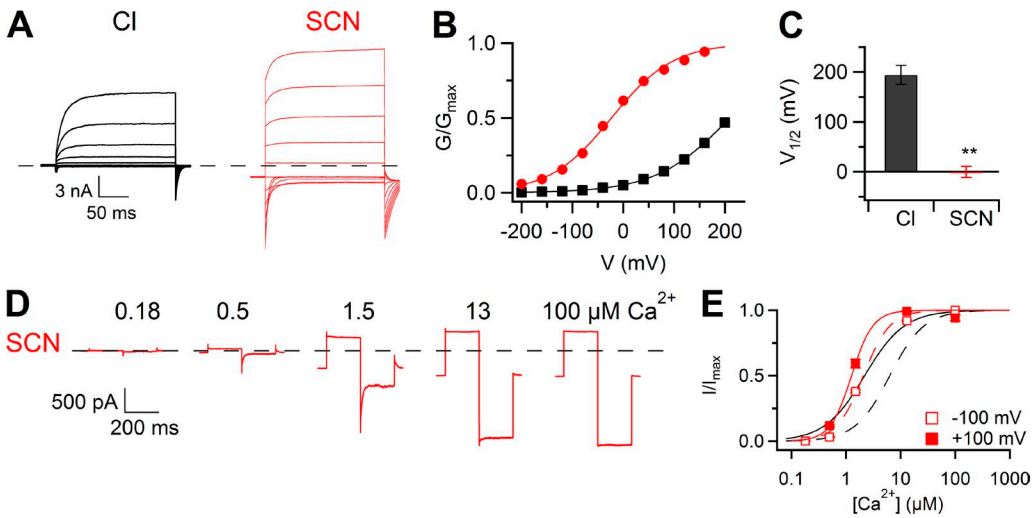

Figure 8. Effect of intracellular SCN^-. (A) Whole-cell recordings at 0.5 μM Ca^{2+} with a standard intracellular solution containing Cl^- (same traces of Fig. 5 A) or SCN^-. Voltage steps as in Fig. 5. (B) Normalized conductances calculated from tail currents at −100 mV after prepulses between −200 and +200 mV plotted versus the prepulse voltage for the experiments shown in A. Lines are the fit to the Boltzmann equation (Eq. 1). (C) Mean $V_{1/2}$ values in the presence of Cl^- ($n = 4$; same data of Fig. 5 I) or SCN^- ($n = 11$; **, $P < 0.01$ unpaired t test). Error bars indicate SEM. (D) Traces from an inside-out patch with SCN^- at the intracellular side. $[Ca^{2+}]_i$ ranged from 0.18 to 100 μM. Voltage steps of 200-ms duration were given from a holding voltage of 0 to +100 mV, followed by a 200-ms step to −100 mV. Leakage currents measured in 0 Ca^{2+} were subtracted. (E) Dose–response relations of activation by Ca^{2+} obtained by normalized currents at −100 or +100 mV ($n = 11$), fitted to the Hill equation (Eq. 2). Black lines are the fit to the Hill equation in symmetrical Cl^- solutions.

Published May 26, 2014

is the limiting step in permeation" (Dawson et al., 1999; Linsdell et al., 2000).

Activation and deactivation kinetics

We found that anions more permeant than Cl^- slowed both the activation and deactivation time constants at 0.5 µM Ca^{2+}. τ_{act} at +100 mV was 7.7 ± 0.4 ms in Cl^- and almost doubled to 14.8 ± 1.2 ms in I^-. τ_{deact} at −60 mV was 4.6 ± 0.3 ms in Cl^- and also increased twice to 9.3 ± 1.4 ms in I^-. For anions less permeant than Cl^-, currents activated by depolarizing voltage steps lost any time dependence; although the τ_{deact} values were shortened in gluconate, τ_{deact} at −60 mV decreased to 1.9 ± 0.2 ms.

These results can be compared with the limited number of previous studies investigating the effects of permeant anions on endogenous CaCCs. Although some differences in permeability sequences were reported in different cells, in each case there was a correlation between changes in kinetics and permeability ratios.

Evans and Marty (1986) reported the following sequence of permeability ratios for CaCCs in isolated cells from lacrimal glands when Cl^- was replaced with some extracellular anions: I^- (2.71) > NO_3^- (2.39) > Br^- (1.59) > Cl^- (1) > F^- (0.18) > isethionate (0.11) = methanesulfonate (0.11) > glutamate (0.05). The same authors investigated current kinetics at 0.5 µM Ca^{2+} and showed that replacement of extracellular Cl^- with the two most permeant anions in these cells, I^- or NO_3^-, led to significant alterations of both τ_{act} at +20 mV and τ_{deact} at −60 mV. The value of τ_{act} in Cl^- was 241 ± 53 ms and was shortened 0.91 and 0.83 times in I^- and NO_3^-, respectively. The value of τ_{deact} was 170 ± 45 ms in Cl^- and increased 1.54 and 1.38 times in I^- and NO_3^-, respectively. Other anions such as Br^-, isethionate, methanesulfonate, or glutamate did not significantly modify current kinetics, indicating that "the more permeant the anion, the greater was its effect on channel kinetics" (Evans and Marty, 1986).

Greenwood and Large (1999) studied the effects of extracellular anions on the deactivation kinetics of CaCCs in smooth muscle cells isolated from rabbit portal vein with the perforated patch-clamp technique. The sequence of permeability ratios was: SCN^- > I^- > Br^- > Cl^- >> isethionate. The same authors reported that τ_{deact} was prolonged by the external anions SCN^-, I^-, and Br^-, which were more permeant than Cl^-, whereas it was accelerated by the less permeant anion isethionate. Indeed, τ_{deact} was 97 ± 7 ms in Cl^-, 278 ± 19 ms in SCN^-, 157 ± 37 ms in I^-, and 67 ± 5 ms in isethionate, showing a strong correlation between permeability ratios and changes in kinetics of deactivation, suggesting that gating is linked to permeability.

In another study, Perez-Cornejo and Arreola (2004) obtained whole-cell recordings from acinar cells dissociated from rat parotid gland and measured the following permeability ratios: SCN^- (4.3) > I^- > (2.6) > NO_3^- (2.0) > Br^- (1.6) > Cl^- (1) > F^- (0.3) > aspartate (0.1) > glutamate (0.05). Kinetics of current activation and deactivation were measured in the presence of 250 nM Ca^{2+}. Activation kinetics increased about fourfold in SCN^- and about twofold in NO_3^-. Deactivation kinetics increased about threefold in SCN^- and about twofold in NO_3^-, whereas it decreased in F^-. As in previous studies, the effects on kinetics largely followed the order of the permeability sequence, with anions with permeability ratios > 1 producing larger effects. Also in this case, SCN^- efficacy was much larger than what was observed with the other more permeant anions, an effect consistent with the high permeability of SCN^-.

Although results from CaCCs on different cells are heterogeneous, all share the same property that τ_{act} and τ_{deact} were affected by extracellular permeant anions according with their permeability ratios, similarly to our results. τ_{deact} was prolonged or shortened by anions more or less permeant than Cl^-, respectively. One important difference from our results is that we found that τ_{act} for the TMEM16B current was prolonged by anions more permeant than Cl^-, whereas in the previous work on endogenous CaCCs, τ_{act} was shortened (Evans and Marty, 1986; Perez-Cornejo and Arreola, 2004). This difference may be the result of the difference in channel proteins, as TMEM16A is most likely the CaCC expressed in lacrimal glands and in parotid acinar cells and/or by the $[Ca^{2+}]_i$. Indeed, we measured τ_{act} at 0.5 µM Ca^{2+}, a concentration at which the TMEM16B current induced by depolarization has a clear time-dependent component, whereas as $[Ca^{2+}]_i$ increases the time-dependent component decreases, and most current has an instantaneous change to the new level (Fig. 7 A). Thus, differences in τ_{act} may be explained by different Ca^{2+} dependencies of the time-dependent component among CaCCs.

Voltage and Ca^{2+} dependence of activation

We measured the voltage-dependent activation of TMEM16B at low Ca^{2+} concentrations, showing that the substitution of both intra- and extracellular Cl^- with the more permeant SCN^- caused a leftward shift of the G-V relation. Also the Cl^- itself is affecting TMEM16B voltage dependence because its substitution with sucrose caused a shift of $V_{1/2}$ to more positive values. Furthermore, dose–response relations for Ca^{2+} showed that the sensitivity for Ca^{2+} depends on the permeant anion and that $K_{1/2}$ at +100 mV decreases as a function of permeability ratios.

Also, these results can be compared with the small number of previous studies which have investigated the effect of permeant anions on endogenous CaCCs. Ishikawa and Cook (1993) recorded in whole cell from sheep parotid secretory cells and measured the following permeability ratios: SCN^- (1.80) > I^- (1.09) > Cl^- (1) > NO_3^- (0.92) > Br^- (0.75). These authors analyzed current amplitudes and showed that both outward and inward currents increased when Cl^- was replaced with

Published May 26, 2014

SCN^-, remained similar in I^-, and decreased both with NO_3^- and Br^-. Thus, the conductance changes followed the order of the permeability sequence. Perez-Cornejo and Arreola (2004) measured G-V relations in the presence of anions more permeant than Cl^-, fit the normalized conductance with the Boltzmann equation, and reported that G-V relations were shifted toward more negative voltages with respect to the value in Cl^-. The shift was larger for anions with higher permeability ratios. Anions with permeability ratios < 1 were not tested. Qu and Hartzell (2000) compared dose–response for Ca^{2+} in inside-out patches from *Xenopus* oocytes, in the presence of Cl^- or SCN^- at the intracellular side. By fitting the data with the Hill equation, they found that at 0 mV, the Ca^{2+} concentration producing 50% of the maximal current was 279 nM in Cl^-, whereas it decreased about twofold, 131 nM, in SCN^-, indicating that a lower $[Ca^{2+}]_i$ is sufficient to open the channels in the presence of the more permeant anion SCN^- compared with Cl^-. These results show that anions more permeant than Cl^- favor channel opening, whereas less permeant anions favor channel closure, in agreement with our results.

TMEM16A and TMEM16B

After the discovery that TMEM16A and TMEM16B are CaCCs, some studies reported the effect of some permeant anion on TMEM16A, whereas this is the first study on TMEM16B. Xiao et al. (2011) obtained whole-cell recordings from HEK293 cell expressing the TMEM16A(ac) isoform and showed that replacement of extracellular Cl^- with NO_3^- or SCN^- shifted G-V relations to more negative voltages. Moreover, replacement of increasing concentrations of extracellular Cl^- with gluconate or sucrose shifted the G-V relations toward increasingly more positive voltages. τ_{act} and τ_{deact} were not reported. These results are in agreement with our data.

Ferrera et al. (2011) reported that whole-cell recordings from Fischer rat thyroid cells stably expressing the TMEM16A(abc) showed an increase or decrease in conductance when extracellular Cl^- was replaced with more or less permeant anions, respectively. Indeed, the conductance increased about twofold in I^- and SCN^-, whereas it decreased by ∼50% in gluconate. Interestingly, the same authors showed that the isoform TMEM16A(0) had some differences in selectivity compared with TMEM16A(abc). P_I/P_{Cl} increased from 3.6 for TMEM16A(abc) to 4.7 for TMEM16A(0), and P_{SCN}/P_{Cl} increased from 3.4 for TMEM16A(abc) to 5.6 for TMEM16A(0). Furthermore, the membrane conductance in I^- and SCN^- increased about sixfold compared with Cl for TMEM16A(0), to be compared with a twofold increase in TMEM16A(abc). τ_{act} and τ_{deact} were not reported. It is likely that a comparison of the regions of the two isoforms may help to shed light on the molecular mechanism at the basis of the effect of permeant anion on gating.

How are permeant anions modifying gating in these channels? Greenwood and Large (1999) first suggested that the slower deactivation measured with more permeant anions could be explained if the more permeant anion favors the channel open state, for example by increasing the mean open time, possibly with a mechanism similar to the "foot in the door," originally observed in potassium channels (Armstrong, 1971) and afterward confirmed in various other ion channels, where the most permeant ions stabilized the open conformation (Yellen, 1997). Our results could be explained by this mechanism, as the most permeant anions also produce an increase in the apparent open probability.

Overall, we found that permeant anions affected the voltage dependence and the apparent Ca^{2+} affinity but not the voltage sensitivity, as measured by the equivalent gating charge *z*. However, it is likely that permeant anions play a more complex role in addition to an increase in open probability. We observed that the substitution of Cl^- with SCN^- both at the extracellular and intracellular side produced a shift of the G-V relation toward more negative values, an increase of the apparent Ca^{2+} affinity, but also a reduction in the voltage dependence of the apparent Ca^{2+} affinity (Fig. 7, C and H), and an increase of the Hill coefficient at positive voltages. These results could suggest that more permeant ions can bind with higher affinity than Cl^- to an allosteric binding site (inside or outside the pore) that may control the gate of the channel.

Interestingly, the effect of permeant anions on gating is not novel for Cl^- channels because it is well known that anion occupancy of the pore is strictly coupled to fast gating in CLC Cl^- channels. For these channels, the movement of the permeating anion in the pore contributes to the voltage dependence of the channel opening (Pusch et al., 1995; Chen and Miller, 1996; Pusch, 1996). However, the ion selectivity sequence for CLC Cl^- channels, $Cl^- > Br^- > I^-$, is very different from that for TMEM16B, and there is no evidence for sequence conservation patterns among CLC and TMEM16 families (Duran et al., 2010), indicating that the molecular mechanisms underlying the effect of permeant anions on gating may be rather different.

Recent work showed that the TMEM16A channel can be gated by direct binding of Ca^{2+} to the TMEM16A protein, rather than by binding to an accessory Ca^{2+}-binding protein or through phosphorylation (Yu et al., 2012, 2014; Terashima et al., 2013). Moreover, mutation of two glutamic acids, E702 and E705, greatly modified the Ca^{2+} sensitivity of the channel and contributed to the revision of the topology of the channel (Yu et al., 2012), a topology which received further support by results obtained with chimeric proteins between TMEM16A and TMEM16B (Scudieri et al., 2013). Yu et al. (2012) also obtained data consistent with amino acids 625 to 630 contributing to an outer vestibule at the extracellular

side of the membrane and with amino acids beyond 635 located deep in the putative pore. To determine whether these amino acids are part of the permeation pathway and modify ion selectivity, Yu et al. (2012) measured the permeability and conductance ratios between I^- and Cl^- after replacement of several amino acids between 625 and 639 with cysteine, but did not find any significant alteration in ion selectivity. Thus, at present, determinants of ion selectivity are still unknown. Future work will have to determine which regions of the protein contribute to the permeation pathway, which amino acids are critical for ion selectivity, and how permeant anions modify gating at the molecular level. Moreover, as TMEM16A and TMEM16B have several important differences and none of the chimeras recently produced had properties reproducing those of TMEM16B (Scudieri et al., 2013), it is likely that the molecular determinants of modifications of gating by permeant anions in the two channels may have some differences.

We thank Sara Migliarini (University of Pisa, Pisa, Italy) for the help with molecular biology and all members of the laboratory for discussions.

This study was supported by a grant from the Italian Ministry of Education, Universities, and Research (MIUR). S. Pifferi is a recipient of a European Union Marie Curie Reintegration Grant (OLF-STOM no. 334404).

The authors declare no competing financial interests.

Lawrence G. Palmer served as editor.

Submitted: 14 February 2014
Accepted: 2 May 2014

REFERENCES

Adomaviciene, A., K.J. Smith, H. Garnett, and P. Tammaro. 2013. Putative pore-loops of TMEM16/anoctamin channels affect channel density in cell membranes. *J. Physiol.* 591:3487–3505. http://dx.doi.org/10.1113/jphysiol.2013.251660

Armstrong, C.M. 1971. Interaction of tetraethylammonium ion derivatives with the potassium channels of giant axons. *J. Gen. Physiol.* 58:413–437. http://dx.doi.org/10.1085/jgp.58.4.413

Berg, J., H. Yang, and L.Y. Jan. 2012. Ca^{2+}-activated Cl^- channels at a glance. *J. Cell Sci.* 125:1367–1371. http://dx.doi.org/10.1242/jcs.093260

Billig, G.M., B. Pál, P. Fidzinski, and T.J. Jentsch. 2011. Ca^{2+}-activated Cl^- currents are dispensable for olfaction. *Nat. Neurosci.* 14:763–769. http://dx.doi.org/10.1038/nn.2821

Caputo, A., E. Caci, L. Ferrera, N. Pedemonte, C. Barsanti, E. Sondo, U. Pfeffer, R. Ravazzolo, O. Zegarra-Moran, and L.J.V. Galietta. 2008. TMEM16A, a membrane protein associated with calcium-dependent chloride channel activity. *Science.* 322:590–594. http://dx.doi.org/10.1126/science.1163518

Cenedese, V., G. Betto, F. Celsi, O.L. Cherian, S. Pifferi, and A. Menini. 2012. The voltage dependence of the TMEM16B/anoctamin2 calcium-activated chloride channel is modified by mutations in the first putative intracellular loop. *J. Gen. Physiol.* 139:285–294. http://dx.doi.org/10.1085/jgp.201110764

Centinaio, E., E. Bossi, and A. Peres. 1997. Properties of the Ca^{2+}-activated Cl− current of *Xenopus* oocytes. *Cell. Mol. Life Sci.* 53:604–610. http://dx.doi.org/10.1007/s000180050079

Chen, T.Y., and C. Miller. 1996. Nonequilibrium gating and voltage dependence of the ClC-0 Cl- channel. *J. Gen. Physiol.* 108:237–250. http://dx.doi.org/10.1085/jgp.108.4.237

Dauner, K., J. Lissmann, S. Jeridi, S. Frings, and F. Möhrlen. 2012. Expression patterns of anoctamin 1 and anoctamin 2 chloride channels in the mammalian nose. *Cell Tissue Res.* 347:327–341. http://dx.doi.org/10.1007/s00441-012-1324-9

Dauner, K., C. Möbus, S. Frings, and F. Möhrlen. 2013. Targeted expression of anoctamin calcium-activated chloride channels in rod photoreceptor terminals of the rodent retina. *Invest. Ophthalmol. Vis. Sci.* 54:3126–3136. http://dx.doi.org/10.1167/iovs.13-11711

Dawson, D.C., S.S. Smith, and M.K. Mansoura. 1999. CFTR: mechanism of anion conduction. *Physiol. Rev.* 79:S47–S75.

Dibattista, M., A. Amjad, D.K. Maurya, C. Sagheddu, G. Montani, R. Tirindelli, and A. Menini. 2012. Calcium-activated chloride channels in the apical region of mouse vomeronasal sensory neurons. *J. Gen. Physiol.* 140:3–15. http://dx.doi.org/10.1085/jgp.201210780

Duran, C., C.H. Thompson, Q. Xiao, and H.C. Hartzell. 2010. Chloride channels: often enigmatic, rarely predictable. *Annu. Rev. Physiol.* 72:95–121. http://dx.doi.org/10.1146/annurev-physiol-021909-135811

Evans, M.G., and A. Marty. 1986. Calcium-dependent chloride currents in isolated cells from rat lacrimal glands. *J. Physiol.* 378:437–460.

Ferrera, L., A. Caputo, I. Ubby, E. Bussani, O. Zegarra-Moran, R. Ravazzolo, F. Pagani, and L.J.V. Galietta. 2009. Regulation of TMEM16A chloride channel properties by alternative splicing. *J. Biol. Chem.* 284:33360–33368. http://dx.doi.org/10.1074/jbc.M109.046607

Ferrera, L., P. Scudieri, E. Sondo, A. Caputo, E. Caci, O. Zegarra-Moran, R. Ravazzolo, and L.J.V. Galietta. 2011. A minimal isoform of the TMEM16A protein associated with chloride channel activity. *Biochim. Biophys. Acta.* 1808:2214–2223. http://dx.doi.org/10.1016/j.bbamem.2011.05.017

Flores, C.A., L.P. Cid, F.V. Sepúlveda, and M.I. Niemeyer. 2009. TMEM16 proteins: the long awaited calcium-activated chloride channels? *Braz. J. Med. Biol. Res.* 42:993–1001. http://dx.doi.org/10.1590/S0100-879X2009005000028

Frings, S., D. Reuter, and S.J. Kleene. 2000. Neuronal Ca^{2+}-activated Cl^- channels—homing in on an elusive channel species. *Prog. Neurobiol.* 60:247–289. http://dx.doi.org/10.1016/S0301-0082(99)00027-1

Galietta, L.J.V. 2009. The TMEM16 protein family: a new class of chloride channels? *Biophys. J.* 97:3047–3053. http://dx.doi.org/10.1016/j.bpj.2009.09.024

Greenwood, I.A., and W.A. Large. 1999. Modulation of the decay of Ca^{2+}-activated Cl^- currents in rabbit portal vein smooth muscle cells by external anions. *J. Physiol.* 516:365–376. http://dx.doi.org/10.1111/j.1469-7793.1999.0365v.x

Hartzell, C., I. Putzier, and J. Arreola. 2005. Calcium-activated chloride channels. *Annu. Rev. Physiol.* 67:719–758. http://dx.doi.org/10.1146/annurev.physiol.67.032003.154341

Hartzell, H.C., K. Yu, Q. Xiao, L.-T. Chien, and Z. Qu. 2009. Anoctamin/TMEM16 family members are Ca^{2+}-activated Cl^- channels. *J. Physiol.* 587:2127–2139. http://dx.doi.org/10.1113/jphysiol.2008.163709

Hengl, T., H. Kaneko, K. Dauner, K. Vocke, S. Frings, and F. Möhrlen. 2010. Molecular components of signal amplification in olfactory sensory cilia. *Proc. Natl. Acad. Sci. USA.* 107:6052–6057. http://dx.doi.org/10.1073/pnas.0909032107

Hille, B. 2001. Ion Channel of Excitable Membranes. Third edition. Sinauer Associates, Inc, Sunderland, MA. 814 pp.

Huang, F., J.R. Rock, B.D. Harfe, T. Cheng, X. Huang, Y.N. Jan, and L.Y. Jan. 2009. Studies on expression and function of the TMEM16A calcium-activated chloride channel. *Proc. Natl. Acad. Sci. USA.* 106:21413–21418. http://dx.doi.org/10.1073/pnas.0911935106

Huang, F., X. Wong, and L.Y. Jan. 2012a. International Union of Basic and Clinical Pharmacology. LXXXV: calcium-activated chloride

channels. *Pharmacol. Rev.* 64:1–15. http://dx.doi.org/10.1124/pr.111.005009

Huang, W.C., S. Xiao, F. Huang, B.D. Harfe, Y.N. Jan, and L.Y. Jan. 2012b. Calcium-activated chloride channels (CaCCs) regulate action potential and synaptic response in hippocampal neurons. *Neuron.* 74:179–192. http://dx.doi.org/10.1016/j.neuron.2012.01.033

Ishikawa, T., and D.I. Cook. 1993. A Ca^{2+}-activated Cl^- current in sheep parotid secretory cells. *J. Membr. Biol.* 135:261–271. http://dx.doi.org/10.1007/BF00211098

Jung, J., J.H. Nam, H.W. Park, U. Oh, J.H. Yoon, and M.G. Lee. 2013. Dynamic modulation of ANO1/TMEM16A HCO_3^- permeability by Ca^{2+}/calmodulin. *Proc. Natl. Acad. Sci. USA.* 110:360–365. http://dx.doi.org/10.1073/pnas.1211594110

Kunzelmann, K., R. Schreiber, A. Kmit, W. Jantarajit, J.R. Martins, D. Faria, P. Kongsuphol, J. Ousingsawat, and Y. Tian. 2012a. Expression and function of epithelial anoctamins. *Exp. Physiol.* 97:184–192.

Kunzelmann, K., Y. Tian, J.R. Martins, D. Faria, P. Kongsuphol, J. Ousingsawat, L. Wolf, and R. Schreiber. 2012b. Airway epithelial cells—Functional links between CFTR and anoctamin dependent Cl^- secretion. *Int. J. Biochem. Cell Biol.* 44:1897–1900. http://dx.doi.org/10.1016/j.biocel.2012.06.011

Kuruma, A., and H.C. Hartzell. 2000. Bimodal control of a Ca^{2+}-activated Cl^- channel by different Ca^{2+} signals. *J. Gen. Physiol.* 115:59–80. http://dx.doi.org/10.1085/jgp.115.1.59

Lalonde, M.R., M.E. Kelly, and S. Barnes. 2008. Calcium-activated chloride channels in the retina. *Channels (Austin).* 2:252–260. http://dx.doi.org/10.4161/chan.2.4.6704

Leblanc, N., J. Ledoux, S. Saleh, A. Sanguinetti, J. Angermann, K. O'Driscoll, F. Britton, B.A. Perrino, and I.A. Greenwood. 2005. Regulation of calcium-activated chloride channels in smooth muscle cells: a complex picture is emerging. *Can. J. Physiol. Pharmacol.* 83:541–556. http://dx.doi.org/10.1139/y05-040

Linsdell, P., A. Evagelidis, and J.W. Hanrahan. 2000. Molecular determinants of anion selectivity in the cystic fibrosis transmembrane conductance regulator chloride channel pore. *Biophys. J.* 78:2973–2982. http://dx.doi.org/10.1016/S0006-3495(00)76836-6

Maurya, D.K., and A. Menini. 2013. Developmental expression of the calcium-activated chloride channels TMEM16A and TMEM16B in the mouse olfactory epithelium. *Dev. Neurobiol.* In press.

Patton, C., S. Thompson, and D. Epel. 2004. Some precautions in using chelators to buffer metals in biological solutions. *Cell Calcium.* 35:427–431. http://dx.doi.org/10.1016/j.ceca.2003.10.006

Perez-Cornejo, P., and J. Arreola. 2004. Regulation of Ca^{2+}-activated chloride channels by cAMP and CFTR in parotid acinar cells. *Biochem. Biophys. Res. Commun.* 316:612–617. http://dx.doi.org/10.1016/j.bbrc.2004.02.097

Petersen, O.H. 2005. Ca^{2+} signalling and Ca^{2+}-activated ion channels in exocrine acinar cells. *Cell Calcium.* 38:171–200. http://dx.doi.org/10.1016/j.ceca.2005.06.024

Pifferi, S., G. Pascarella, A. Boccaccio, A. Mazzatenta, S. Gustincich, A. Menini, and S. Zucchelli. 2006. Bestrophin-2 is a candidate calcium-activated chloride channel involved in olfactory transduction. *Proc. Natl. Acad. Sci. USA.* 103:12929–12934. http://dx.doi.org/10.1073/pnas.0604505103

Pifferi, S., M. Dibattista, and A. Menini. 2009. TMEM16B induces chloride currents activated by calcium in mammalian cells. *Pflugers Arch.* 458:1023–1038. http://dx.doi.org/10.1007/s00424-009-0684-9

Pifferi, S., V. Cenedese, and A. Menini. 2012. Anoctamin 2/TMEM16B: a calcium-activated chloride channel in olfactory transduction. *Exp. Physiol.* 97:193–199.

Ponissery Saidu, S., A.B. Stephan, A.K. Talaga, H. Zhao, and J. Reisert. 2013. Channel properties of the splicing isoforms of the olfactory calcium-activated chloride channel Anoctamin 2. *J. Gen. Physiol.* 141:691–703. http://dx.doi.org/10.1085/jgp.201210937

Pusch, M. 1996. Knocking on channel's door. The permeating chloride ion acts as the gating charge in ClC-0. *J. Gen. Physiol.* 108:233–236. http://dx.doi.org/10.1085/jgp.108.4.233

Pusch, M., U. Ludewig, A. Rehfeldt, and T.J. Jentsch. 1995. Gating of the voltage-dependent chloride channel CIC-0 by the permeant anion. *Nature.* 373:527–531.

Qu, Z., and H.C. Hartzell. 2000. Anion permeation in Ca^{2+}-activated Cl^- channels. *J. Gen. Physiol.* 116:825–844. http://dx.doi.org/10.1085/jgp.116.6.825

Rasche, S., B. Toetter, J. Adler, A. Tschapek, J.F. Doerner, S. Kurtenbach, H. Hatt, H. Meyer, B. Warscheid, and E.M. Neuhaus. 2010. Tmem16b is specifically expressed in the cilia of olfactory sensory neurons. *Chem. Senses.* 35:239–245. http://dx.doi.org/10.1093/chemse/bjq007

Rock, J.R., and B.D. Harfe. 2008. Expression of TMEM16 paralogs during murine embryogenesis. *Dev. Dyn.* 237:2566–2574. http://dx.doi.org/10.1002/dvdy.21676

Sagheddu, C., A. Boccaccio, M. Dibattista, G. Montani, R. Tirindelli, and A. Menini. 2010. Calcium concentration jumps reveal dynamic ion selectivity of calcium-activated chloride currents in mouse olfactory sensory neurons and TMEM16b-transfected HEK 293T cells. *J. Physiol.* 588:4189–4204. http://dx.doi.org/10.1113/jphysiol.2010.194407

Sanders, K.M., M.H. Zhu, F. Britton, S.D. Koh, and S.M. Ward. 2012. Anoctamins and gastrointestinal smooth muscle excitability. *Exp. Physiol.* 97:200–206.

Schroeder, B.C., T. Cheng, Y.N. Jan, and L.Y. Jan. 2008. Expression cloning of TMEM16A as a calcium-activated chloride channel subunit. *Cell.* 134:1019–1029. http://dx.doi.org/10.1016/j.cell.2008.09.003

Scudieri, P., E. Sondo, L. Ferrera, and L.J.V. Galietta. 2012. The anoctamin family: TMEM16A and TMEM16B as calcium-activated chloride channels. *Exp. Physiol.* 97:177–183. http://dx.doi.org/10.1113/expphysiol.2011.058198

Scudieri, P., E. Sondo, E. Caci, R. Ravazzolo, and L.J. Galietta. 2013. TMEM16A-TMEM16B chimaeras to investigate the structure-function relationship of calcium-activated chloride channels. *Biochem. J.* 452:443–455. http://dx.doi.org/10.1042/BJ20130348

Smith, S.S., E.D. Steinle, M.E. Meyerhoff, and D.C. Dawson. 1999. Cystic fibrosis transmembrane conductance regulator. Physical basis for lyotropic anion selectivity patterns. *J. Gen. Physiol.* 114:799–818. http://dx.doi.org/10.1085/jgp.114.6.799

Stephan, A.B., E.Y. Shum, S. Hirsh, K.D. Cygnar, J. Reisert, and H. Zhao. 2009. ANO2 is the cilial calcium-activated chloride channel that may mediate olfactory amplification. *Proc. Natl. Acad. Sci. USA.* 106:11776–11781. http://dx.doi.org/10.1073/pnas.0903304106

Stöhr, H., J.B. Heisig, P.M. Benz, S. Schöberl, V.M. Milenkovic, O. Strauss, W.M. Aartsen, J. Wijnholds, B.H. Weber, and H.L. Schulz. 2009. TMEM16B, a novel protein with calcium-dependent chloride channel activity, associates with a presynaptic protein complex in photoreceptor terminals. *J. Neurosci.* 29:6809–6818. http://dx.doi.org/10.1523/JNEUROSCI.5546-08.2009

Terashima, H., A. Picollo, and A. Accardi. 2013. Purified TMEM16A is sufficient to form Ca^{2+}-activated Cl^- channels. *Proc. Natl. Acad. Sci. USA.* 110:19354–19359. http://dx.doi.org/10.1073/pnas.1312014110

Wray, S., T. Burdyga, and K. Noble. 2005. Calcium signalling in smooth muscle. *Cell Calcium.* 38:397–407. http://dx.doi.org/10.1016/j.ceca.2005.06.018

Wright, E.M., and J.M. Diamond. 1977. Anion selectivity in biological systems. *Physiol. Rev.* 57:109–156.

Xiao, Q., K. Yu, P. Perez-Cornejo, Y. Cui, J. Arreola, and H.C. Hartzell. 2011. Voltage- and calcium-dependent gating of TMEM16A/Ano1 chloride channels are physically coupled by the first intracellular loop. *Proc. Natl. Acad. Sci. USA.* 108:8891–8896. http://dx.doi.org/10.1073/pnas.1102147108

Yang, Y.D., H. Cho, J.Y. Koo, M.H. Tak, Y. Cho, W.-S. Shim, S.P. Park, J. Lee, B. Lee, B.-M. Kim, et al. 2008. TMEM16A confers receptor-activated calcium-dependent chloride conductance. *Nature.* 455: 1210–1215. http://dx.doi.org/10.1038/nature07313

Yellen, G. 1997. Single channel seeks permeant ion for brief but intimate relationship. *J. Gen. Physiol.* 110:83–85. http://dx.doi.org/10.1085/jgp.110.2.83

Yu, K., C. Duran, Z. Qu, Y.Y. Cui, and H.C. Hartzell. 2012. Explaining calcium-dependent gating of anoctamin-1 chloride channels requires a revised topology. *Circ. Res.* 110:990–999. http://dx.doi.org/10.1161/CIRCRESAHA.112.264440

Yu, K., J. Zhu, Z. Qu, Y.Y. Cui, and H.C. Hartzell. 2014. Activation of the Ano1 (TMEM16A) chloride channel by calcium is not mediated by calmodulin. *J. Gen. Physiol.* 143:253–267. http://dx.doi.org/10.1085/jgp.201311047

Zhang, Y., and P.S. Cremer. 2006. Interactions between macromolecules and ions: The Hofmeister series. *Curr. Opin. Chem. Biol.* 10:658–663. http://dx.doi.org/10.1016/j.cbpa.2006.09.020

4.3 Multiple effects of anthracene-9-carboxylic acid on the TMEM16B/anoctamin2 calcium activated chloride channel.

Multiple effects of anthracene-9-carboxylic acid

on the TMEM16B/anoctamin2 calcium-activated chloride channel

O. Lijo Cherian[1], Anna Menini[1], Anna Boccaccio[2]

[1]Neurobiology Group, SISSA, International School for Advanced Studies, Trieste, Italy

[2]Istituto di Biofisica, CNR, Genova, Italy

Corresponding author:

Anna Boccaccio

Istituto di Biofisica - IBF

Consiglio Nazionale delle Ricerche - CNR

Via De Marini 6, 16149 Genova, Italy

phone : +39 010 6475 891, Fax: +39 010 6475500

boccaccio@ge.ibf.cnr.it

KEY WORDS: Ca^{2+}-activated Cl^- channel, patch clamp, ANO2, blocker, A9M, A9C

RUNNING TITLE: Multiple effects of A9C on TMEM16B/anoctamin2

Abstract

We investigated the extracellular effects of anthracene-9-carboxylic acid (A9C) on TMEM16B Ca^{2+}-activated Cl^- channels, expressed in HEK 293T cells, using the whole-cell patch-clamp technique. In the presence of 1.5 μM Ca^{2+}, A9C had multiple effects on TMEM16B-mediated currents. We measured a voltage-dependent block of outward currents and potentiation of transient early inward currents. Moreover, also tail currents recorded at -100 mV after various prepulse voltages were potentiated and their deactivation was slower compared to control. The effectiveness of A9C in potentiating tail current and prolonging their closure increased with higher prior depolarization, thus requiring channel opening.

We evaluated the dependence of current block, potentiation and decay rate on A9C concentration.

To test whether the negative charge of A9C was important, we used anthracene-9-methanol (A9M), a non-charged analogue of A9C. A9M produced a small, not voltage-dependent block of TMEM16B currents, did not produce current potentiation, but prolonged both the activation and deactivation kinetics of TMEM16B. This is the first report of A9M activity on a Ca^{2+} activated chloride current.

The data from present study confirm previous observation on paradoxical effects of A9C on Ca^{2+} activated chloride current in smooth muscle cells (Piper and Greenwood, 2003).

Introduction

Ca^{2+}-activated Cl^- currents (CaCCs) were originally identified in rod segments from the salamander retina (Bader et al., 1982) and in *Xenopus laevis* oocytes (Miledi, 1982). Later they have been observed in diverse tissues including exocrine gland cells, neurons, heart, skeletal and smooth muscle (Large and Wang, 1996; Frings et al., 2000; Hartzell et al., 2005; Leblanc et al., 2005; Petersen, 2005; Wray et al., 2005; Lalonde et al., 2008; Duran et al., 2010; Berg et al., 2012; Huang et al., 2012a).

The molecular identity of CaCCs has been controversial for a long time, until recently, when two members of TMEM16/anoctamin gene family, TMEM16A/anoctamin1 and TMEM16B/ anoctamin2, were shown to mediate CaCCs (Yang et al., 2008; Caputo et al., 2008; Schroeder et al., 2008; Pifferi et al., 2009; Stephan et al., 2009; Stöhr et al., 2009; Sagheddu et al., 2010; Dibattista et al., 2012; Pedemonte and Galietta, 2014).

Since then TMEM16A and B were found to be expressed in many of the cell types known to exhibit CaCCs (Huang et al., 2009, 2012a; Ferrera et al., 2010; Pedemonte and Galietta, 2014). Studies performed with knockout mice for TMEM16A or TMEM16B (Rock and Harfe, 2008; Billig et al., 2011) and knockdown of these channels in specific cell types confirmed their involvement in the generation of CaCCs (Flores et al., 2009; Galietta, 2009; Kunzelmann et al., 2012a; b; Pifferi et al., 2012; Sanders et al., 2012; Scudieri et al., 2012; Huang et al., 2012a).

TMEM16A and TMEM16B are closely related (Pedemonte and Galietta, 2014) and their expression in diverse cell types give rise to voltage-dependent anionic currents, although they somewhat differ in certain respects, as TMEM16B shows faster kinetics and lower sensitivity to cytosolic Ca^{2+} than TMEM16A (Yang et al., 2008; Caputo et al., 2008; Schroeder et al., 2008; Pifferi et al., 2009; Stephan et al., 2009; Scudieri et al., 2013).

Selective and specific blockers are a valuable research tool to study ion channel structure-function relations, to explore the properties of channel pore and to elucidate the physiological relevance of native currents (Hille, 2001). Diverse classes of compounds were reported to block CaCCs in various cell types, like fenamates (flufenamic acid, niflumic acid; (White and Aylwin, 1990; Hogg et al., 1994b; Greenwood and Large, 1995)), stilbene derivatives (4,4-diisothiocyanato-stilbene-2,2-disulfonic acid, known as DIDS; (Hogg et al., 1994a)) and anthracene-9-carboxylic acid (A9C;(Hogg et al., 1994a)). Unfortunately, these compounds lack specificity and high affinity. Other blockers, such as eugenol (Yao et al., 2012), digallic and tannic acid (Namkung et al., 2010), benzbromarone (Huang et al., 2012b), CaCCinh-A01 (De La Fuente et al., 2008) and the novel T16Ainh-A01 (Namkung et al., 2011) and MONNA (Oh et al., 2013) have been identified recently. The investigation of their specificity and blocking mode is still in progress.

Anthracene-9-carboxylic acid (A9C) is an organic molecule traditionally used to block and identify CaCCs in various cell types, like diverse smooth muscle cells (from portal vein Hogg et al., 1993, 1994a; esophageal Akbarali and Giles, 1993; urethral Cotton et al., 1997; anococcygeal Wayman et al., 1997 and lymphatic smooth muscle cells Toland et al., 2000), but also in epithelial cells (Qu et al., 2003), in salivary gland cells (Romanenko et al., 2010) and in *Xenopus laevis* oocytes (Qu and Hartzell, 2001).

A9C has been described as a low-affinity open channel voltage-dependent blocker of CaCCs measured in excised patches from *Xenopus laevis* oocytes, being more efficient at depolarizing voltages and acting from the extracellular side (Qu and Hartzell, 2001).

Piper and Greenwood (Piper and Greenwood, 2003) observed an anomalous and more complex action of A9C on CaCCs recorded in rabbit pulmonary artery smooth muscle cells,

consisting of a weak block of outward currents and an increase of the amplitude of instantaneous inward currents recorded at hyperpolarizing potential.

In this study we investigated the effect of extracellular A9C on TMEM16B Ca^{2+}-activated Cl^- currents, recorded in HEK 293T cells using the whole-cell patch-clamp technique. In the presence of intracellular 1.5 μM Ca^{2+}, A9C had multiple effects on TMEM16B-mediated currents: a voltage-dependent block of outward currents and a strong potentiation of transient early inward currents. These complex effect was not replicated when we used an electrically neutral analogue of A9C, anthracene-9-methanol (A9M).

Materials and Methods:

Cell culture and heterologous expression of TMEM16B

The full length isoform of TMEM16B cDNA in pCMV-Sport6 mammalian expression plasmid was obtained from RZPD (clone identification IRAV p968H1167D; NCBI protein database accession number NP_705817.1). This is the retinal isoform with the same start site of the olfactory isoform used in Stephan et al. (2009) and contained the exon 14 (Ponissery Saidu et al., 2013), named exon 13 in (Stephan et al., 2009). 2µg cDNA coding for TMEM16B together with 0.2µg of pEGFP-C1 (Takara Bio Inc.) were transfected into HEK293T cells using FuGENE 6 or X-tremeGENE 9 (Roche). Cell were used for patch clamp experiments within 48 hours of transfection.

Electrophysiology

Experiments were performed in the whole cell voltage clamp configuration at room temperature (22-25 ^{0}C) as previously described (Pifferi et al., 2006, 2009; Cenedese et al., 2012; Betto et al., 2014). Patch pipettes, made of borosilicate glass had a pipette resistance of ~3-5 MΩ when immersed in bath solution. Whole cell currents were recorded with an Axopatch 1D amplifier controlled by pClamp 9.2 via a Digidata 1332A (Axon instruments, Molecular devices). Data were low pass filtered at 5kHz and sampled at 10kHz. Complete exchange of extracellular solution in close vicinity of patched cell was achieved using a gravity fed perfusion system (Perfusion Fast Step SF-77B, Warner Instruments Corp.) in a continuously perfused bath. Bath was grounded using a 3MKCl agar salt bridge connected to an Ag/AgCl reference electrode. Liquid junction potentials were of few mV and were not corrected. Stimulation protocol consisted of voltage steps of

200ms duration from a holding potential of 0mV (or -60mV) ranging from -100mV to +140mV with an interval of 20mV, followed by a step to -100mV.

Solutions

The standard extracellular solutions (mammalian Ringer) contained (in mM): 140 NaCl, 5 KCl, 2 $CaCl_2$, 1 $MgCl_2$, 10 glucose and 10 HEPES adjusted to pH 7.4 with NaOH. The standard intracellular solutions contained (in mM): 140 CsCl, 10 HEPES, 10 HEDTA, adjusted to pH 7.2 with CsOH, and various amounts of $CaCl_2$, as calculated with the program WinMAXC (C. Patton, Stanford University, Stanford, CA), to obtain free Ca^{2+} 1.5 and 13 μM (Patton et al., 2004). Anthracene-9-carboxylic acid, A9C, was dissolved in DMSO at a stock concentration of 1M and stored at -20^{0}C. Final concentrations of A9C were achieved by diluting the desired volume of stock into bath solution and sonicating for 30 mins at 37 ^{0}C. Anthracene-9-methanol, A9M, was dissolved in chloroform at a concentration of 100 mM and diluted in bath solution to final concentration of 300μM. Solution was sonicated till it became clear and was left open under chemical hood to evaporate the remaining chloroform. The maximal nominal concentration of chloroform in the final solution was 0.3%. All the preparations and experiments with A9C and A9M were done minimizing solutions' light exposure. All the chemicals were purchased from Sigma-Aldrich.

Data analysis

IGOR Pro software (WaveMetrics, Lake Oswego, OR, USA) was used for data analysis and figures. Data are usually presented as mean ± SEM and the number of cells (n).

For the sake of clarity in the figures the capacitive transients of some traces were trimmed.

Results

Voltage-dependent A9C block of TMEM16B currents

To measure the extracellular effect of A9C on TMEM16B-mediated currents, we recorded from HEK293T cells transiently transfected with TMEM16B using the whole cell patch clamp configuration in the presence of 1.5 or 13 µM free Ca^{2+} in the intracellular solution.

In a first set of experiments, currents were activated by 13 µM Ca^{2+}, a concentration that almost fully activates TMEM16B-induced currents. Indeed, the Ca^{2+} concentration necessary to activate 50% of the maximal current between -100 and +100 mV in TMEM16B ranges between approximately 1 and 4 µM (Pifferi et al., 2009; Stephan et al., 2009). Figure 1 A shows representative whole-cell recordings measured in control and in the presence of 1 mM A9C, obtained in response to voltage steps between -100 and +140 mV, from a holding potential of 0 mV, followed by a step to -100 mV. I-V relations at the end of voltage steps show that outward currents were partially reduced by A9C (Fig. 1 B). The average ratios between current in A9C and control (I_{A9C}/ I_{CT}) plotted versus voltage reveal that the block was voltage-dependent and was more efficient at high depolarizing voltages (Fig. 1C).

Multiple effects of A9C

In a second set of experiments, we reduced intracellular Ca^{2+} to 1.5 µM. Figure 2 A shows that addition of 1 mM A9C produced not only a voltage-dependent block of outward currents, but also a transient increase of early inward currents and of tail currents at -100 mV (see also Fig. 2C and Fig. 3). Figure 2 B shows currents recorded from the same cell

as in A, from a holding potential of -60 mV. In the presence of 1 mM A9C, the voltage-dependent block of outward currents was similar to that measured from a holding potential of 0 mV (Figs. 2 A, B and D), whereas the amplitude of transient early inward currents did not change compared to control (Fig. 2 C). Potentiation of tail currents at -100 mV was still present (Fig. 2 B and). Similar results were obtained in n=5 cells.

These results show that 1 mM A9C has multiple effects on TMEM16B in the presence of 1.5 μM Ca^{2+}, consisting of voltage-dependent block of outward currents and potentiation of transient early inward currents and tail currents at -100 mV. In addition, early inward current potentiation was elicited by 1 mM A9C from a holding potential of 0 mV, whereas no potentiation was observed from a holding potential of -60 mV.

Figure 3 A shows that the kinetics of deactivation of tail currents recorded at -100 mV after several prepulse voltages in the presence of 1 mM A9C was often biphasic, whereas deactivation in control could be well described by a single exponential function. To quantify tail current potentiation after each prepulse voltage, we evaluated the maximal tail currents with respect to the values measured at steady state at -100 mV. In control, we calculated the current value obtained from a single-exponential fit of tail currents extrapolated to the beginning of the step to -100 mV (Fig. 3 B, green line). In the presence of A9C, we usually measured the current peak that developed between 2.5 and 3 ms after the voltage step to -100 mV. Both in control and in A9C the corresponding values of steady state currents at -100 mV were subtracted from the above values. Figure 3 C shows the maximal tail current amplitudes in A9C and control versus the prepulse voltages. The amplitudes of maximal tail currents in A9C were similar to control from negative prepulse voltages up to -40 mV, whereas increased in A9C when the prepulse voltage was >-20 mV.

To quantify the tail current decay kinetics, we measured the decay time necessary to reach 50% of the maximal tail current (Fig. 3 B, dotted blue line) recorded at -100 mV. Figure 3 D shows that t_{50} did not change with voltage in control, whereas increased with voltage in 1 mM A9C.

These results show that both transient tail current potentiation and t_{50} increased with depolarization of the prepulse voltage.

Concentration dependence of A9C effects

Figure 4 A shows representative whole-cell recordings at 1.5 μM Ca^{2+} in control and in the presence of various concentrations of A9C from 33 μM to 1 mM. All the effects of A9C, block, potentiation and change in kinetics were reversible, as shown by the wash out traces in the right column of Fig. 4 A. I-V relations measured at the end of voltage steps are shown in Fig. 4 B. Interestingly, the inset of Fig. 4 B illustrates that at 300 μM A9C and at intermediate depolarizing potentials (20-60 mV) there was a small potentiation of outward currents. Average fractional currents as a function of voltage (Fig. 4 C; n=4 to 8 for each concentration) show the presence of a voltage-dependent block at every A9C concentration, but also an outward current potentiation (I_{A9C}/ I_{CT} >1) in 300 μM A9C between +20 and +60 mV. Outward current potentiation was present in most experiments at 300 μM A9C and its amplitude was quite variable.

As the presence of potentiation prevents a correct evaluation of the blocking potency of A9C at every voltage, we made a rough evaluation of the concentration-dependent block between +80 and +140 mV and we did not consider values at 300 μM A9C because potentiation obscured the blocking effect especially at this concentration. Figure 5A shows

the fractional current I_{A9C} / I_{CT} plotted versus A9C concentration at the diverse potentials, while the continuous lines correspond to the fit according to a Michaelis-Menten equation, I_{A9C} / I_{CT} = (1-[A9C] / K_D)$^{-1}$, where K_D is the apparent dissociation constant. In panel B is plotted the K_D in function of the membrane potential and the line corresponds to the fit with a Woodhull equation, log K_D (V_m) = log K_D^{0mV} - δV_mF/(2.3*RT), with δ equal to 0.57 and an apparent K_D^{0mV} of 4450 μM.

We quantified the potentiation of tail currents and the deactivation kinetics at -100 mV at various A9C concentrations as previously described in Fig. 3. Figure 6 A and B show respectively the maximal tail currents at -100 mV after a prepulse to +120 mV and t_{50} as a function of A9C concentration.

These results showed that tail current potentiation increased up to 300 μM A9C and then decreased as A9C further increased (Fig. 6 A), while t_{50} monotonically increased with A9C concentration (Fig. 6 B).

Effects of A9M, a non-charged analogue of A9C

To test the hypothesis that the negatively charged side chain of A9C is involved in the voltage dependence of block, we used anthracene-9-methanol (A9M), a non-charged analogue of A9C and compared the effect of A9C and A9M at 300 μ*M.* Figures 7 A-B show that A9M had a very small blocking effect on outward currents and did not cause potentiation of inward currents. In the same cell, 300 μM A9C had the typical voltage-dependent effect, blocking outward currents at high depolarizing voltages (Fig. 7 A-C) and potentiated early inward currents and tail currents at -100 mV, in agreement with Figs. 4 and 6, while potentiation was not present in 300 μM A9M.

Figure 7 C shows that the small block by A9M was not voltage-dependent (average values from 4 experiments, the broken line refer to the experiment in panel A). Moreover, it is important to note that the blocking efficacy of 300 μM A9M was lower than that of A9C at high depolarizing voltages (V_m>+60 mV), similar at about +60 mV, and higher than that of A9C at low positive voltages (+20<V_m<+40mV), which is the voltage range in which we observed potentiation by A9C. Thus, the blocking effect by A9C is underestimated at low positive voltages because of simultaneous potentiating effect.

In addition, we observed that A9M slowed activation kinetics, with τ_{act} of about 2.5 fold larger than those in control. A9M weakly blocked TMEM16B currents recorded in the presence of 1.5 μM Ca^{2+}, but produced a strong and reversible prolongation of the activation kinetics (Fig. 7 A, D).

We also compared the effect of A9M and A9C on the tail currents measured at -100 mV after prepulse voltages from -100 to +140 mV. Figure 8A shows tail currents from the same experiment of Fig. 7 A on an expanded time scale: A9C greatly potentiated tail currents as previously shown (Figs. 3,4 and 6), while A9M caused a small block of tail currents and a prolongation of the deactivation kinetics. Figure 8 B and C show respectively the ratios of the maximal tail currents in A9M and A9C with respect to control and t_{50} recorded at -100 mV, following a depolarization to +120 mV.

Taken together, these results show that 300 μM A9M produced a small, not voltage-dependent current block of outward currents, did not potentiate currents, but prolonged both the activation and deactivation kinetics of TMEM16B.

Discussion

In this study we applied the traditional blocker A9C to CaCC currents elicited in TMEM16B transfected cells. It is apparent that A9C has a bimodal effect, it inhibits currents at positive voltages, while it enhances tail currents at negative potentials. Additionally, A9C application strongly modifies current kinetics, prolonging channel closure.

Voltage dependent A9C block of TMEM16B currents

We measured A9C block of TMEM16B mediated currents in presence of high and intermediate Ca^{2+} concentration (Fig.1,2 and 4), where current is respectively fully or only partially activated (Cenedese et al., 2012). In both cases we observed a voltage dependent block of outward currents (Fig.1, 2 and 4), being A9C more effective at high depolarizing potentials.

We could not carefully evaluate the voltage dependence at all potentials because in our working conditions we observed also a potentiatory effect of A9C at intermediate positive potentials when TMEM16B current was activated with 1.5 μM Ca^{2+}. However, from a rough evaluation of the apparent K_D in the range 80-140mV we estimated that the blocking agent (to which we associated a negative charge of -1) experienced 57% of the voltage drop calculated from the outside of the channels (Hille, 2001; Woodhull, 1973).

The voltage dependence of A9C block was first described by Hogg et al (Hogg et al., 1993, 1994a) in smooth muscle cells from rabbit portal vein, and analyzed in detail by Qu and Hartzell in *Xenopus laevis* oocytes (Qu and Hartzell, 2001).

Qu and Hartzell (Qu and Hartzell, 2001) performed experiments in excised patches and activated the CaCC current with a saturating Ca^{2+}-concentration. In this experimental

condition they found that the blocker was sensitive to 60% of the electric field, similarly to what we reported. However, they found that the blocker was much more efficient, with a 15 times higher affinity, 18 μM, at +100 mV in respect to what we measured for TMEM16B. This difference can be due to the fact that CaCC in *Xenopus laevis* oocyte is generated by TMEM16A (Schroeder et al., 2008), that might be more sensitive to A9C.

Bradley et al. (Bradley et al., 2014) recently reported A9C block of hTMEM16A-*acd* mediated currents, measured in HEK293 transfected cell in the whole cell configuration. They found a higher affinity of A9C to TMEM16A, 56 μM at +80 mV, in respect to our data on TMEM16B. The value obtained by Bradley et al are similar to what has been reported in CaCC from rabbit portal vein (Hogg et al., 1994a). These reports, together with Qu and Hartzell (Qu and Hartzell, 2001), suggest a higher block efficacy of A9C to TMEM16A in respect to TMEM16B. However, further studies are needed, since not all reports agree on the relative high sensitivity of A9C to TMEM16A (see Romanenko et al., 2010).

Nonetheless, since the voltage dependence of the block is commonly interpreted to reflect binding of the blocker to a site in the permeation pathway, the analogy with the voltage dependence found by Qu and Hartzell (Qu and Hartzell, 2001) confirms a strong similarity among TMEM16A and TMEM16B.

Potentiation

Application of 1mM A9C to TMEM16B currents, activated with 1.5 μM Ca^{2+} in the patch pipette, blocked outward directed currents, but increased notably tail currents recorded at -100mV (Fig.2A and B). Additionally A9C increased the amplitude of transient inward

currents (I_{early} in the result section, identified by the green line in Fig.2 A) following a holding potential of 0 mV, but not of -60 mV, suggesting that potentiation requires prior channel opening. Indeed in presence of 1.5 μM Ca^{2+} a consistent fraction of channels, but not all, are open at a holding potential of 0 mV (Fig2A,D; Fig4 in Cenedese et al., 2012), while are mostly closed when the holding potential is held at -60 mV (Fig.2B).

Analysis of tail currents recorded at -100 mV following a test potential varying from -100 to +140 mV in Fig. 3C, show indeed that currents recorded in presence of 1mM A9C increase in respect to control when the prior potential is more depolarized, corresponding to higher number of open channels. At very high potentials the increase is counterbalanced by block. Interestingly a considerable current potentiation is already present at prepulses to -20 / +20 mV where the block is negligible or masked by potentiation (Fig 3C). This observation is confirmed by application of lower concentration of A9C (Fig 4 33 μM, Fig5A) that produces a clear potentiation although the block is minimal.

The potentiation of inward currents had a biphasic dependence on A9C concentration (Fig4 and 6A), reaching a maximal almost 3-fold increase at 300 μM. Higher concentrations were less efficacious, probably due to the prevalence of the blocking action. We did not observe potentiation of current amplitude in presence of 13 μM intracellular Ca^{2+}, probably due to the fact that in this condition channels are already maximally activated. (Fig 4 in Cenedese et al., 2012)

Summarizing, our data suggest that current potentiation depends on the degree of activation, but not on the block.

Slowing of deactivation

The potentiation of inward currents was accompanied by a marked slowing of channels' closure (Fig.3), more effective when preceded by a depolarizing potential (Fig. 3D), suggesting that also in this case prior channel opening is required. Additionally the time of 50% current decay, t_{50}, recorded at -100 mV increased monotonically with the A9C concentration (Fig. 4, 6B).

In presence of A9C a peak was clearly visible in the tail current recorded at -100 mV (Fig3). This feature, although without potentiation, is usually observed in presence of open channel blockers that have to leave for channel closure (Cahalan and Almers, 1979).

Previous studies on CaCCs

Several studies used A9C to identify CaCC currents in different tissues and paradoxical effects have been observed, not only for A9C, but also with other blockers.

An anomalous effect of A9C on calcium-activated chloride currents was reported by Piper and Greenwood (Piper and Greenwood, 2003) in rabbit pulmonary artery smooth muscle cells. Application of 500μM A9C, producing a small inhibition of the maximum outward Cl^- current at +70 mV, augmented the amplitude of the instantaneous inward relaxation at -80 mV by 3.7 times (Fig.1B, C in Piper and Greenwood, 2003). Additionally, they also reported the appearance of a peak in the tail current in presence of A9C (inset in Fig1B in Piper and Greenwood, 2003). They pointed out that the potentiation of inward current at -80 was more prominent than block at +70 mV (Fig 2B in Piper and Greenwood, 2003). We agree on this aspect and we explored higher potentials to see an effective block at lower concentrations (Fig. 4), at which A9C was already effective in potentiating.

Additionally, Piper and Greenwood did not observe a significant slowing of the deactivation kinetics (Piper and Greenwood, 2003) at -80 mV following a depolarization to +70 mV, but only at less negative potentials. Hereof, the different relaxation kinetics of CaCC in rabbit pulmonary artery smooth muscle cells in respect to the much faster TMEM16B can justify this difference. Again likely this currents are underlined by the slower TMEM16A.

Bradley et al. found a reduction of outward currents by 1mM A9C and a potentiation and slowing of inward tail current A9C in HEK cells expressing hTMEM16A-*acd* cells (Fig1-2 in Bradley et al., 2014).

A bimodal action is not unique to A9C interaction with CaCC, indeed it has been reported also for NFA, DCDPC on CaCCs (Piper et al., 2002; Ledoux et al., 2005) and recently for NFA, flufenamic acid and NPPB in TMEM16A transfected cells (Bradley et al., 2014; Liu et al., 2014). With respect to A9C, potentiation in presence of these agents is smaller and at high concentrations is masked by the block (Liu et al., 2014). These compounds also have a slowing effect on current kinetics, the most effective being NFA (Bradley et al., 2014; Liu et al., 2014). However newer agents such as T16Ainh-A01 do not produce these effects (Bradley et al., 2014, Davis et al., 2013).

A9M

Since A9C block is voltage-dependent we used the A9M, an analogue of A9C, but with an electrically neutral side-chain. This compound is scarcely used due to its low solubility. We succeeded to dissolve in Ringer bath solution at a maximal concentration of 300 μM. To our knowledge this is the first report showing the action of A9M on a CaCC current. The application of 300μM A9M produced a voltage independent weak block of TMEM16B

mediated currents. Interestingly at all potentials A9M slowed the kinetics of current activation and deactivation, and was no longer effective in potentiating the current.

This means that the negative charge is required only for the voltage dependence of the block, but not for the block itself. Interestingly, the charge is also required for the potentiation. We do not know if this is a direct effect or if it could be mediated by the interaction with the permeating anion, that would differ whether the blocking agent is charged, as A9C, or neutral, as A9M.

Sideness of block

Since A9C and A9M are hydrophobic molecules, although A9C is negatively charged, it is possible that they traverse the membrane bilayer and block from the intracellular side. Qu and Hartzell showed that block of CaCC in *Xenopus laevis* oocytes by A9C was much faster and about 6 fold more efficient in outside-out rather than inside-out patches, showing that it occurs from the extracellular side of the membrane (Qu and Hartzell, 2001). In our experimental condition, we observed a fast and reversible block both for A9C and A9M, compatible with the time of complete solution exchange, supporting an action from the extracellular side. Additionally we performed experiments with intracellular 1mM A9C in the pipette and TMEM16B current was still present and could be blocked by the successive application of 1 mM bath A9C (data not shown).

Specificity

A9C has been reported to block diverse Cl conductances in different tissues, not only CaCC calcium-dependent currents, but also CFTR and CLC-1 (Zhou et al., 1997; Astill et

al., 1996; Steinmeyer et al., 1991), although the proteins underlying these currents are not structurally related.

A9C, acting from the intracellular side, shows both potentiation and voltage dependent inhibitory effects on CFTR mediated currents (Zhou et al., 1997; Ai et al., 2004). Interestingly, its electro-neutral analogue A9M fails to block CFTR current, but has nearly identical potentiatory effect (Ai et al., 2004).

In summary, in this paper we described for the first time the interaction of the traditional CaCC blocker A9C and its electro-neutral analogue A9M with TMEM16B. A9C inhibited TMEM16B currents at positive voltages, while it enhances tail currents at negative potentials and strongly prolonged channel closure. A9M blocked TMEM16B currents weakly, modified current kinetics, but was not effective in potentiating tail currents.

Further studies are needed to comprehend the nature of this dual effect of A9C on the TMEM16B and A channel and to identify the molecular mechanisms and the channel's region responsible for potentiation and block.

Acknowledgments

We thank all members of the laboratories for discussions. This study was supported by a grant from the Italian Ministry of Education, University and Research (MIUR) and a grant from the Fondazione Compagnia di San Paolo.

The authors declare no competing financial interest.

References

Ai, T., S.G. Bompadre, Y. Sohma, X. Wang, M. Li, and T.-C. Hwang. 2004. Direct effects of 9-anthracene compounds on cystic fibrosis transmembrane conductance regulator gating. *Pflüg. Arch. Eur. J. Physiol.* 449:88–95. doi:10.1007/s00424-004-1317-y.

Akbarali, H.I., and W.R. Giles. 1993. Ca2+ and Ca(2+)-activated Cl- currents in rabbit oesophageal smooth muscle. *J. Physiol.* 460:117–133.

Astill, D.S., G. Rychkov, J.D. Clarke, B.P. Hughes, M.L. Roberts, and A.H. Bretag. 1996. Characteristics of skeletal muscle chloride channel C1C-1 and point mutant R304E expressed in Sf-9 insect cells. *Biochim. Biophys. Acta*. 1280:178–186.

Bader, C.R., D. Bertrand, and E.A. Schwartz. 1982. Voltage-activated and calcium-activated currents studied in solitary rod inner segments from the salamander retina. *J. Physiol.* 331:253–284.1.

Berg, J., H. Yang, and L.Y. Jan. 2012. Ca2+-activated Cl− channels at a glance. *J. Cell Sci.* 125:1367–1371. doi:10.1242/jcs.093260.

Betto, G., O.L. Cherian, S. Pifferi, V. Cenedese, A. Boccaccio, and A. Menini. 2014. Interactions between permeation and gating in the TMEM16B/anoctamin2 calcium-activated chloride channel. *J. Gen. Physiol.* 143:703–718. doi:10.1085/jgp.201411182.

Billig, G.M., B. Pál, P. Fidzinski, and T.J. Jentsch. 2011. Ca2+-activated Cl− currents are dispensable for olfaction. *Nat. Neurosci.* 14:763–769. doi:10.1038/nn.2821.

Bradley, E., S. Fedigan, T. Webb, M.A. Hollywood, K.D. Thornbury, N.G. McHale, and G.P. Sergeant. 2014. Pharmacological characterization of TMEM16A currents. *Channels Austin Tex*. 8.

Cahalan, M.D., and W. Almers. 1979. Block of sodium conductance and gating current in squid giant axons poisoned with quaternary strychnine. *Biophys. J.* 27:57–73. doi:10.1016/S0006-3495(79)85202-9.

Caputo, A., E. Caci, L. Ferrera, N. Pedemonte, C. Barsanti, E. Sondo, U. Pfeffer, R. Ravazzolo, O. Zegarra-Moran, and L.J.V. Galietta. 2008. TMEM16A, a membrane protein associated with calcium-dependent chloride channel activity. *Science*. 322:590–594. doi:10.1126/science.1163518.

Cenedese, V., G. Betto, F. Celsi, O.L. Cherian, S. Pifferi, and A. Menini. 2012. The voltage dependence of the TMEM16B/anoctamin2 calcium-activated chloride channel is modified by mutations in the first putative intracellular loop. *J. Gen. Physiol.* 139:285–294. doi:10.1085/jgp.201110764.

Cotton, K.D., M.A. Hollywood, N.G. McHale, and K.D. Thornbury. 1997. Ca2+ current and Ca(2+)-activated chloride current in isolated smooth muscle cells of the sheep urethra. *J. Physiol.* 505 (Pt 1):121–131.

Dibattista, M., A. Amjad, D.K. Maurya, C. Sagheddu, G. Montani, R. Tirindelli, and A. Menini. 2012. Calcium-activated chloride channels in the apical region of mouse vomeronasal sensory neurons. *J. Gen. Physiol.* 140:3–15. doi:10.1085/jgp.201210780.

Duran, C., C.H. Thompson, Q. Xiao, and H.C. Hartzell. 2010. Chloride channels: often enigmatic, rarely predictable. *Annu. Rev. Physiol.* 72:95–121. doi:10.1146/annurev-physiol-021909-135811.

Ferrera, L., A. Caputo, and L.J.V. Galietta. 2010. TMEM16A Protein: A New Identity for Ca2+-Dependent Cl− Channels. *Physiology*. 25:357–363. doi:10.1152/physiol.00030.2010.

Flores, C.A., L.P. Cid, F.V. Sepúlveda, and M.I. Niemeyer. 2009. TMEM16 proteins: the long awaited calcium-activated chloride channels? *Braz. J. Med. Biol. Res. Rev. Bras. Pesqui. Médicas E Biológicas Soc. Bras. Biofísica Al*. 42:993–1001.

Frings, S., D. Reuter, and S.J. Kleene. 2000. Neuronal Ca2+ -activated Cl- channels--homing in on an elusive channel species. *Prog. Neurobiol.* 60:247–289.

Galietta, L.J.V. 2009. The TMEM16 protein family: a new class of chloride channels? *Biophys. J.* 97:3047–3053. doi:10.1016/j.bpj.2009.09.024.

Greenwood, I.A., and W.A. Large. 1995. Comparison of the effects of fenamates on Ca-activated chloride and potassium currents in rabbit portal vein smooth muscle cells. *Br. J. Pharmacol.* 116:2939–2948.

Hartzell, C., I. Putzier, and J. Arreola. 2005. Calcium-activated chloride channels. *Annu. Rev. Physiol.* 67:719–758. doi:10.1146/annurev.physiol.67.032003.154341.

Hille, B. 2001. Ion Channels of Excitable Membranes, Third Edition. 3rd Edition edition. Sinauer Associates, Sunderland, Mass. 814 pp.

Hogg, R.C., Q. Wang, and W.A. Large. 1993. Time course of spontaneous calcium-activated chloride currents in smooth muscle cells from the rabbit portal vein. *J. Physiol.* 464:15–31.

Hogg, R.C., Q. Wang, and W.A. Large. 1994a. Effects of Cl channel blockers on Ca-activated chloride and potassium currents in smooth muscle cells from rabbit portal vein. *Br. J. Pharmacol.* 111:1333–1341.

Hogg, R.C., Q. Wang, and W.A. Large. 1994b. Action of niflumic acid on evoked and spontaneous calcium-activated chloride and potassium currents in smooth muscle cells from rabbit portal vein. *Br. J. Pharmacol.* 112:977–984.

Huang, F., J.R. Rock, B.D. Harfe, T. Cheng, X. Huang, Y.N. Jan, and L.Y. Jan. 2009. Studies on expression and function of the TMEM16A calcium-activated chloride channel. *Proc. Natl. Acad. Sci.* 106:21413–21418. doi:10.1073/pnas.0911935106.

Huang, F., X. Wong, and L.Y. Jan. 2012a. International Union of Basic and Clinical Pharmacology. LXXXV: Calcium-Activated Chloride Channels. *Pharmacol. Rev.* 64:1–15. doi:10.1124/pr.111.005009.

Huang, F., H. Zhang, M. Wu, H. Yang, M. Kudo, C.J. Peters, P.G. Woodruff, O.D. Solberg, M.L. Donne, X. Huang, D. Sheppard, J.V. Fahy, P.J. Wolters, B.L.M. Hogan, W.E. Finkbeiner, M. Li, Y.-N. Jan, L.Y. Jan, and J.R. Rock. 2012b. Calcium-activated chloride channel TMEM16A modulates mucin secretion and airway smooth muscle contraction. *Proc. Natl. Acad. Sci. U. S. A.* 109:16354–16359. doi:10.1073/pnas.1214596109.

Kunzelmann, K., R. Schreiber, A. Kmit, W. Jantarajit, J.R. Martins, D. Faria, P. Kongsuphol, J. Ousingsawat, and Y. Tian. 2012a. Expression and function of epithelial anoctamins. *Exp. Physiol.* 97:184–192. doi:10.1113/expphysiol.2011.058206.

Kunzelmann, K., Y. Tian, J.R. Martins, D. Faria, P. Kongsuphol, J. Ousingsawat, L. Wolf, and R. Schreiber. 2012b. Airway epithelial cells--functional links between CFTR and anoctamin dependent Cl- secretion. *Int. J. Biochem. Cell Biol.* 44:1897–1900. doi:10.1016/j.biocel.2012.06.011.

De La Fuente, R., W. Namkung, A. Mills, and A.S. Verkman. 2008. Small-molecule screen identifies inhibitors of a human intestinal calcium-activated chloride channel. *Mol. Pharmacol.* 73:758–768. doi:10.1124/mol.107.043208.

Lalonde, M.R., M.E. Kelly, and S. Barnes. 2008. Calcium-activated chloride channels in the retina. *Channels Austin Tex*. 2:252–260.

Large, W.A., and Q. Wang. 1996. Characteristics and physiological role of the Ca(2+)-activated Cl- conductance in smooth muscle. *Am. J. Physiol.* 271:C435–454.

Leblanc, N., J. Ledoux, S. Saleh, A. Sanguinetti, J. Angermann, K. O'Driscoll, F. Britton, B.A. Perrino, and I.A. Greenwood. 2005. Regulation of calcium-activated chloride channels in smooth muscle cells: a complex picture is emerging. *Can. J. Physiol. Pharmacol.* 83:541–556. doi:10.1139/y05-040.

Ledoux, J., I.A. Greenwood, and N. Leblanc. 2005. Dynamics of Ca2+-dependent Cl- channel modulation by niflumic acid in rabbit coronary arterial myocytes. *Mol. Pharmacol.* 67:163–173. doi:10.1124/mol.104.004168.

Liu, Y., H. Zhang, D. Huang, J. Qi, J. Xu, H. Gao, X. Du, N. Gamper, and H. Zhang. 2014. Characterization of the effects of Cl(-) channel modulators on TMEM16A and bestrophin-1 Ca(2+) activated Cl (-) channels. *Pflugers Arch.* doi:10.1007/s00424-014-1572-5.

Miledi, R. 1982. A calcium-dependent transient outward current in Xenopus laevis oocytes. *Proc. R. Soc. Lond. Ser. B Contain. Pap. Biol. Character R. Soc. G. B.* 215:491–497.

Namkung, W., J.R. Thiagarajah, P.-W. Phuan, and A.S. Verkman. 2010. Inhibition of Ca2+-activated Cl- channels by gallotannins as a possible molecular basis for health benefits of red wine and green tea. *FASEB J. Off. Publ. Fed. Am. Soc. Exp. Biol.* 24:4178–4186. doi:10.1096/fj.10-160648.

Namkung, W., P.-W. Phuan, and A.S. Verkman. 2011. TMEM16A inhibitors reveal TMEM16A as a minor component of calcium-activated chloride channel conductance in airway and intestinal epithelial cells. *J. Biol. Chem.* 286:2365–2374. doi:10.1074/jbc.M110.175109.

Oh, S.-J., S.J. Hwang, J. Jung, K. Yu, J. Kim, J.Y. Choi, H.C. Hartzell, E.J. Roh, and C.J. Lee. 2013. MONNA, a potent and selective blocker for transmembrane protein with unknown function 16/anoctamin-1. *Mol. Pharmacol.* 84:726–735. doi:10.1124/mol.113.087502.

Patton, C., S. Thompson, and D. Epel. 2004. Some precautions in using chelators to buffer metals in biological solutions. *Cell Calcium*. 35:427–431. doi:10.1016/j.ceca.2003.10.006.

Pedemonte, N., and L.J.V. Galietta. 2014. Structure and function of TMEM16 proteins (anoctamins). *Physiol. Rev.* 94:419–459. doi:10.1152/physrev.00039.2011.

Petersen, O.H. 2005. Ca2+ signalling and Ca2+-activated ion channels in exocrine acinar cells. *Cell Calcium*. 38:171–200. doi:10.1016/j.ceca.2005.06.024.

Pifferi, S., G. Pascarella, A. Boccaccio, A. Mazzatenta, S. Gustincich, A. Menini, and S. Zucchelli. 2006. Bestrophin-2 is a candidate calcium-activated chloride channel involved in olfactory transduction. *Proc. Natl. Acad. Sci. U. S. A.* 103:12929–12934. doi:10.1073/pnas.0604505103.

Pifferi, S., M. Dibattista, and A. Menini. 2009. TMEM16B induces chloride currents activated by calcium in mammalian cells. *Pflüg. Arch. Eur. J. Physiol.* 458:1023–1038. doi:10.1007/s00424-009-0684-9.

Pifferi, S., V. Cenedese, and A. Menini. 2012. Anoctamin 2/TMEM16B: a calcium-activated chloride channel in olfactory transduction. *Exp. Physiol.* 97:193–199. doi:10.1113/expphysiol.2011.058230.

Piper, A.S., I.A. Greenwood, and W.A. Large. 2002. Dual effect of blocking agents on Ca2+-activated Cl(-) currents in rabbit pulmonary artery smooth muscle cells. *J. Physiol.* 539:119–131.

Piper, A.S., and I.A. Greenwood. 2003. Anomalous effect of anthracene-9-carboxylic acid on calcium-activated chloride currents in rabbit pulmonary artery smooth muscle cells. *Br. J. Pharmacol.* 138:31–38. doi:10.1038/sj.bjp.0705000.

Ponissery Saidu, S., A.B. Stephan, A.K. Talaga, H. Zhao, and J. Reisert. 2013. Channel properties of the splicing isoforms of the olfactory calcium-activated chloride channel Anoctamin 2. *J. Gen. Physiol.* 141:691–703. doi:10.1085/jgp.201210937.

Qu, Z., and H.C. Hartzell. 2001. Functional geometry of the permeation pathway of Ca2+-activated Cl-channels inferred from analysis of voltage-dependent block. *J. Biol. Chem.* 276:18423–18429. doi:10.1074/jbc.M101264200.

Qu, Z., R.W. Wei, and H.C. Hartzell. 2003. Characterization of Ca2+-activated Cl- currents in mouse kidney inner medullary collecting duct cells. *Am. J. Physiol. Renal Physiol.* 285:F326–335. doi:10.1152/ajprenal.00034.2003.

Rock, J.R., and B.D. Harfe. 2008. Expression of TMEM16 paralogs during murine embryogenesis. *Dev. Dyn. Off. Publ. Am. Assoc. Anat.* 237:2566–2574. doi:10.1002/dvdy.21676.

Romanenko, V.G., M.A. Catalán, D.A. Brown, I. Putzier, H.C. Hartzell, A.D. Marmorstein, M. Gonzalez-Begne, J.R. Rock, B.D. Harfe, and J.E. Melvin. 2010. Tmem16A encodes the Ca2+-activated Cl- channel in mouse submandibular salivary gland acinar cells. *J. Biol. Chem.* 285:12990–13001. doi:10.1074/jbc.M109.068544.

Sagheddu, C., A. Boccaccio, M. Dibattista, G. Montani, R. Tirindelli, and A. Menini. 2010. Calcium concentration jumps reveal dynamic ion selectivity of calcium-activated chloride currents in mouse olfactory sensory neurons and TMEM16b-transfected HEK 293T cells. *J. Physiol.* 588:4189–4204. doi:10.1113/jphysiol.2010.194407.

Sanders, K.M., M.H. Zhu, F. Britton, S.D. Koh, and S.M. Ward. 2012. Anoctamins and gastrointestinal smooth muscle excitability. *Exp. Physiol.* 97:200–206. doi:10.1113/expphysiol.2011.058248.

Schroeder, B.C., T. Cheng, Y.N. Jan, and L.Y. Jan. 2008. Expression cloning of TMEM16A as a calcium-activated chloride channel subunit. *Cell*. 134:1019–1029. doi:10.1016/j.cell.2008.09.003.

Scudieri, P., E. Sondo, L. Ferrera, and L.J.V. Galietta. 2012. The anoctamin family: TMEM16A and TMEM16B as calcium-activated chloride channels. *Exp. Physiol.* 97:177–183. doi:10.1113/expphysiol.2011.058198.

Scudieri, P., E. Sondo, E. Caci, R. Ravazzolo, and L.J.V. Galietta. 2013. TMEM16A-TMEM16B chimaeras to investigate the structure-function relationship of calcium-activated chloride channels. *Biochem. J.* 452:443–455. doi:10.1042/BJ20130348.

Steinmeyer, K., C. Ortland, and T.J. Jentsch. 1991. Primary structure and functional expression of a developmentally regulated skeletal muscle chloride channel. *Nature*. 354:301–304. doi:10.1038/354301a0.

Stephan, A.B., E.Y. Shum, S. Hirsh, K.D. Cygnar, J. Reisert, and H. Zhao. 2009. ANO2 is the cilial calcium-activated chloride channel that may mediate olfactory amplification. *Proc. Natl. Acad. Sci. U. S. A.* 106:11776–11781. doi:10.1073/pnas.0903304106.

Stöhr, H., J.B. Heisig, P.M. Benz, S. Schöberl, V.M. Milenkovic, O. Strauss, W.M. Aartsen, J. Wijnholds, B.H.F. Weber, and H.L. Schulz. 2009. TMEM16B, a novel protein with calcium-dependent chloride channel activity, associates with a presynaptic protein complex in photoreceptor terminals. *J. Neurosci. Off. J. Soc. Neurosci.* 29:6809–6818. doi:10.1523/JNEUROSCI.5546-08.2009.

Toland, H.M., K.D. McCloskey, K.D. Thornbury, N.G. McHale, and M.A. Hollywood. 2000. Ca(2+)-activated Cl(-) current in sheep lymphatic smooth muscle. *Am. J. Physiol. Cell Physiol.* 279:C1327–1335.

Wayman, C.P., I. McFadzean, A. Gibson, and J.F. Tucker. 1997. Cellular mechanisms underlying carbachol-induced oscillations of calcium-dependent membrane current in smooth muscle cells from mouse anococcygeus. *Br. J. Pharmacol.* 121:1301–1308. doi:10.1038/sj.bjp.0701279.

White, M.M., and M. Aylwin. 1990. Niflumic and flufenamic acids are potent reversible blockers of Ca2(+)-activated Cl- channels in Xenopus oocytes. *Mol. Pharmacol.* 37:720–724.

Woodhull, A.M. 1973. Ionic Blockage of Sodium Channels in Nerve. *J. Gen. Physiol.* 61:687–708. doi:10.1085/jgp.61.6.687.

Wray, S., T. Burdyga, and K. Noble. 2005. Calcium signalling in smooth muscle. *Cell Calcium*. 38:397–407. doi:10.1016/j.ceca.2005.06.018.

Yang, Y.D., H. Cho, J.Y. Koo, M.H. Tak, Y. Cho, W.-S. Shim, S.P. Park, J. Lee, B. Lee, B.-M. Kim, R. Raouf, Y.K. Shin, and U. Oh. 2008. TMEM16A confers receptor-activated calcium-dependent chloride conductance. *Nature*. 455:1210–1215. doi:10.1038/nature07313.

Yao, Z., W. Namkung, E.A. Ko, J. Park, L. Tradtrantip, and A.S. Verkman. 2012. Fractionation of a Herbal Antidiarrheal Medicine Reveals Eugenol as an Inhibitor of Ca2+-

Activated Cl− Channel TMEM16A. *PLoS ONE*. 7:e38030. doi:10.1371/journal.pone.0038030.

Zhou, S.S., A. Takai, M. Tominaga, and Y. Okada. 1997. Phosphatase-mediated enhancement of cardiac cAMP-activated Cl-conductance by a Cl- channel blocker, anthracene-9-carboxylate. *Circ. Res.* 81:219–228.

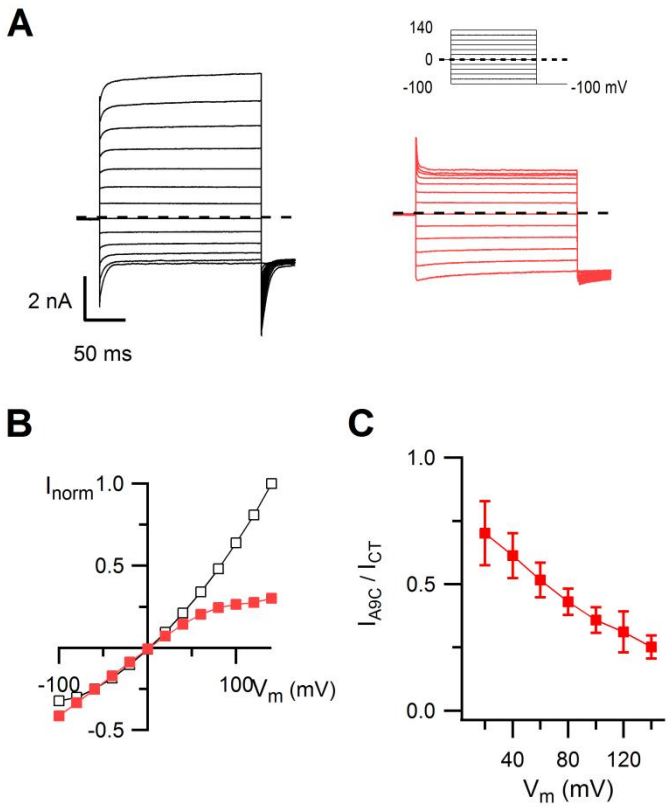

Figure 1. Voltage dependence of A9C block in 13 μM Ca^{2+}. (A) Whole-cell currents recorded in the presence of 13 μM intracellular Ca^{2+}, with voltage steps from -100 to +140 mV from a holding potential of 0 mV in control (black) or in presence of 1 mM A9C (red). Stimulation protocol in shown in top right side. (B) I-V relations measured at the end of the voltage steps from the cell shown in A normalized to the control value at +140 mV. (C) Average fractional current (I_{A9C}/I_{CT}) as a function of voltage (n=4).

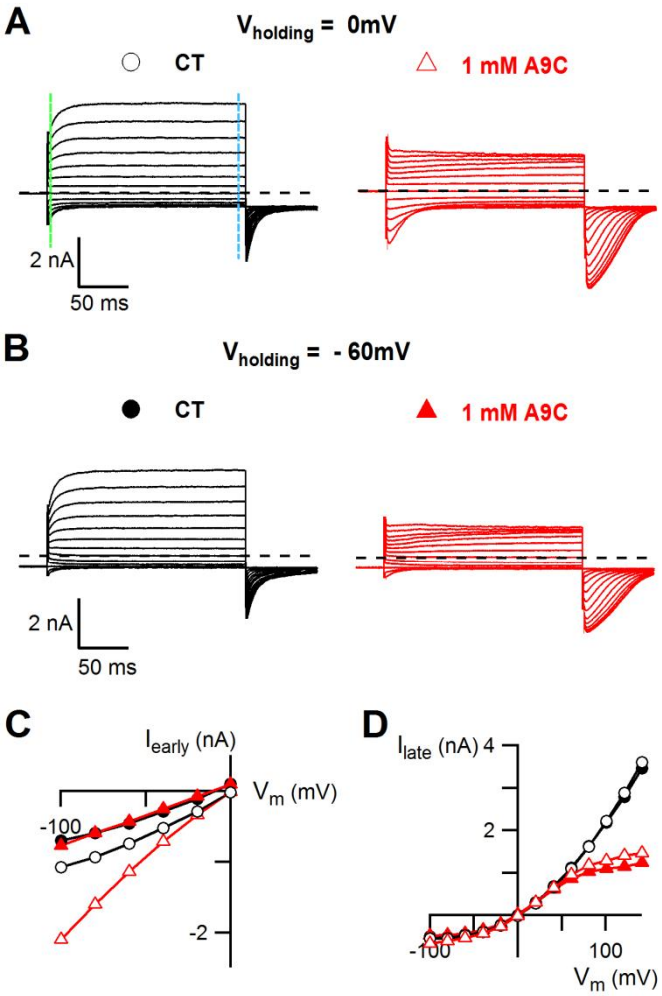

Figure 2. Holding potential affects early inward current potentiation. Whole-cell currents recorded in the same cell in the presence of 1.5 μM intracellular Ca^{2+}, with voltage steps from -100 to +140 mV from a holding potential ($V_{holding}$) of 0 mV (A) or -60 mV (B), in control (black) or in 1 mM A9C (red). (C) I-V relations of early peak inward currents evaluated at the time indicated by the green vertical line for the cell shown in A, B. Peak inward currents were strongly potentiated in A9C when $V_{holding}$ was 0, but not -60 mV. (D) I-V relations at the end of the voltage steps (at the time of the blue vertical line) for experiments shown in A and B.

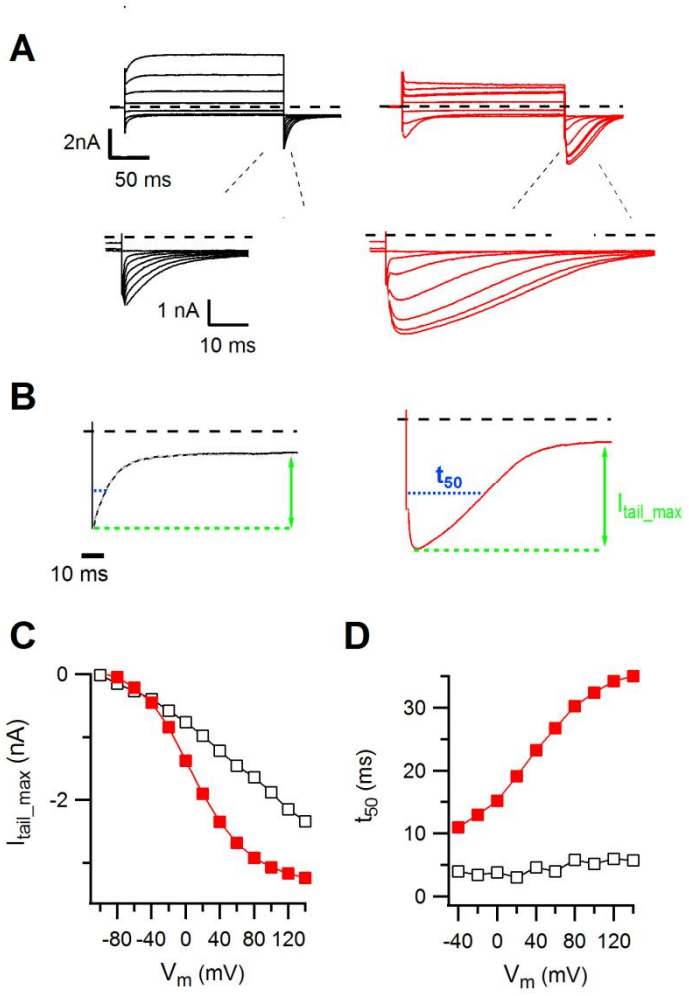

Figure 3. Multiple effects of A9C. (A) Current recordings from the same cell in Fig. 2, with voltage steps from -100 to +140 mV from a holding potential of 0 mV in control (black) or in presence of 1 mM A9C (red). Only recordings every 40 mV are shown. (B) Tail current decay shown in enlarged scale. To evaluate potentiation and slowing of current decay, maximal tail current amplitudes and time of 50% current decay, t_{50}, were calculated with respect to steady-state current at -100 mV. (C) Maximal tail currents, I_{tail_max}, plotted versus membrane potential in control and in 1 mM A9C for the experiment shown in A. (D) Time of 50% current decay, t_{50}, versus membrane potential.

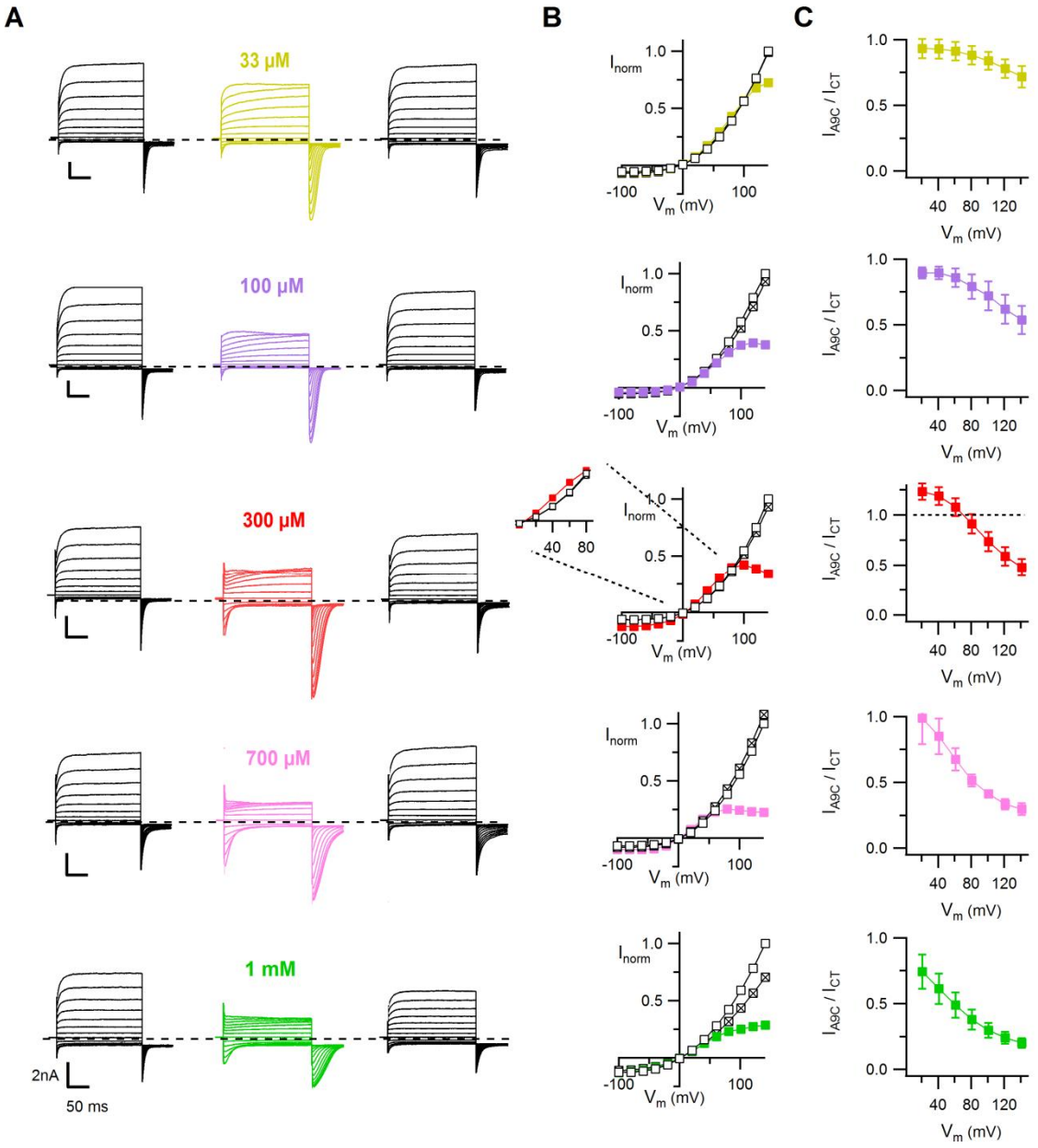

Figure 4. Concentration dependence of A9C effects. (A) representative whole-cell recordings in 1.5 µM intracellular Ca^{2+}. Voltage protocol as in Fig. 1. Each cell was exposed to control (black traces on the left), to the indicated concentration of A9C, followed by wash out (black traces on the right). (B) I-V relations measured at the end of the voltage steps from the cells shown in A in control (empty square), A9C (filled squares), or after wash out (cross squares). Currents were normalized to the value in control at 140

mV. The inset shows the IV on expanded scale for the cell exposed to 300 μM A9C and the potentiating effect of the compound on the current. (C) Average fractional current (I_{A9C} / I_{CT}) as a function of voltage (mean±SEM n=4-8 for each A9C concentration).

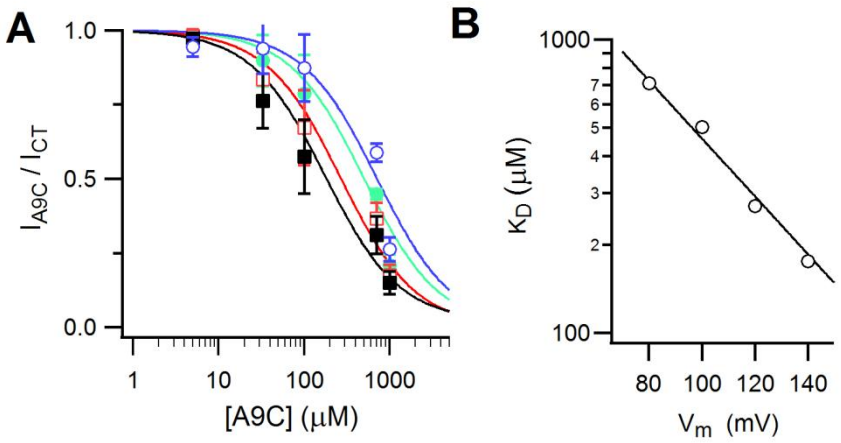

Figure 5. Concentration dependence of A9C block. (A) Concentration dependence of fractional current (I_{A9C} / I_{CT}) recorded at +140 (black squares), +120 (red empty squares), +100 (green circles), +80 mV (blue empty circles) in cells recorded in 1.5 μM Ca^{2+} (mean ± SEM; n=4-8 for each A9C concentration). Continuous lines are the best fit according to a Michaelis-Menten equation with K_D of 176, 270, 502 and 711 μM respectively at +140, +120, +100, +80 mV. (B) K_D Continuous line is the best fit with the Woodhull equation log K_D (V_m) = log K_D^{0mV} - δV_mF/(2.3*RT), with δ equal to 0.57 and an apparent K_D^{0mV} of 4450 μM.

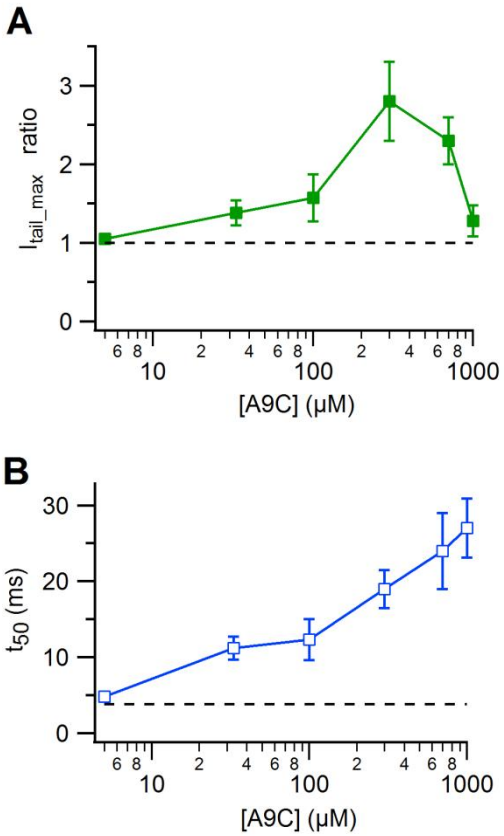

Figure 6. Concentration dependence of A9C tail current potentiation and prolongation of deactivation kinetics, evaluated as described in Fig3B. (A) Average ratios between maximal tail currents, I_{tail_max}, in A9C and control and (B) time of 50% current decay, t_{50}, evaluated at -100mV, after a prepulse to +120 mV, plotted as a function of A9C concentration (mean ± SEM n =4 to 8 for each A9C concentration). Broken line in A and B represent respectively I_{tail_max} and t_{50} in control.

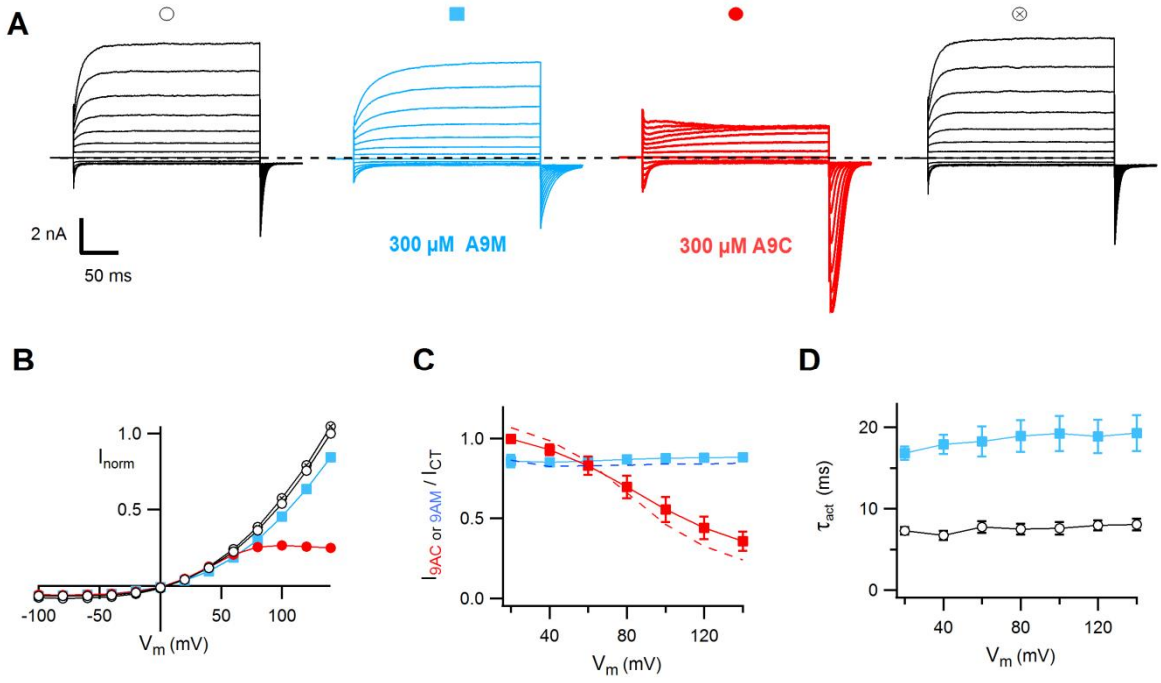

Figure 7. Effect of A9M, a non-charged analog of A9C. (A) TMEM16B currents recorded in presence of 1.5 µM intracellular calcium. The same cell exposed to control solution (black), 300 µM A9M (blue), 300 µM A9C (red) and back to control (black). (B) I-V relations measured at the end of the voltage steps from the cell in A. (C) Comparison of fractional currents ($I_{A9C\ or\ A9M}$ / I_{CT}) in A9M or A9C and control as a function of voltage (n=5). Broken line refers to the experiment in fig. A. (D) Time constant of activation in A9M and control as a function of voltage, showing that application of A9M slowed the activation kinetics (n=5).

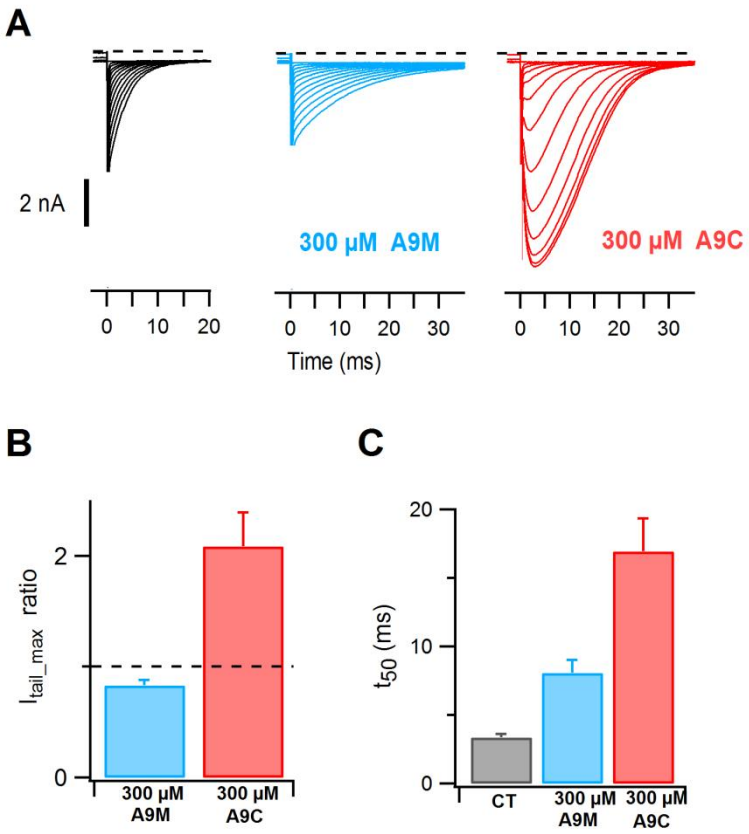

Figure 8. Comparison of tail currents in A9M and A9C. (A) Tail currents at -100 mV from the same cell in Fig. 7 A, shown on an expanded time scale. Currents were recorded in presence of 1.5 µM intracellular calcium in control bath, 300 µM A9M and A9C. (B) Ratio with respect to control of maximal current amplitudes in the presence of 300 µM A9M or A9C, recorded at -100 mV from a prepulse of +120 mV. Broken line refers to control. (n=5). (C) Time of 50% current decay, t_{50}, in control, 300 µM A9C and 300 µM A9M (n=5).

5. Discussion

Calcium and voltage dependent activation is a biophysical signature of endogenous CaCCs and is also observed for TMEM16A and TMEM16B (Yang et al., 2008; Caputo et al., 2008; Schroeder et al., 2008; Stephan et al., 2009; Pifferi et al., 2009a). However, the molecular mechanisms underlying these biophysical characteristics are still unknown. Research in this thesis is focused towards understanding the properties and molecular mechanisms of activation of TMEM16B, which has been very scarcely studied.

Comprehensive analysis of amino acid sequences does not reveal the presence of a canonical calcium binding site or a dedicated S4 like voltage sensor in TMEM16B. However, there are few conserved acidic residues in the first putative intracellular loop that may represent a potential calcium binding site or play a role in channel gating. We mutated the glutamic acids present at $_{367}$E, $_{386}$EEEEE$_{390}$, and $_{399}$EYE$_{401}$, and performed an extensive biophysical characterization and comparison with the properties of the wild type TMEM16B. Our results show that the consecutive five glutamates and a single glutamate at 367 position in the first putative intracellular loop are not involved in calcium sensitivity of TMEM16B, but they have a role in voltage dependent activation of TMEM16B. How the residues from the first intracellular loop contribute towards channel gating is still an open question.

When extracellular or intracellular anions were changed, we measured additional gating modifications of TMEM16B. Permeant anions like SCN^- increased open probability of the channel, with a shift in the activation curve towards less positive voltage and also an increase in the apparent calcium sensitivity. Our findings are in line with previous studies done on either endogenous CaCCs in *Xenopus* oocytes and salivary glands, or on TMEM16A expressed in heterologous system (Qu and Hartzell, 2000; Perez-Cornejo et al., 2004; Xiao et al., 2011).

A recent paper reported that TMEM16A(*ac*) channel can be gated by direct binding of calcium to glutamic acids $_{702}$E and $_{705}$E in the third intracellular loop (Yu et al., 2012). Interestingly, these residues are also conserved in the TMEM16B protein in spite of 10-fold lower calcium sensitivity in comparison to TMEM16A. Scudieri et al., (2013) replaced the third intracellular loop of TMEM16A which contains $_{702}$E and $_{705}$E with that of TMEM16B and observed a decrease in calcium sensitivity resembling TMEM16B. Therefore additional amino acids in the third intracellular loop are also important in determining the calcium sensitivity. Indeed this hypothesis is confirmed from the recent structural-functional characterization of TMEM16A(*a*) by Tien et al., 2014. They found two more residues at $_{730}$E and $_{734}$D to be involved in direct calcium binding.

These findings also modified the initially proposed topology of TMEM16A, in which the loop between 5th and 6th transmembrane segments formed a re-entrant loop (Das et al., 2008). A mutation of single arginine residues ($_{620}$R; TMEM16A(*a*) in Yang et al., 2008) in this re-entrant loop changed the selectivity of the channel, so tentatively featuring the pore lining (Yang et al., 2008). However, Yu et al 2012 remodeled the re-entrant loop between 5th and 6th transmembrane and proposed that it forms the third intracellular loop. Moreover, unlike Yang et al., 2008 they did not observe any change in selectivity with mutation of $_{620}$R under their experimental condition. Our study on TMEM16B shows a coupling between permeant anion and gating. However, determinants of ion selectivity are still unknown and future work should dissect further the molecular mechanism of this coupling.

The ability of a compound to modify channel gating is a desirable property not just for therapeutic purposes but also for structural-functional studies (Hille, 2001). A9C has been shown to have anomalous effect on endogenous CaCCs from smooth muscle cells in rabbit pulmonary artery (Piper and Greenwood, 2003). We studied the effect of extracellular A9C on heterologous expressed TMEM16B channels. Our results show that the interaction of A9C with TMEM16B is voltage and concentration dependent. The block of TMEM16B current by extracellular A9C was more efficient at positive voltages. In addition, A9C also had a potentiation effect, which was more evident at

negative potentials and prolonged the channel closure. In fact, the amplitude of current potentiation depended on the degree of activation, but not on the block. We also tested an electrically non-charged analog A9M on TMEM16B current. Extracellular A9M still blocked TMEM16B current weakly and modified the current kinetics, but unlike A9C, A9M was not effective in potentiating the current. Future studies focused to understand the molecular mechanism behind the A9C‘s bimodal effect on TMEM16B currents would be essential for the rational design of potent and selective modifiers of TMEM16B members of the same protein family.

Our findings presented in this thesis clearly portray a complex interplay between calcium, voltage and permeant anions in gating of TMEM16B. The mutational approach followed in our study along with other studies on TMEM16A and TMEM16B clearly shows involvement of multiple regions, spread throughout the primary amino acid sequences, and are involved in the channel function. However, future structure-function studies are required also to identify the pore region, probably where the effect of calcium, voltage and permeant anions play important role in channel activation. Structure-function studies with charged compounds like A9C, as reported for CLC in Estévez et al., 2003 should steer the use of similar compounds in the biophysical characterization of members of the TMEM16 protein family.

7. References

Adomaviciene, A., K.J. Smith, H. Garnett, and P. Tammaro. 2013. Putative pore-loops of TMEM16/anoctamin channels affect channel density in cell membranes. *J. Physiol.* 591:3487–3505. doi:10.1113/jphysiol.2013.251660.

Akbarali, H.I., and W.R. Giles. 1993. Ca^{2+} and Ca^{2+}-activated Cl- currents in rabbit oesophageal smooth muscle. *J. Physiol.* 460:117–133.

Åkervall, J.A., Y. Jin, J.P. Wennerberg, U.K. Zätterström, E. Kjellén, F. Mertens, R. Willén, N. Mandahl, S. Heim, and F. Mitelman. 1995. Chromosomal abnormalities involving 11q13 are associated with poor prognosis in patients with squamous cell carcinoma of the head and neck. Cancer. 76:853–859. doi:10.1002/1097-0142(19950901)76.

Arreola, J., J.E. Melvin, and T. Begenisich. 1996. Activation of calcium-dependent chloride channels in rat parotid acinar cells. *J. Gen. Physiol.* 108:35–47. doi:10.1085/jgp.108.1.35.

Bader, C.R., D. Bertrand, and E.A. Schwartz. 1982. Voltage-activated and calcium-activated currents studied in solitary rod inner segments from the salamander retina. *J. Physiol.* 331:253–284.1.

Bao, L., C. Kaldany, E.C. Holmstrand, and D.H. Cox. 2004. Mapping the BK_{Ca} Channel's "Ca^{2+} Bowl" Side-chains Essential for Ca2+ Sensing. *J. Gen. Physiol.* 123:475–489. doi:10.1085/jgp.200409052.

Barish, M.E. 1983. A transient calcium-dependent chloride current in the immature Xenopus oocyte. *J. Physiol.* 342:309–325.

Bevers, E.M., and P.L. Williamson. 2010. Phospholipid scramblase: an update. *FEBS Lett.* 584:2724–2730. doi:10.1016/j.febslet.2010.03.020.

Bradley, E., S. Fedigan, T. Webb, M.A. Hollywood, K.D. Thornbury, N.G. McHale, and G.P. Sergeant. 2014. Pharmacological characterization of TMEM16A currents. *Channels Austin Tex.* 8.

Caputo, A., E. Caci, L. Ferrera, N. Pedemonte, C. Barsanti, E. Sondo, U. Pfeffer, R. Ravazzolo, O. Zegarra-Moran, and L.J.V. Galietta. 2008. TMEM16A, a membrane protein associated with calcium-dependent chloride channel activity. *Science.* 322:590–594. doi:10.1126/science.1163518.

Cotton, K.D., M.A. Hollywood, N.G. McHale, and K.D. Thornbury. 1997. Ca^{2+} current and Ca^{2+}-activated chloride current in isolated smooth muscle cells of the sheep urethra. *J. Physiol.* 505 (Pt 1):121–131.

Cunningham, S.A., M.S. Awayda, J.K. Bubien, I.I. Ismailov, M.P. Arrate, B.K. Berdiev, D.J. Benos, and C.M. Fuller. 1995. Cloning of an epithelial chloride channel from bovine trachea. *J. Biol. Chem.* 270:31016–31026.

Das, S., Y. Hahn, D.A. Walker, S. Nagata, M.C. Willingham, D.M. Peehl, T.K. Bera, B. Lee, and I. Pastan. 2008. Topology of NGEP, a prostate-specific cell:cell junction protein widely expressed in many cancers of different grade level. *Cancer Res.* 68:6306–6312. doi:10.1158/0008-5472.CAN-08-0870.

Davis, A.J., J. Shi, H.A.T. Pritchard, P.S. Chadha, N. Leblanc, G. Vasilikostas, Z. Yao, A.S. Verkman, A.P. Albert, and I.A. Greenwood. 2013. Potent vasorelaxant activity of the TMEM16A inhibitor $T16A_{inh}$ -A01. *Br. J. Pharmacol.* 168:773–784. doi:10.1111/j.1476-5381.2012.02199.x.

De La Fuente, R., W. Namkung, A. Mills, and A.S. Verkman. 2008. Small-molecule screen identifies inhibitors of a human intestinal calcium-activated chloride channel. *Mol. Pharmacol.* 73:758–768. doi:10.1124/mol.107.043208.

Duran, C., and H.C. Hartzell. 2011. Physiological roles and diseases of Tmem16/Anoctamin proteins: are they all chloride channels? *Acta Pharmacol. Sin.* 32:685–692. doi:10.1038/aps.2011.48.

Duran, C., C.H. Thompson, Q. Xiao, and H.C. Hartzell. 2010. Chloride channels: often enigmatic, rarely predictable. *Annu. Rev. Physiol.* 72:95–121. doi:10.1146/annurev-physiol-021909-135811.

Duvvuri, U., D.J. Shiwarski, D. Xiao, C. Bertrand, X. Huang, R.S. Edinger, J.R. Rock, B.D. Harfe, B.J. Henson, K. Kunzelmann, R. Schreiber, R.S. Seethala, A.M. Egloff, X. Chen, V.W. Lui, J.R. Grandis, and S.M. Gollin. 2012. TMEM16A Induces MAPK and Contributes Directly to Tumorigenesis and Cancer Progression. Cancer Res. 72:3270–3281. doi:10.1158/0008-5472.CAN-12-0475-T.

Eggermont, J. 2004. Calcium-activated chloride channels: (un)known, (un)loved? *Proc. Am. Thorac. Soc.* 1:22–27. doi:10.1513/pats.2306010.

Espinosa, I., C.-H. Lee, M.K. Kim, B.-T. Rouse, S. Subramanian, K. Montgomery, S. Varma, C.L. Corless, M.C. Heinrich, K.S. Smith, Z. Wang, B. Rubin, T.O. Nielsen, R.S. Seitz, D.T. Ross, R.B. West, M.L. Cleary, and M. van de Rijn. 2008. A novel monoclonal antibody against DOG1 is a sensitive and specific marker for gastrointestinal stromal tumors. *Am. J. Surg. Pathol.* 32:210–218. doi:10.1097/PAS.0b013e3181238cec.

Estévez, R., B.C. Schroeder, A. Accardi, T.J. Jentsch, and M. Pusch. 2003. Conservation of chloride channel structure revealed by an inhibitor binding site in ClC-1. *Neuron*. 38:47–59.

Evans, M.G., and A. Marty. 1986. Calcium-dependent chloride currents in isolated cells from rat lacrimal glands. *J. Physiol.* 378:437–460.

Fallah, G., T. Römer, S. Detro-Dassen, U. Braam, F. Markwardt, and G. Schmalzing. 2011. TMEM16A(a)/anoctamin-1 shares a homodimeric architecture with CLC chloride channels. *Mol. Cell. Proteomics MCP.* 10:M110.004697. doi:10.1074/mcp.M110.004697.

Ferrera, L., A. Caputo, I. Ubby, E. Bussani, O. Zegarra-Moran, R. Ravazzolo, F. Pagani, and L.J.V. Galietta. 2009. Regulation of TMEM16A chloride channel properties by alternative splicing. *J. Biol. Chem.* 284:33360–33368. doi:10.1074/jbc.M109.046607.

Ferrera, L., P. Scudieri, E. Sondo, A. Caputo, E. Caci, O. Zegarra-Moran, R. Ravazzolo, and L.J.V. Galietta. 2011a. A minimal isoform of the TMEM16A protein associated with chloride channel activity. *Biochim. Biophys. Acta BBA - Biomembr.* 1808:2214–2223. doi:10.1016/j.bbamem.2011.05.017.

Ferrera, L., O. Zegarra-Moran, and L.J.V. Galietta. 2011b. Ca^{2+}-activated Cl^- channels. *Compr. Physiol.* 1:2155–2174. doi:10.1002/cphy.c110017.

Flores, C.A., L.P. Cid, F.V. Sepúlveda, and M.I. Niemeyer. 2009. TMEM16 proteins: the long awaited calcium-activated chloride channels? *Braz. J. Med. Biol. Res. Rev. Bras. Pesqui. Médicas E Biológicas Soc. Bras. Biofísica Al.* 42:993–1001.

Frings, S., D. Reuter, and S.J. Kleene. 2000. Neuronal Ca^{2+} -activated Cl^- channels--homing in on an elusive channel species. *Prog. Neurobiol.* 60:247–289.

Galietta, L.J.V. 2009. The TMEM16 protein family: a new class of chloride channels? *Biophys. J.* 97:3047–3053. doi:10.1016/j.bpj.2009.09.024.

Galindo, B.E., and V.D. Vacquier. 2005. Phylogeny of the TMEM16 protein family: some members are overexpressed in cancer. *Int. J. Mol. Med.* 16:919–924.

Greenwood, I.A., and W.A. Large. 1995. Comparison of the effects of fenamates on Ca-activated chloride and potassium currents in rabbit portal vein smooth muscle cells. *Br. J. Pharmacol.* 116:2939–2948.

Greenwood, I.A., and W.A. Large. 1999. Modulation of the decay of Ca^{2+}-activated Cl^- currents in rabbit portal vein smooth muscle cells by external anions. *J. Physiol.* 516 (Pt 2):365–376.

Greenwood, I.A., J. Ledoux, and N. Leblanc. 2001. Differential regulation of Ca2+-activated Cl− currents in rabbit arterial and portal vein smooth muscle cells by Ca^{2+}-calmodulin-dependent kinase. *J. Physiol.* 534:395–408. doi:10.1111/j.1469-7793.2001.00395.x.

Hartzell, C., I. Putzier, and J. Arreola. 2005. Calcium-activated chloride channels. *Annu. Rev. Physiol.* 67:719–758. doi:10.1146/annurev.physiol.67.032003.154341.

Hartzell, H.C., Z. Qu, K. Yu, Q. Xiao, and L.-T. Chien. 2008. Molecular physiology of bestrophins: multifunctional membrane proteins linked to best disease and other retinopathies. *Physiol. Rev.* 88:639–672. doi:10.1152/physrev.00022.2007.

Hartzell, H.C., K. Yu, Q. Xiao, L.-T. Chien, and Z. Qu. 2009. Anoctamin/TMEM16 family members are Ca^{2+}-activated Cl^- channels. *J. Physiol.* 587:2127–2139. doi:10.1113/jphysiol.2008.163709.

Hille, B. 2001. Ion Channels of Excitable Membranes, Third Edition. 3rd Edition edition. Sinauer Associates, Sunderland, Mass. 814 pp.

Hogg, R.C., Q. Wang, and W.A. Large. 1993. Time course of spontaneous calcium-activated chloride currents in smooth muscle cells from the rabbit portal vein. *J. Physiol.* 464:15–31.

Hogg, R.C., Q. Wang, and W.A. Large. 1994a. Effects of Cl channel blockers on Ca-activated chloride and potassium currents in smooth muscle cells from rabbit portal vein. *Br. J. Pharmacol.* 111:1333–1341.

Hogg, R.C., Q. Wang, and W.A. Large. 1994b. Action of niflumic acid on evoked and spontaneous calcium-activated chloride and potassium currents in smooth muscle cells from rabbit portal vein. *Br. J. Pharmacol.* 112:977–984.

Huang, F., X. Wong, and L.Y. Jan. 2012a. International Union of Basic and Clinical Pharmacology. LXXXV: Calcium-Activated Chloride Channels. *Pharmacol. Rev.* 64:1–15. doi:10.1124/pr.111.005009.

Huang, F., H. Zhang, M. Wu, H. Yang, M. Kudo, C.J. Peters, P.G. Woodruff, O.D. Solberg, M.L. Donne, X. Huang, D. Sheppard, J.V. Fahy, P.J. Wolters, B.L.M. Hogan, W.E. Finkbeiner, M. Li, Y.-N. Jan, L.Y. Jan, and J.R. Rock. 2012b. Calcium-activated chloride channel TMEM16A modulates mucin secretion and airway smooth muscle contraction. *Proc. Natl. Acad. Sci. U. S. A.* 109:16354–16359. doi:10.1073/pnas.1214596109.

Huang, P., J. Liu, A. Di, N.C. Robinson, M.W. Musch, M.A. Kaetzel, and D.J. Nelson. 2001. Regulation of human CLC-3 channels by multifunctional Ca2+/calmodulin-dependent protein kinase. *J. Biol. Chem.* 276:20093–20100. doi:10.1074/jbc.M009376200.

Huang, X., S.M. Gollin, S. Raja, and T.E. Godfrey. 2002. High-resolution mapping of the 11q13 amplicon and identification of a gene, TAOS1, that is amplified and overexpressed in oral cancer cells. Proc. Natl. Acad. Sci. 99:11369–11374. doi:10.1073/pnas.172285799.

Jentsch, T.J., V. Stein, F. Weinreich, and A.A. Zdebik. 2002. Molecular structure and physiological function of chloride channels. *Physiol. Rev.* 82:503–568. doi:10.1152/physrev.00029.2001.

Jung, J., J.H. Nam, H.W. Park, U. Oh, J.-H. Yoon, and M.G. Lee. 2013. Dynamic modulation of ANO1/TMEM16A HCO_3^- permeability by Ca^{2+}/calmodulin. *Proc. Natl. Acad. Sci. U. S. A.* 110:360–365. doi:10.1073/pnas.1211594110.

Kaneko, H., F. Möhrlen, and S. Frings. 2006. Calmodulin contributes to gating control in olfactory calcium-activated chloride channels. *J. Gen. Physiol.* 127:737–748. doi:10.1085/jgp.200609497.

Kunzelmann, K., B. Nilius, G. Owsianik, R. Schreiber, J. Ousingsawat, L. Sirianant, P. Wanitchakool, E.M. Bevers, and J.W.M. Heemskerk. 2014. Molecular functions of anoctamin 6 (TMEM16F): a chloride channel, cation channel, or phospholipid scramblase? *Pflüg. Arch. Eur. J. Physiol.* 466:407–414. doi:10.1007/s00424-013-1305-1.

Kunzelmann, K., R. Schreiber, A. Kmit, W. Jantarajit, J.R. Martins, D. Faria, P. Kongsuphol, J. Ousingsawat, and Y. Tian. 2012. Expression and function of epithelial anoctamins. *Exp. Physiol.* 97:184–192. doi:10.1113/expphysiol.2011.058206.

Kuruma, A., and H.C. Hartzell. 2000. Bimodal control of a Ca^{2+}-activated Cl^- channel by different Ca^{2+} signals. *J. Gen. Physiol.* 115:59–80.

Ledoux, J., I.A. Greenwood, and N. Leblanc. 2005. Dynamics of Ca^{2+}-dependent Cl^- channel modulation by niflumic acid in rabbit coronary arterial myocytes. *Mol. Pharmacol.* 67:163–173. doi:10.1124/mol.104.004168.

Liu, Y., H. Zhang, D. Huang, J. Qi, J. Xu, H. Gao, X. Du, N. Gamper, and H. Zhang. 2014. Characterization of the effects of Cl^- channel modulators on TMEM16A and bestrophin-1 Ca^{2+} activated Cl^- channels. *Pflugers Arch.* doi:10.1007/s00424-014-1572-5.

Loewen, M.E., and G.W. Forsyth. 2005. Structure and function of CLCA proteins. *Physiol. Rev.* 85:1061–1092. doi:10.1152/physrev.00016.2004.

Matsuda, J.J., M.S. Filali, M.M. Collins, K.A. Volk, and F.S. Lamb. 2010. The ClC-3 Cl-/H+ antiporter becomes uncoupled at low extracellular pH. *J. Biol. Chem.* 285:2569–2579. doi:10.1074/jbc.M109.018002.

Mazzone, A., S.T. Eisenman, P.R. Strege, Z. Yao, T. Ordog, S.J. Gibbons, and G. Farrugia. 2012. Inhibition of Cell Proliferation by a Selective Inhibitor of the Ca^{2+}-activated Cl^- Channel, Ano1. *Biochem. Biophys. Res. Commun.* 427:248–253. doi:10.1016/j.bbrc.2012.09.022.

Miledi, R. 1982. A calcium-dependent transient outward current in *Xenopus laevis* oocytes. *Proc. R. Soc. Lond. Ser. B Contain. Pap. Biol. Character R. Soc. G. B.* 215:491–497.

Milenkovic, V.M., M. Brockmann, H. Stöhr, B.H. Weber, and O. Strauss. 2010. Evolution and functional divergence of the anoctamin family of membrane proteins. *BMC Evol. Biol.* 10:319. doi:10.1186/1471-2148-10-319.

Namkung, W., P.-W. Phuan, and A.S. Verkman. 2011. TMEM16A inhibitors reveal TMEM16A as a minor component of calcium-activated chloride channel conductance in airway and intestinal epithelial cells. *J. Biol. Chem.* 286:2365–2374. doi:10.1074/jbc.M110.175109.

Namkung, W., J.R. Thiagarajah, P.-W. Phuan, and A.S. Verkman. 2010. Inhibition of Ca^{2+}-activated Cl^- channels by gallotannins as a possible molecular basis for health benefits of red wine and green tea. *FASEB J. Off. Publ. Fed. Am. Soc. Exp. Biol.* 24:4178–4186. doi:10.1096/fj.10-160648.

Nilius, B., and G. Droogmans. 2003. Amazing chloride channels: an overview. *Acta Physiol. Scand.* 177:119–147. doi:10.1046/j.1365-201X.2003.01060.x.

Nilius, B., J. Prenen, T. Voets, K. Van den Bremt, J. Eggermont, and G. Droogmans. 1997. Kinetic and pharmacological properties of the calcium-activated chloride-current in macrovascular endothelial cells. *Cell Calcium*. 22:53–63.

O'Driscoll, K.E., R.A. Pipe, and F.C. Britton. 2011. Increased complexity of Tmem16a/Anoctamin 1 transcript alternative splicing. *BMC Mol. Biol.* 12:35. doi:10.1186/1471-2199-12-35.

Oh, S.-J., S.J. Hwang, J. Jung, K. Yu, J. Kim, J.Y. Choi, H.C. Hartzell, E.J. Roh, and C.J. Lee. 2013. MONNA, a potent and selective blocker for transmembrane protein with unknown function 16/anoctamin-1. *Mol. Pharmacol.* 84:726–735. doi:10.1124/mol.113.087502.

Ousingsawat, J., P. Kongsuphol, R. Schreiber, and K. Kunzelmann. 2011. CFTR and TMEM16A are separate but functionally related Cl^- channels. *Cell. Physiol. Biochem. Int. J. Exp. Cell. Physiol. Biochem. Pharmacol.* 28:715–724. doi:10.1159/000335765.

Papassotiriou, J., J. Eggermont, G. Droogmans, and B. Nilius. 2001. Ca^{2+}-activated Cl^- channels in Ehrlich ascites tumor cells are distinct from mCLCA1, 2 and 3. *Pflüg. Arch. Eur. J. Physiol.* 442:273–279.

Patton, C., S. Thompson, and D. Epel. 2004. Some precautions in using chelators to buffer metals in biological solutions. *Cell Calcium*. 35:427–431. doi:10.1016/j.ceca.2003.10.006.

Pedemonte, N., and L.J.V. Galietta. 2014. Structure and function of TMEM16 proteins (anoctamins). *Physiol. Rev.* 94:419–459. doi:10.1152/physrev.00039.2011.

Perez-Cornejo, P., J.A. De Santiago, and J. Arreola. 2004. Permeant anions control gating of calcium-dependent chloride channels. *J. Membr. Biol.* 198:125–133. doi:10.1007/s00232-004-0659-x.

Pifferi, S., M. Dibattista, and A. Menini. 2009a. TMEM16B induces chloride currents activated by calcium in mammalian cells. *Pflüg. Arch. Eur. J. Physiol.* 458:1023–1038. doi:10.1007/s00424-009-0684-9.

Pifferi, S., M. Dibattista, C. Sagheddu, A. Boccaccio, A. Al Qteishat, F. Ghirardi, R. Tirindelli, and A. Menini. 2009b. Calcium-activated chloride currents in olfactory sensory neurons from mice lacking bestrophin-2. *J. Physiol.* 587:4265–4279. doi:10.1113/jphysiol.2009.176131.

Piper, A.S., and I.A. Greenwood. 2003. Anomalous effect of anthracene-9-carboxylic acid on calcium-activated chloride currents in rabbit pulmonary artery smooth muscle cells. *Br. J. Pharmacol.* 138:31–38. doi:10.1038/sj.bjp.0705000.

Piper, A.S., I.A. Greenwood, and W.A. Large. 2002. Dual effect of blocking agents on Ca2+-activated Cl(-) currents in rabbit pulmonary artery smooth muscle cells. *J. Physiol.* 539:119–131.

Planells-Cases, R., and T.J. Jentsch. 2009. Chloride channelopathies. *Biochim. Biophys. Acta*. 1792:173–189. doi:10.1016/j.bbadis.2009.02.002.

Ponissery Saidu, S., A.B. Stephan, A.K. Talaga, H. Zhao, and J. Reisert. 2013. Channel properties of the splicing isoforms of the olfactory calcium-activated chloride channel Anoctamin 2. *J. Gen. Physiol.* 141:691–703. doi:10.1085/jgp.201210937.

Qu, Z., and H.C. Hartzell. 2000. Anion permeation in Ca^{2+}-activated Cl^- channels. *J. Gen. Physiol.* 116:825–844.

Qu, Z., and H.C. Hartzell. 2001. Functional geometry of the permeation pathway of Ca^{2+}-activated Cl^- channels inferred from analysis of voltage-dependent block. *J. Biol. Chem.* 276:18423–18429. doi:10.1074/jbc.M101264200.

Qu, Z., R.W. Wei, and H.C. Hartzell. 2003a. Characterization of Ca^{2+}-activated Cl^- currents in mouse kidney inner medullary collecting duct cells. *Am. J. Physiol. Renal Physiol.* 285:F326–335. doi:10.1152/ajprenal.00034.2003.

Qu, Z., R.W. Wei, W. Mann, and H.C. Hartzell. 2003b. Two bestrophins cloned from *Xenopus laevis* oocytes express Ca^{2+}-activated Cl^- currents. *J. Biol. Chem.* 278:49563–49572. doi:10.1074/jbc.M308414200.

Romanenko, V.G., M.A. Catalán, D.A. Brown, I. Putzier, H.C. Hartzell, A.D. Marmorstein, M. Gonzalez-Begne, J.R. Rock, B.D. Harfe, and J.E. Melvin. 2010. Tmem16A encodes the Ca^{2+}-activated Cl^- channel in mouse submandibular salivary gland acinar cells. *J. Biol. Chem.* 285:12990–13001. doi:10.1074/jbc.M109.068544.

Sagheddu, C., A. Boccaccio, M. Dibattista, G. Montani, R. Tirindelli, and A. Menini. 2010. Calcium concentration jumps reveal dynamic ion selectivity of calcium-activated chloride currents in mouse olfactory sensory neurons and TMEM16b-transfected HEK 293T cells. *J. Physiol.* 588:4189–4204. doi:10.1113/jphysiol.2010.194407.

Scudieri, P., E. Sondo, E. Caci, R. Ravazzolo, and L.J.V. Galietta. 2013. TMEM16A-TMEM16B chimaeras to investigate the structure-function relationship of calcium-activated chloride channels. Biochem. J. 452:443–455. doi:10.1042/BJ20130348.

Schroeder, B.C., T. Cheng, Y.N. Jan, and L.Y. Jan. 2008. Expression cloning of TMEM16A as a calcium-activated chloride channel subunit. *Cell*. 134:1019–1029. doi:10.1016/j.cell.2008.09.003.

Segawa, K., J. Suzuki, and S. Nagata. 2011. Constitutive exposure of phosphatidylserine on viable cells. *Proc. Natl. Acad. Sci. U. S. A.* 108:19246–19251. doi:10.1073/pnas.1114799108.

Sheridan, J.T., E.N. Worthington, K. Yu, S.E. Gabriel, H.C. Hartzell, and R. Tarran. 2011. Characterization of the oligomeric structure of the Ca^{2+}-activated Cl^- channel Ano1/TMEM16A. *J. Biol. Chem.* 286:1381–1388. doi:10.1074/jbc.M110.174847.

Sondo, E., P. Scudieri, V. Tomati, E. Caci, A. Mazzone, G. Farrugia, R. Ravazzolo, and L.J.V. Galietta. 2014. Non-canonical translation start sites in the TMEM16A chloride channel. *Biochim. Biophys. Acta*. 1838:89–97. doi:10.1016/j.bbamem.2013.08.010.

Stephan, A.B., E.Y. Shum, S. Hirsh, K.D. Cygnar, J. Reisert, and H. Zhao. 2009. ANO2 is the cilial calcium-activated chloride channel that may mediate olfactory amplification. *Proc. Natl. Acad. Sci. U. S. A.* 106:11776–11781. doi:10.1073/pnas.0903304106.

Suzuki, M., and A. Mizuno. 2004. A novel human Cl^- channel family related to Drosophila flightless locus. *J. Biol. Chem.* 279:22461–22468. doi:10.1074/jbc.M313813200.

Terashima, H., A. Picollo, and A. Accardi. 2013. Purified TMEM16A is sufficient to form Ca^{2+}-activated Cl^- channels. *Proc. Natl. Acad. Sci. U. S. A.* 110:19354–19359. doi:10.1073/pnas.1312014110.

Tian, Y., P. Kongsuphol, M. Hug, J. Ousingsawat, R. Witzgall, R. Schreiber, and K. Kunzelmann. 2011. Calmodulin-dependent activation of the epithelial calcium-dependent chloride channel TMEM16A. *FASEB J. Off. Publ. Fed. Am. Soc. Exp. Biol.* 25:1058–1068. doi:10.1096/fj.10-166884.

Tien, J., H.Y. Lee, D.L. Minor, Y.N. Jan, and L.Y. Jan. 2013. Identification of a dimerization domain in the TMEM16A calcium-activated chloride channel (CaCC). *Proc. Natl. Acad. Sci. U. S. A.* 110:6352–6357. doi:10.1073/pnas.1303672110.

Tien, J., C.J. Peters, X.M. Wong, T. Cheng, Y.N. Jan, L.Y. Jan, and H. Yang. 2014. A comprehensive search for calcium binding sites critical for TMEM16A calcium-activated chloride channel activity. *eLife*. e02772. doi:10.7554/eLife.02772.

Toland, H.M., K.D. McCloskey, K.D. Thornbury, N.G. McHale, and M.A. Hollywood. 2000. Ca^{2+}-activated Cl^- current in sheep lymphatic smooth muscle. *Am. J. Physiol. Cell Physiol.* 279:C1327–1335.

Tsunenari, T., J. Nathans, and K.-W. Yau. 2006. Ca^{2+}-activated Cl^- Current from Human Bestrophin-4 in Excised Membrane Patches. *J. Gen. Physiol.* 127:749–754. doi:10.1085/jgp.200609527.

Tsunenari, T., H. Sun, J. Williams, H. Cahill, P. Smallwood, K.-W. Yau, and J. Nathans. 2003. Structure-function analysis of the bestrophin family of anion channels. *J. Biol. Chem.* 278:41114–41125. doi:10.1074/jbc.M306150200.

Verkman, A.S., and L.J.V. Galietta. 2009. Chloride channels as drug targets. *Nat. Rev. Drug Discov.* 8:153–171. doi:10.1038/nrd2780.

Vocke, K., K. Dauner, A. Hahn, A. Ulbrich, J. Broecker, S. Keller, S. Frings, and F. Möhrlen. 2013. Calmodulin-dependent activation and inactivation of anoctamin calcium-gated chloride channels. *J. Gen. Physiol.* 142:381–404. doi:10.1085/jgp.201311015.

Wayman, C.P., I. McFadzean, A. Gibson, and J.F. Tucker. 1997. Cellular mechanisms underlying carbachol-induced oscillations of calcium-dependent membrane current in smooth muscle cells from mouse anococcygeus. *Br. J. Pharmacol.* 121:1301–1308. doi:10.1038/sj.bjp.0701279.

West, R.B., C.L. Corless, X. Chen, B.P. Rubin, S. Subramanian, K. Montgomery, S. Zhu, C.A. Ball, T.O. Nielsen, R. Patel, J.R. Goldblum, P.O. Brown, M.C. Heinrich, and M. van de Rijn. 2004. The Novel Marker, DOG1, Is Expressed Ubiquitously in Gastrointestinal Stromal Tumors Irrespective of KIT or PDGFRA Mutation Status. *Am. J. Pathol.* 165:107–113.

White, M.M., and M. Aylwin. 1990. Niflumic and flufenamic acids are potent reversible blockers of Ca^{2+}-activated Cl^- channels in Xenopus oocytes. *Mol. Pharmacol.* 37:720–724.

Wright, E.M., and J.M. Diamond. 1977. Anion selectivity in biological systems. *Physiol. Rev.* 57:109–156.

Xiao, Q., and Y. Cui. 2014. Acidic Amino Acids in the First Intracellular Loop Contribute to Voltage- and Calcium- Dependent Gating of Anoctamin1/TMEM16A. *PLoS ONE*. 9:e99376. doi:10.1371/journal.pone.0099376.

Xiao, Q., K. Yu, P. Perez-Cornejo, Y. Cui, J. Arreola, and H.C. Hartzell. 2011. Voltage- and calcium-dependent gating of TMEM16A/Ano1 chloride channels are physically coupled by the first intracellular loop. *Proc. Natl. Acad. Sci. U. S. A.* 108:8891–8896. doi:10.1073/pnas.1102147108.

Yang, Y.D., H. Cho, J.Y. Koo, M.H. Tak, Y. Cho, W.-S. Shim, S.P. Park, J. Lee, B. Lee, B.-M. Kim, R. Raouf, Y.K. Shin, and U. Oh. 2008. TMEM16A confers receptor-activated calcium-dependent chloride conductance. *Nature*. 455:1210–1215. doi:10.1038/nature07313.

Yao, Z., W. Namkung, E.A. Ko, J. Park, L. Tradtrantip, and A.S. Verkman. 2012. Fractionation of a Herbal Antidiarrheal Medicine Reveals Eugenol as an Inhibitor of Ca^{2+}-Activated Cl^- Channel TMEM16A. *PLoS ONE*. 7:e38030. doi:10.1371/journal.pone.0038030.

Yu, K., C. Duran, Z. Qu, Y.-Y. Cui, and H.C. Hartzell. 2012. Explaining calcium-dependent gating of anoctamin-1 chloride channels requires a revised topology. *Circ. Res.* 110:990–999. doi:10.1161/CIRCRESAHA.112.264440.

Yu, K., J. Zhu, Z. Qu, Y.-Y. Cui, and H.C. Hartzell. 2014. Activation of the Ano1 (TMEM16A) chloride channel by calcium is not mediated by calmodulin. *J. Gen. Physiol.* 143:253–267. doi:10.1085/jgp.201311047.

Zhang, Y., and P.S. Cremer. 2006. Interactions between macromolecules and ions: the Hofmeister series. *Curr. Opin. Chem. Biol.* 10:658–663. doi:10.1016/j.cbpa.2006.09.020.